Regulation of chromosome congression: Focus on the function of hSpindly and the kinetochore recruitment of the Ska complex

Inauguraldissertation
zur
Erlangung der Würde eines Doktors der Philosophie
vorgelegt der
Philosophisch-Naturwissenschaftlichen Fakultät
der Universität Basel

von

Ying Wai Chan
aus Hong Kong, China

Basel, 2011

Genehmigt von der Philosophisch-Naturwissenschaftlichen Fakultät

auf Antrag von

Prof. Erich A. Nigg, Prof. Thomas U. Mayer, Prof. Patrick Meraldi and
Dr. Anna Santamaria
(Mitglieder des Dissertationskomitees)

Basel, den 18.10.2011
Prof. Martin Spiess
– Dekan –

The experiments displayed in this thesis have been performed from September 2007 to October 2011 in the laboratory of Prof. Erich A. Nigg, in the Department of Cell Biology at the Max-Planck Institute of Biochemistry and at the Biozentrum (Growth & Development), University of Basel.

Parts of this thesis have been published in:

Chan, Y.W., Fava, L.L., Uldschmid, A., Schmitz, M.H.A., Gerlich, D.W., Nigg, E.A. and Santamaria, A. Mitotic control of kinetochore-associated dynein and spindle orientation by human Spindly. *Journal of Cell Biology* 185: 859-874 (2009)

Chan, Y.W., Nigg, E.A. and Santamaria, A. Aurora B controls kinetochore-microtubules attachments by modulating the interaction between the Ska complex and the KMN network. *Journal of Cell Biology* under revision (2011)

I herewith declare that major passages in this thesis have been adapted from the above stated publications. I am primarily responsible for the work described in this publication

Figure 21, Figure 27A-B were performed by Dr. Anna Santamaria and Luca Fava, respectively.

Table of Contents

Summary

Mitosis is a process in which cells divide their genetic materials equally into two daughter cells. During mitosis, specialized structures called kinetochores (KTs), located at the centromeric regions of chromosomes, are captured by microtubules (MTs) radiated from spindle poles. Subsequently, the chromosomes align at the metaphase plate, a process called congression. This process needs to be tightly controlled in order to maintain genomic stability, as subsequent chromosome segregation depends critically on KT-MT interactions. However, how KT-MT attachments are regulated remains largely unknown. Therefore, identification of novel KT/spindle proteins and thorough examination of their functions and regulation will increase our understanding on chromosome congression mechanisms and thus mitotic progression.

This thesis focuses on the study of two KT and spindle components previously identified in a survey of the human mitotic spindle and it is therefore divided into two parts. The first part describes the functional characterization of a novel KT and spindle localizing protein, human Spindly (hSpindly, previously called CCDC99), which is the human homologue of *Drosophila* Spindly. We show that hSpindly specifically recruits dynein/dynactin to KTs. Localization of hSpindly is in turn controlled by the Rod/ZW10/Zwilch (RZZ) complex and Aurora B kinase. hSpindly depletion results in reduced inter-KT tension, unstable KT-MT fibers (K-fibers), and extensive prometaphase delay and severe chromosome misalignment. Moreover, depletion of hSpindly induces a striking spindle rotation, which can be rescued by co-depletion of dynein. However, in contrast to *Drosophila*, hSpindly depletion does not abolish the removal of MAD2 and ZW10 from KTs. Collectively, our data reveal hSpindly-mediated dynein functions and highlight a critical role of KT dynein in spindly orientation.

In the second part of this thesis, the regulation of the Ska complex (composed of Ska1, Ska2 and Ska3) has been studied. We show that Aurora B activity negatively regulates the localization of the Ska complex to KTs. Furthermore, recruitment of the Ska complex to KTs depends on the KNL-1/Mis12/Ndc80 (KMN) network. In agreement with this, we have identified interactions between members of the KMN and Ska complexes and demonstrate that the interaction between the two complexes is regulated by Aurora B activity. Aurora B can directly phosphorylate Ska1 and Ska3 *in vitro*, and expression of phosphomimetic mutants of Ska1 and Ska3 impairs Ska KT recruitment and formation of stable K-fibers, disrupting mitotic progression. We propose that Aurora B phosphorylation antagonizes the interaction between the

Ska complex and the KMN network, thereby controlling Ska KT recruitment and stabilization of KT-MT attachments.

Together, we conclude that hSpindly and the Ska complex, two important components of KTs in metazoans, are involved in the regulation of chromosome congression by recruiting KT dynein and stabilizing KT-MT attachments, respectively. Both their function and localization are tightly regulated by mitotic kinases and upstream structural components.

Introduction

1. The cell cycle and checkpoints

Cell reproduction is a fundamental process for the development of life. It occurs by a highly regulated and orderly sequence of events, termed the cell cycle. In the mitotic cell cycle, the duplication and the division of the cellular components are tightly controlled to ensure the production of two identical daughter cells. The genetic information of the cell consist of discrete DNA molecules, the chromosomes and it is particularly important for them to be first duplicated with no error and then equally segregated during any cell cycle into the two daughter cells. In unicellular organism, one cell cycle leads to two new organisms. For multicellular organism, numberless cell divisions lead to the diverse populations of cells that make up tissues and organs.

In eukaryotic cells, the stages of cell cycle are defined on the chromosomal events and are divided into four phases. The DNA is replicated once during S (synthesis) phase, resulting in duplicated chromosomes referred as sister chromatids. Later, sister chromatids and other cellular components are segregated equally into two daughter cells during M phase, which is composed of two events: mitosis (segregation of sister chromatids) and cytokinesis (cell division). There are two gap phases between S and M phase, known as G1 and G2. G1 occurs after M phase while G2 occurs after S phase. Both gap phases provide additional time for cell growth and preparation of next cell cycle events. During G1, if the cells is under unfavorable growth conditions (e.g. in the absence of growth factors) or receives inhibitory signals, they may enter a prolonged non-cycling state, called G0 phase (quiescent state). Cells in G0 phase are capable of re-entering the cell cycle if they receive appropriate extracellular signals. Cell cycle phases other than M phase are collectively referred as interphase (Figure 1) (Morgan, 2007).

A key concept of the eukaryotic cell cycle is that S phase must always follow M phase and that M phase must not start until S phase has been completed. The unidirectional nature of the cell cycle is ensured by the oscillation of the activities of different cyclin-dependent kinases (CDKs). Different types of cyclin are produced at different phases and lead to the formation and activation of different cyclin-CDK complexes. In brief, cyclin D-CDK4/6 enables G1 progression; Cyclin E/A-CDK2 initiates DNA replication and centrosome duplication; Cyclin A/B-CDK1 triggers mitotic entry while cyclin B-CDK1 also controls mitotic progression (Figure 1) (Garrett, 2001; Morgan, 2007; Nurse, 2000).

To make sure that cells do not transit to the next cell cycle phase if the previous one has

not finished or there is presence of damage, various checkpoint mechanisms have evolved to monitor the cell cycle events, stopping cell cycle progression at specific points (Garrett, 2001; Hartwell and Weinert, 1989). The checkpoints transmit signals and act directly on the cell cycle machinery (i.e. the cyclin-CDKs) to prevent cell cycle progression. The essential checkpoints include: the G1-S transition checkpoint that senses damaged DNA and prevents activation of the S phase cyclin-CDK; the G2-M transition checkpoint that senses both damaged and unreplicated DNA and prevents activation of the M phase cyclin-CDK; the intra S phase checkpoint that responds to replication stress and inhibits the S-phase cyclin-CDK. Finally, proper attachment of chromosomes to the spindle apparatus is monitored during M phase by the spindle assembly checkpoint to ensure correct segregation of the chromosomes to the daughter cells (this checkpoint will be described later section in more detail).

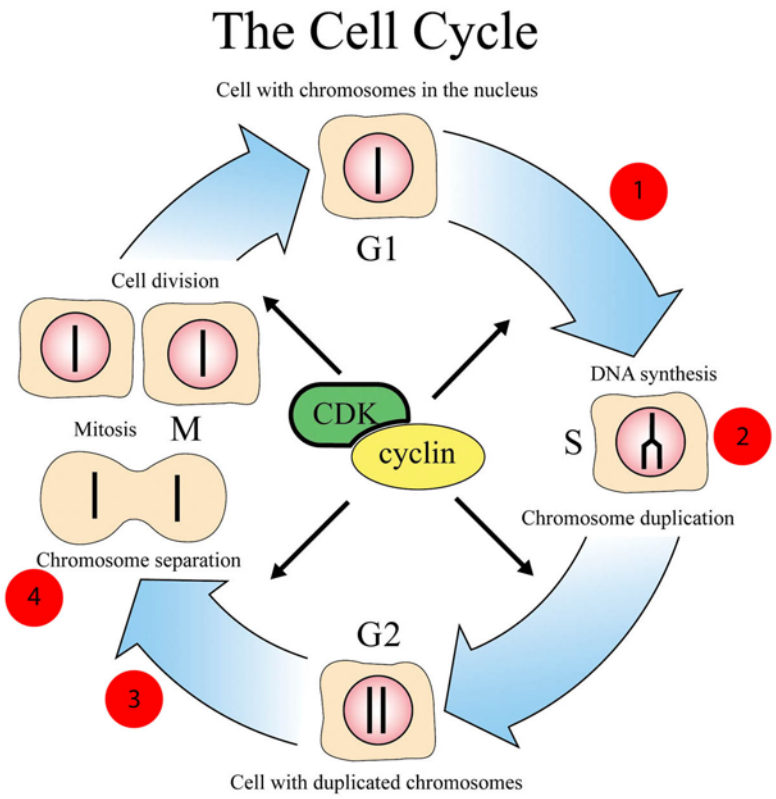

Figure 1. The eukaryotic cell cycle. Cell cycle is divided into four main stages: S phase when DNA replication occurs, M phase when mitosis and cell division occurs, and the two gap phases, G1 and G2. Different cyclin-CDK complexes drive different phases of the cell cycle. The red circles represent the four key checkpoints, 1: G1-S checkpoint, 2: intra S checkpoint, 3: G2-M checkpoint and 4: spindle-assembly checkpoint. *Illustration adapted and modified from "The Nobel Prize in Physiology or Medicine 2001, Press release", nobelprize.org.*

2. An overview of mitosis

In 1882, the German anatomist Walther Flemming was the first one to visualize and describe chromosome behavior during the cell cycle, which was published in his book "Zellsubstanz, Kern und Kerntheilung" and the expressions he coined (e.g. chromatin, equatorial plate) are still in use today. Despites the lack of sufficient knowledge to interpret his results at that time, Flemming's cytological data provided clear information of the key features of mitosis and became foundation of further research (Figure 2) (Paweletz, 2001). Around 100 years later, Leland H. Hartwell, Tim Hunt and Sir Paul M. Nurse received the Nobel Prize in Physiology and Medicine in 2001 for the discovery of key molecular components (i.e. the cyclin-CDKs) and mechanisms behind Flemming's initial observations.

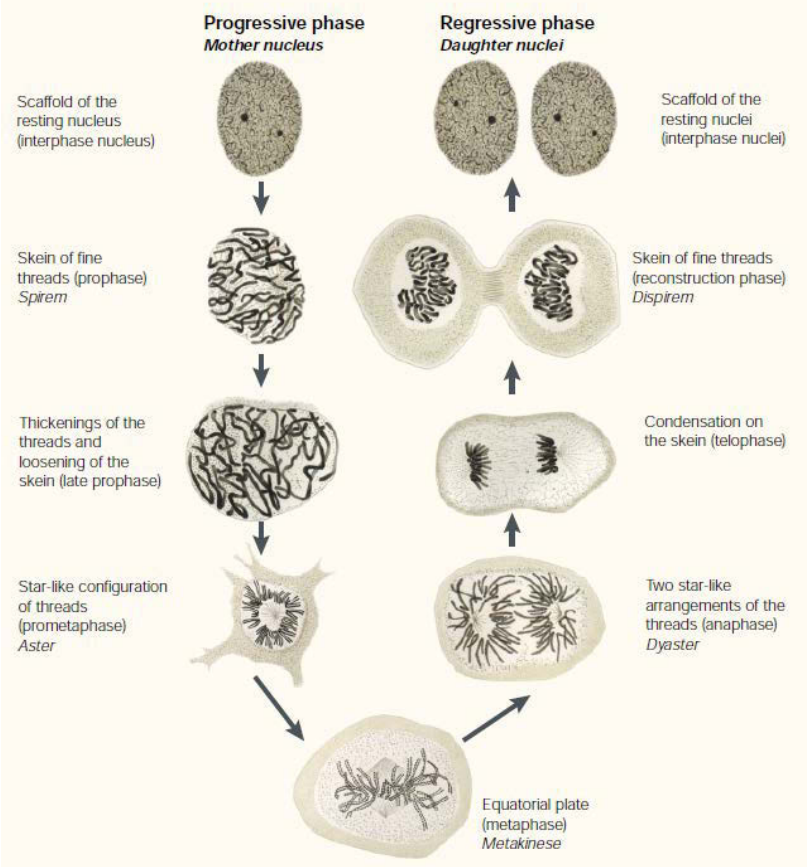

Figure 2. The progression of cell division visualized by Flemming's staining procedure. Key events such as chromosome condensation, bipolar spindle formation, chromosome congression and segregation can be clearly seen. *Illustration adapted from Paweletz N, Nature Reviews Mol Cell Biol, 2001, original images reproduced from Flemming, 1882*

Today, mitosis and cell division have been studied in great detail. Sister chromatids segregate during mitosis, which comprises five morphologically distinct phases. First, in prophase, interphase chromatin condenses to become well-defined chromosomes. The two centrosomes that have been duplicated during S phase start to move to the opposite poles and nucleate highly dynamic MTs. At the onset of the second phase, prometaphase, the nuclear envelope breaks down and the MTs emanating from the separated spindle poles are then able to capture chromosomes at their KTs on both sister chromatids. Each chromatid contains one KT at its centromeric region and each sister chromatids should be attached to MTs emanating from opposite poles in a configuration that is called bi-orientation. After interacting with MTs, chromosomes are then moved to the equator of the cell, a process called congression. Metaphase (the third phase) is a state when all chromosomes have achieved bi-orientation and aligned at the equatorial or metaphase plate. Shortly after metaphase, cohesion between sister chromatids is lost. The sister chromatids are subsequently pulled apart to the opposite side of the cell, this phase is called anaphase. Anaphase is divided into two parts. First, in anaphase A, the chromosome separation is driven mainly by depolymerization of MTs that attach to KTs. In anaphase B, spindle elongation increasing the pole-to-pole distance furthers the poleward movement of the chromosomes. In telophase, the fifth and last phase of mitosis, chromosomes decondense and the nuclear envelope reforms around the chromosomes and other nuclear components (Figure 3) (Nigg, 2001).

Mitosis is followed by cytokinesis (Figure 3). It requires the formation of the contractile ring in the late anaphase, formed by accumulation of actin and myosin II under the plasma membrane in the central region (or called the region of furrow). The contraction of the ring leads to compaction of central spindle into midbody (the process is referred as furrow ingression). Finally abscission takes place, resulting into two separated daughter cells.

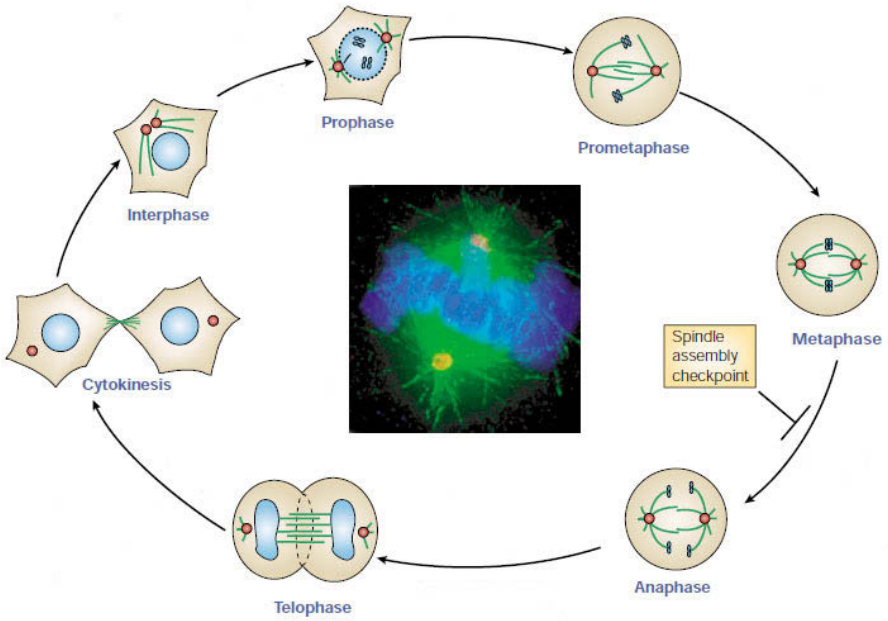

Figure 3. The principal events typical of animal M phase. Prophase, prometaphase, metaphase, anaphase, telophase the final cytokinesis are shown. The spindle assembly checkpoint is operated to prevent anaphase onset until metaphase is properly achieved. *Illustration adapted and modified from Nigg EA, Nature Reviews Mol Cell Biol, 2001*.

3. The mitotic spindle and motor proteins

The central function of mitosis is to separate the sister chromatids into two cells. This process is carried out by a MT-based structure called mitotic spindle. The MTs in the spindle are organized in a bipolar array with the minus-ends embedded in the spindle pole and the plus-ends pointing outward. Three morphologically different populations of MTs are found on the mitotic spindle (Figure 4). MTs interacting with KTs are referred as KT-MTs. KT-MTs bundle together to form a stable KT fiber (K-fiber). Interpolar MTs refer to MTs pointing to spindle poles with their plus-ends overlapping to form the spindle midzone. The third type is the astral MTs, which extend away from the spindle poles and interact with the cell cortex. The astral MTs are important to maintain the spindle orientation and positioning (Gadde and Heald, 2004). The spindle MTs are highly dynamics and undergo continuous growth and shrinkage during mitosis. To maintain the bipolar configuration and to provide suitable force for chromosome movement, the behavior of the mitotic spindle is regulated by various motor proteins and MT-associated proteins (MAPs).

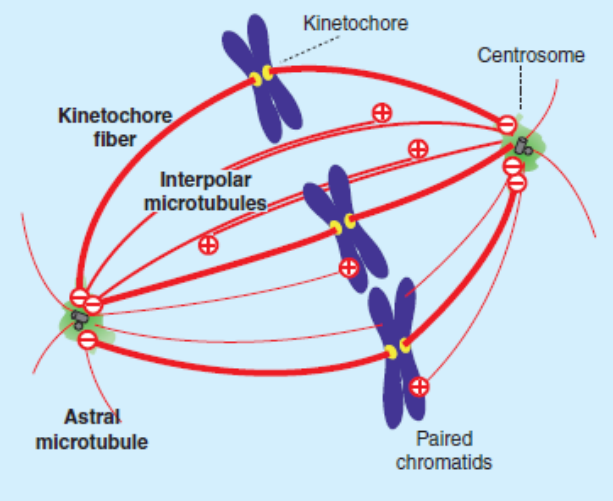

Figure 4. Three types of spindle MTs. K-fibers: bundled MTs connecting spindle pole and KT. Interpolar MTs: MTs forming an overlapping antiparallel array in the central spindle. Astral MTs: MTs extending away from the spindle, contacting the cell cortex. *Illustration adapted from Gadde and Heald, Curr Biol, 2004*

3.1 Centrosome-dependent "capture and search" model

In most vertebrate cells, the formation of the mitotic spindle is mainly driven by the centrosomes, which serves as MT-organizing center (MTOC). The centrosome contains two interconnected centrioles. Each centriole consists of a short array of MT triplets arranged in a nine-fold symmetry and is surrounded by the pericentriolar material (PCM). Key component of the PCM is the γ-tubulin ring complex (γTuRC), which contains a special version of tubulin called γ-tubulin. γ-tubulin forms a circular array, providing a cap for the minus-end and allowing the nucleation of MTs (Moritz et al., 2000).

After nuclear envelope breakdown, the highly dynamic MTs radiated from the centrosomes explore the cytoplasm until they are captured by KTs. KT-bound MTs are then selectively stabilized, leading to the formation of the K-fibers (Figure 5A). This mechanism is referred as to "search-and-capture model" (Hayden et al., 1990; Kirschner and Mitchison, 1986; Rieder and Alexander, 1990). This model predicts that chromosomes play a passive role in the assembly of the spindle and they are only randomly captured by MTs that are continuously growing and shrinking. Although the "search-and-capture" model rapidly gained acceptance, its stochastic nature cannot explain the observed high kinetics of K-fiber formation in animal cells, and much longer time is required to align all the chromosomes if human cells only employ this mechanism (Rieder, 2005; Wollman et al., 2005). Although a centrosome-independent mechanism has been shown to be involved in the assembly of the mitotic spindle (see below), the centrosome-mediated pathway offers several advantages. First, the astral MTs from the

centrosomes can search the cytoplasm and integrate the centrosome-independent spindle components, facilitating the whole spindle assembly process. Second, the astral MTs interacting with the cell cortex ensure correct positioning and orientation of the spindle. Finally, centrosomes may increase the fidelity of chromosome segregation by ensuring bipolar spindle formation (Nigg, 2002; Pearson and Bloom, 2004; Wadsworth and Khodjakov, 2004).

3.2 Chromosome-induced spindle assembly

A centrosome-independent mechanism to drive spindle assembly exists in cells containing no centrosomes, including plant cells and many of the animal oocytes for instance. Our understanding of this mechanism came mainly from studies using *Xenopus* oocyte extracts to analyze spindle assembly. In these extract, MTs can be nucleated around the vicinity of chromosomes and finally self-assemble to from bipolar spindles and drive chromosome congression without centrosomes (Figure 5B). Later, the small GTPase Ran has been shown to be the key factor regulating the chromosome-induced self-assembly of the mitotic spindle. It has two forms: the inactive GDP-bound form (RanGDP) and the active GTP-bound form (RanGTP), able to stimulate spindle formation. Chromosomes contain RCC1, a GTP exchange factor (GEF) for Ran, which binds directly to Ran and induces the rapid formation of RanGTP around the chromosomes. In the cytoplasm, the GTPase of Ran (RanGAP) catalyzes the formation of RanGDP. Therefore, a gradient of RanGTP is generated (with higher concentration around the chromosomes than in the cytoplasm), favoring the assembly of the spindle in the vicinity of chromosomes (Carazo-Salas et al., 2001; Heald et al., 1997; Rieder, 2005). Cytoplamic dynein, a minus-end directed motor, then focuses the minus-ends of the spindle MTs and allows spindle pole formation even in the absence of centrosomes (Heald et al., 1997; Wadsworth and Khodjakov, 2004).

Despite being essential in acentrosomal cells, it was not clear whether the RanGTP guided self-assembly pathway is also employed by cells containing centrosomes. The existence of this mechanism in cells containing centrosomes was confirmed by the fact that vertebrate cells can still form the mitotic spindle when their centrosomes were removed either by microsurgery or laser-ablation (Hinchcliffe et al., 2001; Khodjakov et al., 2000). Importantly, capture of chromosome-mediated K-fibers by the astral MT followed by the transport towards the centrosomes has been observed by live cell imaging (Khodjakov et al., 2003; Maiato et al., 2004).

These results strongly support the idea that both mechanisms cooperate to form the bipolar spindle in cells containing centrosomes (Figure 5C) (Gadde and Heald, 2004; Rieder, 2005).

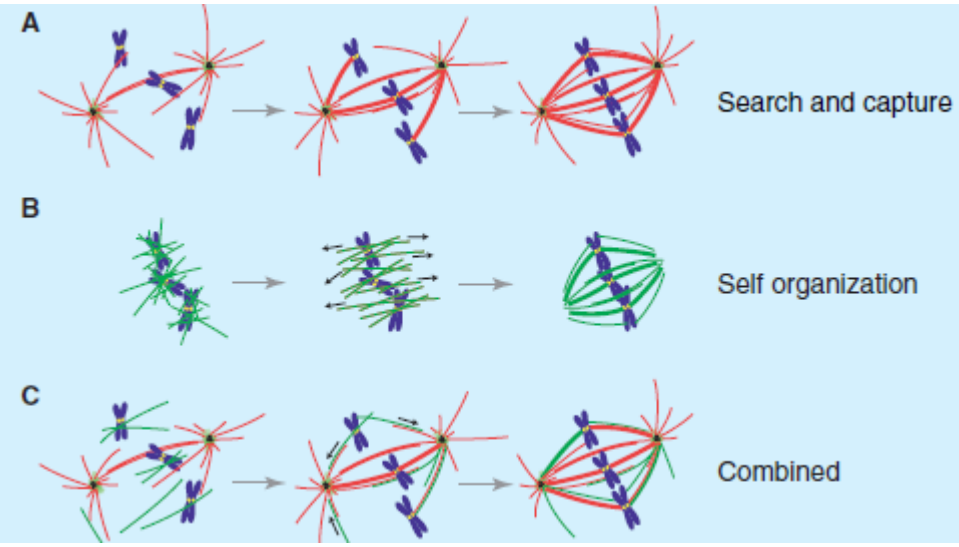

Figure 5. Spindle assembly models. (A) The centrosome-mediated "search-and-capture" model. **(B)** The RanGTP-regulated self-assembly model. **(C)** Combined model: MTs emanating from chromosomes are captured and incorporated in to the centrosomal MT array. *Illustration adapted from Gadde and Heald, Curr Biol, 2004*

3.3 Regulation of spindle assembly and chromosome movement by MT motors

Proper spindle assembly requires various MT motors which transport their cargo unidirectionally along MTs. They provide the essential forces for bipolar spindle formation and chromosome motion. MT motors generally consist of a catalytic domain to hydrolyze ATP (ATPase), a dimerization domain and domains that bind MT and other proteins. There are two classes of MT motors: (1) the kinesins that move towards the MT plus-ends (with the exception of the kinesin-14 family) (Gatlin and Bloom, 2010; Wittmann et al., 2001). (2) The cytoplasmic dynein (a minus-end-directed motor) together with its activator dynactin (referred as the dynein/dynactin complex) that moves towards the minus-ends of MTs (Kardon and Vale, 2009).

There are several essential kinesins involved in spindle assembly and chromosome movement. The kinesin-5/BimC family (Eg5 in human) crosslinks anti-parallel MTs with their overlapped plus-ends and induces spindle poles separation for establishing bipolarity. (Figure 6) (Gadde and Heald, 2004; Gatlin and Bloom, 2010). The kinesin-14 family (HSET in human), a minus-end-directed kinesin, is required for focusing the minus-ends at the spindle poles (Figure 6) (Mountain et al., 1999; Sharp et al., 2000). The kinesin-10 family (chromokinesin Kid in human)

localizes both on chromosome and spindle and generates polar ejection force to push the chromosome arms towards the equator (Figure 6) (Levesque and Compton, 2001). CENP-E, a plus-end directed motor, localizes at KTs during prometaphase and transports mono-oriented chromosomes to the equator (Kapoor et al., 2006). The Kif18a, a plus-end directed motor belonging to the kinesin-8 family, localizes to the plus-ends of the KT-MTs and promotes proper chromosome congression by depolymerizing KT-MTs (Mayr et al., 2007; Stumpff et al., 2008).

Cytoplasmic dynein accounts for most of the minus-end directed transport within cytoplasm and it is a giant multi-subunits-complex. The heavy chain subunit of dynein contains a catalytic ATPase domain and a MT binding domain in its C terminus. The N-terminus of the heavy chain is involved in dimerization and also mediates interactions with five non-catalytic subunits (dynein intermediate chain (IC), light intermediate chain (LIC), light chain 7 and 8 (LC7 and LC8), and TCTEX1). The non-catalytic subunits are important for mediating interactions with other proteins. The most important dynein-interacting partner is dynactin (binding to IC) which is an activator of dynein, involved in nearly all dynein functions. Dynactin increases the processivity of dynein and targets it to specific locations (Kardon and Vale, 2009). During mitosis, the dynein/dynactin complex is recruited to different cellular locations and is involved in various mitotic functions. Together with NuMA, the dynein/dynactin complex localizes to spindle MTs, crosslinking MTs and inducing spindle pole focusing (Figure 6) (Gaglio et al., 1996; Sharp et al., 2000; Wittmann et al., 2001). The dynein/dynactin complex is also highly concentrated at KTs during early mitosis, mediating the initial interaction with spindle MTs and powering the poleward movement of the chromosomes (King et al., 2000; Rieder and Alexander, 1990; Vorozhko et al., 2008). KT dynein has also been proposed to be involved in silencing the spindle-assembly checkpoint by removing checkpoint proteins from KTs (see later section). Finally, the dynein/dynactin complex also localizes to the cortex, this promotes positioning and orientation of the spindle (Figure 6) (Pearson and Bloom, 2004).

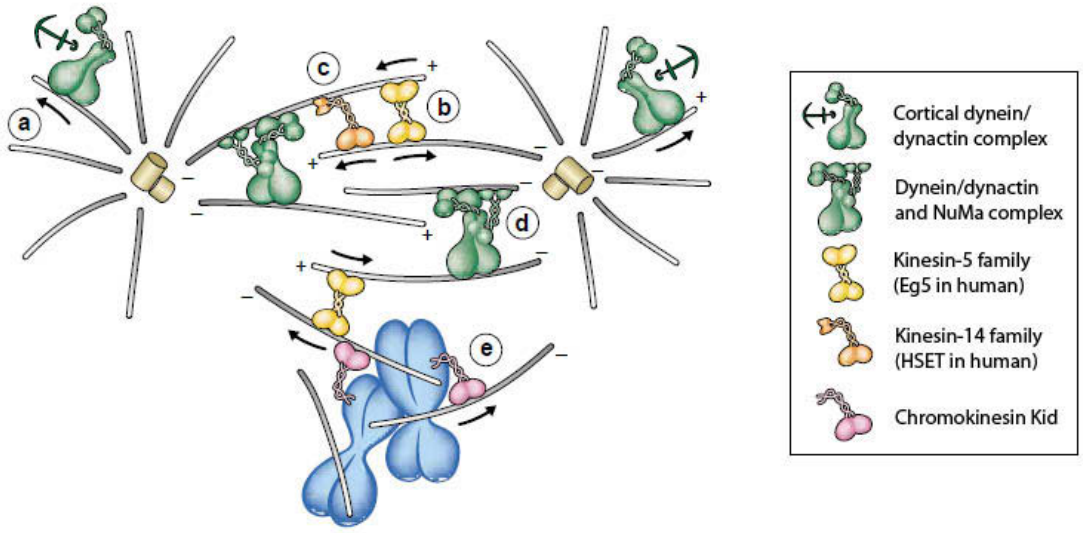

Figure 6. Microtubule-associated motors in spindle assembly. (a)The cortical dynein/dynactin promotes spindle positioning. (b and d) The spindle associated dynein/dynactin/NuMA complex and HSET involve in spindle pole focusing. (c) Eg5 separates two spindle poles. (e) Kid powers the polar ejection force. *Illustration adapted and modified from Wittmann et al., Nature Cell Biol, 2001*

4. Assembly and functions of the centromere/KT region

The KT is a specialized proteinaceous structure that plays multiple essential roles in mitosis. KTs are built on chromosomes at a specialized locus known as centromere (see below) (Santaguida and Musacchio, 2009; Torras-Llort et al., 2009). Electron microscopy experiments distinguished a trilaminar morphology (Figure 7): The inner KT contacts with the centromere, the outer KT contacts spindle MTs. A central region lies between the inner and outer KT. When MTs are depolymerized, there is a dense array of fibers extended away from the outer KT. This layer is referred as fibrous corona (Cheeseman and Desai, 2008; Cleveland et al., 2003).

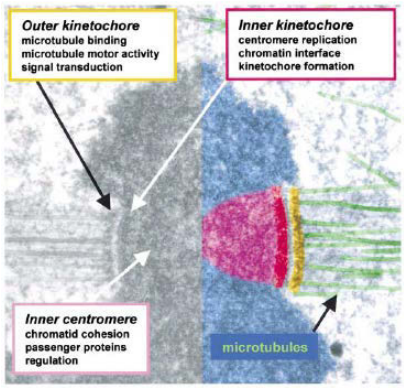

Figure 7. Organization of the vertebrate centromere/KT. The left side shows the trilaminar organization of the KT seen by electron microscopy. The right side shows the key elements with pseudo colors, pink for centromere, red for inner KT, yellow for outer KT and green for KT-MTs. *Illustration adapted from Cleveland et al., Cell, 2003*

In the vertebrate centromere/KT, there are more than 100 proteins identified that control the fidelity of mitosis in different aspects (Figure 8). These include the specialization of the centromere (by proper loading of CENP-A, see below section 4.1), the proper assembly of the KT through multiple protein-protein interactions (e.g., the assembly of the CCAN complex, see below section 4.2), the direct interaction between MTs and KTs (mediated by many outer KT proteins; prominent among these are the KMN network and Ska complex, see section 5 and Results) and various control mechanisms which monitor MT attachments (such as the Aurora B-mediated error correction and the spindle-assembly checkpoint, see section 6 and Results).

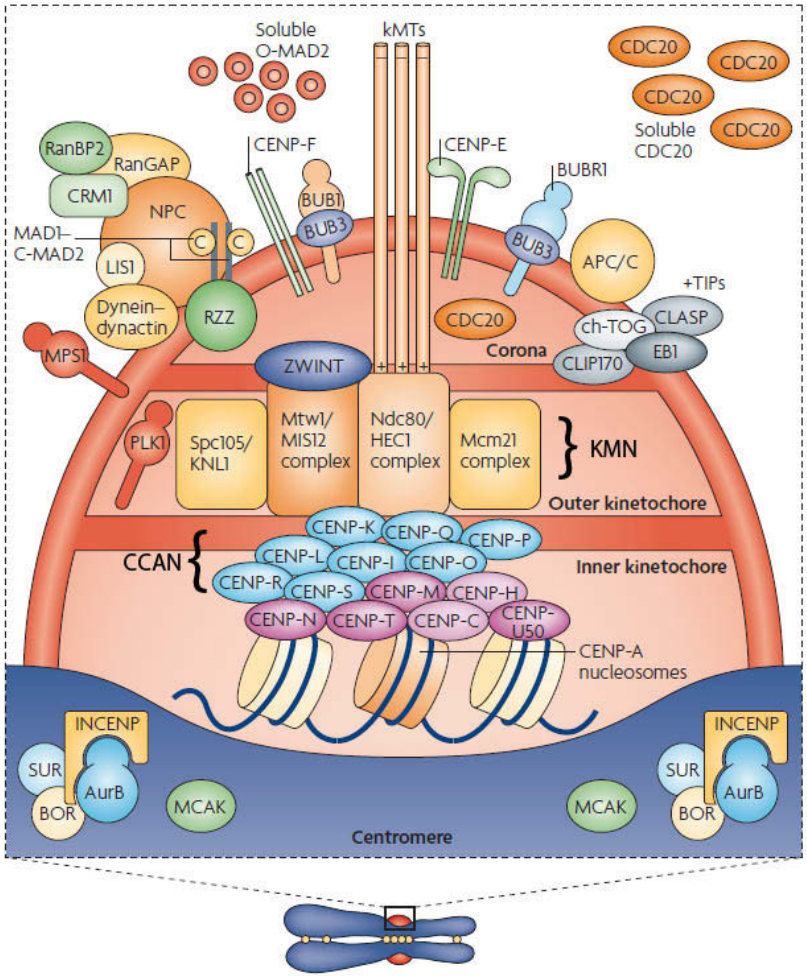

Figure 8. The vertebrate centromere/KT region. Schematic illustration of the spatial distribution of centromere and KT associated proteins. The CENP-A containing nucleosomes specify the centromere and direct the assembly of the KT, which depends on various protein-protein interactions. The CCAN complex, which is immediately associated with CENP-A, recruits the KMN network during mitosis. Other important regulatory proteins, including Aurora B and the spindle assembly-checkpoint proteins are involved in monitoring KT-MT attachments. *Illustration adapted and modified from Musacchio and Salmon, Nature Review Mol Cell Biol, 2007*

4.1 The control of centromere specification and propagation

All eukaryotic centromeres are specialized by the presence of the centromeric-specific variant of histone H3, called CENP-A (also called CenH3). The centromere comprising only one CENP-A containing nucleosome is referred as point centromere (e.g., in budding yeast), while the one containing multiple CENP-A nucleosomes is referred as regional centromere (e.g., in fission yeast and human). The point centromere forms a single MT attachment site per chromosome while regional centromeres form multiple attachment sites per chromosome (Torras-Llort et al., 2009; Verdaasdonk and Bloom, 2011). In human, centromere consists of a highly ordered array of repetitive DNA sequences, known as α-1 satellite DNA repeats. However, the DNA sequence is neither necessary nor sufficient to support centromere identity. Instead, centromere identity is specified epigenetically by the incorporation of CENP-A and histone modifications (Earnshaw and Migeon, 1985; Gieni et al., 2008; Verdaasdonk and Bloom, 2011). The canonical histone H3 within the centromere is methylated at Lys4, a modification associated with euchromatin (Figure 9). This modification is shown to be important for CENP-A incorporation. Centromere is also flanked by the highly condensed heterochromatic regions in which their histone H3 and H4 are methylated at Lys9 and Lys20 (H3K9me, H4K9me and H4K20me).

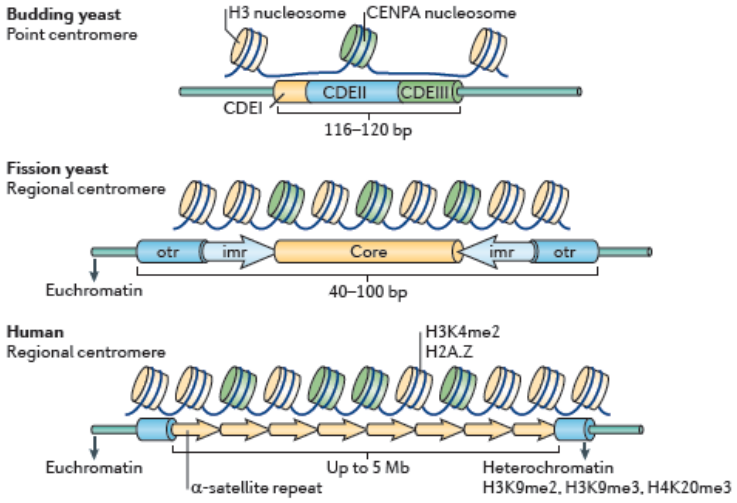

Figure 9. Basic characteristics of point and regional centromeres. Point centromere contains a single CENP-A nucleosome while regional centromere contains multiple CENP-A nucleosomes. In human, both the centromeric and pericentromeric histones are modified. *Illustration adapted from Verdaasdonk and Bloon, Nature Reviews Mol Cell Biol, 2011*

Therefore, the loading of CENP-A onto chromatin during cell cycle is critical for centromere identity. In every round of the cell cycle, the level of CENP-A becomes halved on each sister chromatid after DNA replication and new CENP-A molecules need to be loaded to

maintain centromere identity. Incorporation of new CENP-A into centromeres occurs during late telophase and early G1. (Figure 10) (Hemmerich et al., 2008; Jansen et al., 2007; Torras-Llort et al., 2009). The Mis16/18 complex is crucial for CENP-A incorporation onto chromatin (Fujita et al., 2007). This complex is recruited to the centromere during anaphase and released from the chromatin in G1 (Figure 10). (Verdaasdonk and Bloom, 2011). Loading of CENP-A is also regulated by proteolytic degradation of CENP-A. When bound to non-centromeric DNA, CENP-A becomes unstable while centromeric CENP-A shows extremely low turnover (Conde e Silva et al., 2007; Hemmerich et al., 2008; Moreno-Moreno et al., 2006).

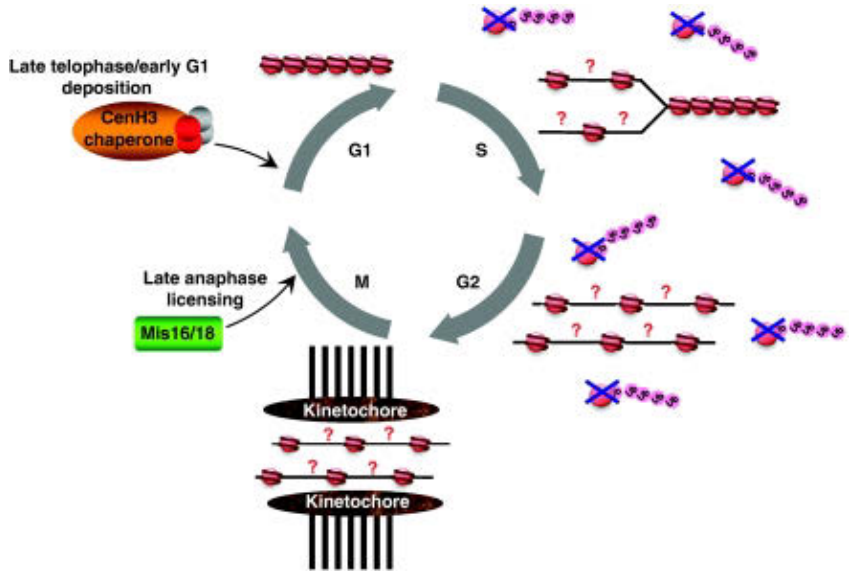

Figure 10. Loading of CENP-A during cell cycle. CENP-A is loaded onto chromatin only in late mitosis and early G1. The Mis16/18 complex is an important licensing factor for loading of CENP-A. Non-centromeric CENP-A is prone to degradation. *Illustration adapted from Torras-Llort et al., EMBO J, 2011*

4.2 Assembly of the inner KT: The CCAN complex

KT assembly at centromere involves complex pathways of hierarchical protein-protein interaction (Torras-Llort et al., 2009). Purification of human CENP-A nucleosomes and has led to the identification of a group of proteins that is directly associated with the centromere. This class of centromeric proteins (CENPs) is referred as CENP-A NAC (CENP-A-nucleosome associated complex, including CENP-C/H//I/M/N/T/U). Another class of CENPs, called CENP-A CAD (CENP-A-nucleosome distal components, including CENP-O/P/R/Q/S/U/K), was further identified by purification of the CENP-A NAC (Foltz et al., 2006) (Figure 11). CENP-C is another CENP that binds directly to DNA. Its localization is dependent on CENP-A and *vice-versa*. CENP-C directly binds to both CENP-$A^{NAC/CAD}$ and the KMN network (see below), serving as a link between centromeric proteins and KT components (Carroll et al., 2010;

Przewloka et al., 2011; Screpanti et al., 2011; Verdaasdonk and Bloom, 2011). As CENPs are constitutively associated with the centromere, thus the CENP-C and CENP-A$^{NAC/CAD}$ are collectively referred as CCAN (constitutive centromere-associated network) (Figure 11) (Cheeseman and Desai, 2008). The CCAN is the upstream structural platform for KT assembly and it is itself recruited by CENP-A. The CCAN can be divided into several sub-complexes. The CENP-T/W complex directly interacts with DNA at centromeric region containing canonical histone H3 and recruits CENP-H/I/K complex. The CENP-H/I/K complex in turn recruits CENP-P/O/Q/U complex. The CENP-L/M/N/S also interacts with CENP-H/I/K and their localizations are dependent on each other (Figure 11) (Foltz et al., 2006; Hori et al., 2008a; Hori et al., 2008b; Okada et al., 2006). Except being a structural scaffold for KT assembly, the CCAN may also be directly involved in some KT functions. For example, CENP-O has been suggested to be involved in bipolar spindle formation. CENP-H has been shown to control KT-MTs plus-ends turnover and CENP-Q can bind MT directly *in vitro* (Amaro et al., 2010; McClelland et al., 2007; Toso et al., 2009).

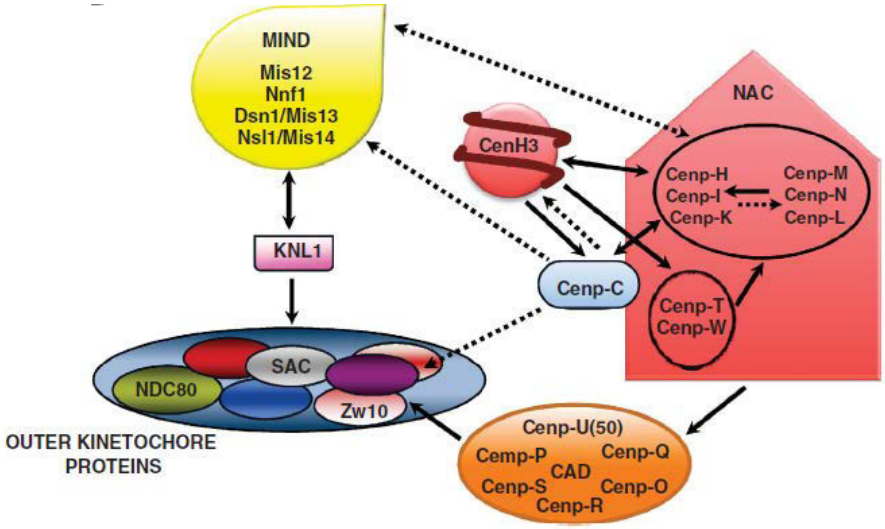

Figure 11. The KT assembly directed by CENP-A nucleosome and the CCAN. CENP-A is at the bottom of the hierarchy, it recruits the CCAN, which in turn leads to the assembly of the KT by recruiting the KMN network and other KT proteins. *Illustration adapted from Torras-Llort et al., EMBO J, 2011*

5. The KMN network and MT attachment

One of the key functions of KTs is to form an attachment interface between chromosome and MT. As spindle MTs explore space randomly and dynamically, KTs may initially interact spindle MTs laterally. The lateral attachments are subsequently converted into end-on attachment,

in which MT plus-ends embedded in KTs. The ability to stabilize and bundle MTs, forming K-fibers is one of the crucial properties of KTs (see above). The other remarkable feature of KTs is that they can generate load-bearing attachments (i.e. The KT is able to maintain end-on attachment by continuous polymerizing and depolymerizing MTs) (Santaguida and Musacchio, 2009; Tanaka and Desai, 2008). The conserved KMN network, composed of KNL-1 protein, the Mis12 complex and the Ndc80 complex, has emerged as a core attachment site for the generation of load-bearing attachments. Inhibition of any of the KMN members, by RNAi-mediated depletion or antibodies microinjection, results in severe attachment defects, which are referred as KT-null phenotype (Cheeseman et al., 2004; DeLuca et al., 2005; Desai et al., 2003; Kiyomitsu et al., 2007; Kline et al., 2006; Vorozhko et al., 2008).

The Ndc80 complex is composed of four subunits, namely Hec1, Nuf2, Spc24 and Spc25. The four proteins form a ~170 kDa stable complex with a ~55 nm rod-like structure, vertically crossing the inner and outer KT plate with two globular domains in each end separated by a long coiled-coil region (Figure 12) (Ciferri et al., 2005; Ciferri et al., 2008; Wei et al., 2005). The globular domain at the outer KT region is formed by the N-terminal parts of Hec1-Nuf2 sub-complex, while the one facing the inner KT region is formed by the C-terminal parts of Spc24-Spc25 sub-complex. The Spc24-Spc25 dimer binds to the Mis12 complex, linking the Ndc80 complex to the inner KT (Joglekar et al., 2009; Kiyomitsu et al., 2007; Wan et al., 2009). On the other hand, the Hec1-Nuf2 dimer, which contains two calponin-homology (CH) domains in each protein, binds directly to MTs *in vitro* (Ciferri et al., 2008). More significantly, when microbeads are coated with Ndc80 complexes, they are able to track both polymerizing and depolymerizing MTs. This result suggests that the Ndc80 can serve as a microtubule coupler to form the load-bearing MT attachments at KTs. (McIntosh et al., 2008; Powers et al., 2009).

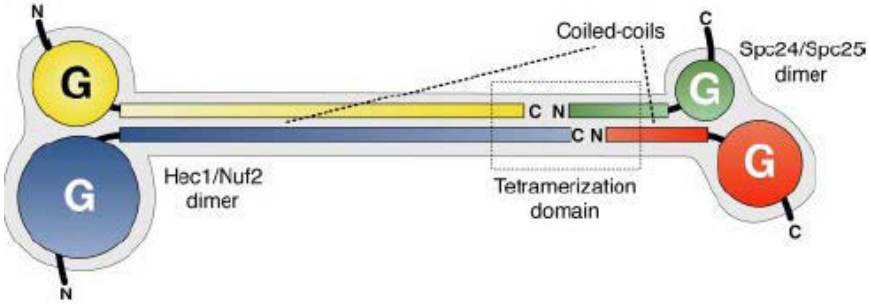

Figure 12. Topology of the Ndc80 complex. Hec1-Nuf2 dimer contains two CH domains at its N-terminus followed by the coiled-coil region that mediates tetramerization with the Spc24-Spc25 dimer. The Spc24-Spc25 dimer has a coiled-coil domain at N-terminal and globular domain at C-terminus which is responsible for binding to the inner KT via the Mis12 complex (see below). *Illustration adapted from Ciferri et al., Journal of Biological Chemistry, 2005*

KNL-1 is a large protein (~300 kDa), which has also been shown to directly interact with MTs weakly *in vitro*, although the region responsible for MT binding is unknown (Cheeseman et al., 2006). KNL-1 also directly interacts with multiple KT proteins. Its N-terminal region directly interacts with checkpoint proteins Bub1 and BubR1 while the C-terminal region interacts with the Mis12 complex and Zwint-1(Kiyomitsu et al., 2007; Petrovic et al., 2010).

The Mis12 complex (~110 kDa) is composed of four subunits, namely Mis12, Mis13, Mis14 and Nnf1. Although the Mis12 complex itself does not bind to MTs, it serves as a scaffold for forming the entire KMN network with Mis13 and Mis14 interacting directly with KNL-1 and Spc24-Spc25 dimer, respectively (Cheeseman et al., 2006; Petrovic et al., 2010). The Mis12 complex also binds directly to the centromeric proteins, CENP-C and HP1, providing a direct linkage between KT components and the centromere (Kiyomitsu et al., 2010; Przewloka et al., 2011; Screpanti et al., 2011). The formation of the whole KMN network synergistically increases the MT binding affinity of the Ndc80 complex and KNL-1. The KNM network also displays a concentration-dependent increase of binding affinity, suggesting the multiple MT binding sites in the complex display cooperative binding (Figure 13) (Cheeseman et al., 2006). Electron microscopy-based tomographic reconstruction of KT in PtK1 cells reveals the presence of fibrils linking KT to the protofilaments of depolymerizing MT. As the eukaryotic KT contains multiple copies of the KMN network per MT binding site (Joglekar et al., 2008; Joglekar et al., 2006), the KMN could be the major component of such fibrils, acting as a MT coupler at KT (Joglekar and DeLuca, 2009; McIntosh et al., 2008; Powers et al., 2009).

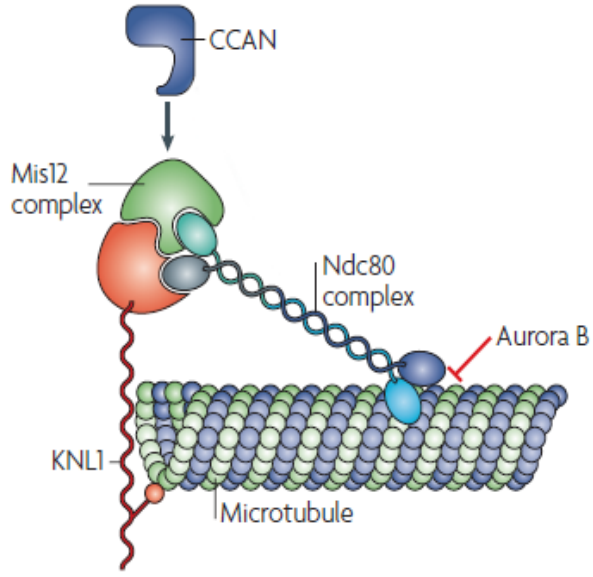

Figure 13. The core KT-MT attachment site formed by the KMN network. The components of the KMN network are conserved throughout the eukaryotic kingdom. Both KNL-1 and Ndc80 interact directly with MTs while Mis12 provides the binding to inner KT/centromere components. Aurora B kinase acts to inhibit the binding between KMN and MTs (see later) *Illustration adapted and modified from Cheeseman and Desai, Nature Reviews Mol Cell Biol, 2008*

6. Aurora B and its role on error correction

Aurora B kinase is an essential mitotic regulator controlling multiple functions and stages of mitosis. The functions of Aurora B include chromatin modification, assembly of the centromere/KT region, spindle formation, spindle assembly checkpoint signaling, correction of improper KT-MT attachment and completion of cytokinesis (Ruchaud et al., 2007). The Aurora B kinase forms a tight complex with three non-enzymatic subunits, namely INCENP (the inner centromere protein), the BIR domain-containing protein survivin and Borealin (also called Dasra B). The whole complex is referred as the CPC (the chromosomal passenger complex). Activation of Aurora B requires the interaction with INCENP, followed by the autophosphorylation of the T-loop on Aurora B and phosphorylation of the TSS-motif on INCENP (Bishop and Schumacher, 2002; Honda et al., 2003; Yasui et al., 2004). Mps1-mediated phosphorylation of Borealin has also been shown to modulate Aurora B kinase activity (Jelluma et al., 2008). Survivin is important for targeting the CPC to centromeres (Lens et al., 2006). During early mitosis (i.e. from prophase to metaphase) the CPC is concentrated at the inner centromere, the region located between the two sister-KTs. Later, in anaphase and telophase, the CPC relocalizes from the centromere to the central spindle and midbody.

One of the key functions of Aurora B is to mediate correction of erroneous MT attachments at KT by destabilizing them and generating unattached KT (Nezi and Musacchio, 2009; Ruchaud et al., 2007). As biorientation (i.e. when sister KTs acquire amphitelic attachments) is the requirement for correct segregation of sister chromatids, syntelic and merotelic attachments need to be corrected before cells entering anaphase (Figure 14).

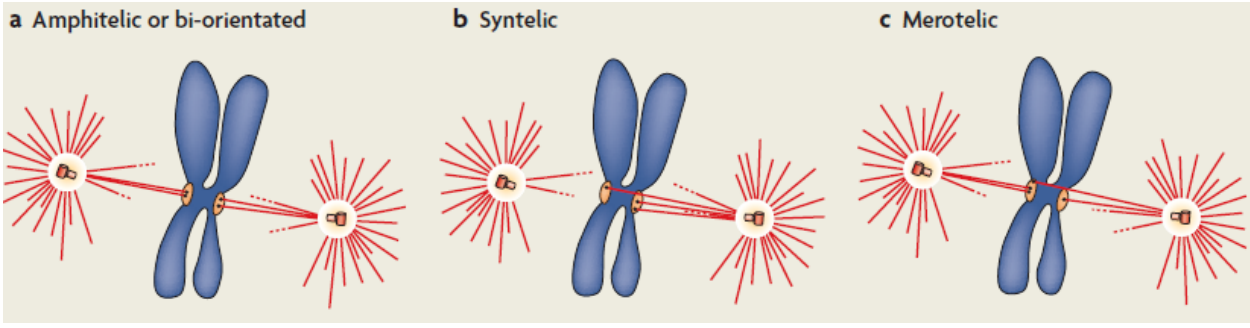

Figure 14. Different types of KT-MT attachments. Amphitelic attachment: each sister KT binds MTs from opposite poles. Syntelic attachment: both sister KTs bind to the same pole. Merotelic attachment: One of the sister KTs binds to both opposite poles. *Illustration adapted from Ruchaud et. al., Nature Reviews Mol Cell Biol, 2007*

The requirement of Aurora B in error correction was first demonstrated in budding yeast. The budding yeast homolog of Aurora B, Ipl1, was shown to be required for resolving syntelic attachments (Tanaka et al., 2002). When budding yeast cells cannot replicate their DNA but remain able to duplicate their spindle poles, KTs continuously detach from both spindle poles in Ipl1-positive cells. However, in the case of Ipl1-deficient cells, KTs remain attached to the old pole. This experiment strongly suggested that Aurora B is required to promote the turnover of KT-MTs in response to lack of tension (Tanaka et al., 2002). Similarly, the requirement of the Aurora B kinase activity for correcting wrong attachments has also been observed in mammalian cells. Syntelic and merotelic attachments are frequently observed in cells with compromised Aurora B activity (Cimini et al., 2006; Ditchfield et al., 2003b; Hauf et al., 2003). When monopolar spindles are induced in cells using the Eg5 inhibitor monastrol (Kapoor et al., 2000; Mayer et al., 1999), most of the syntelic attactments generated under this condition cannot be corrected after monastrol wash-out, if Aurora B activity is inhibited (Figure 15) (Lampson et al., 2004).

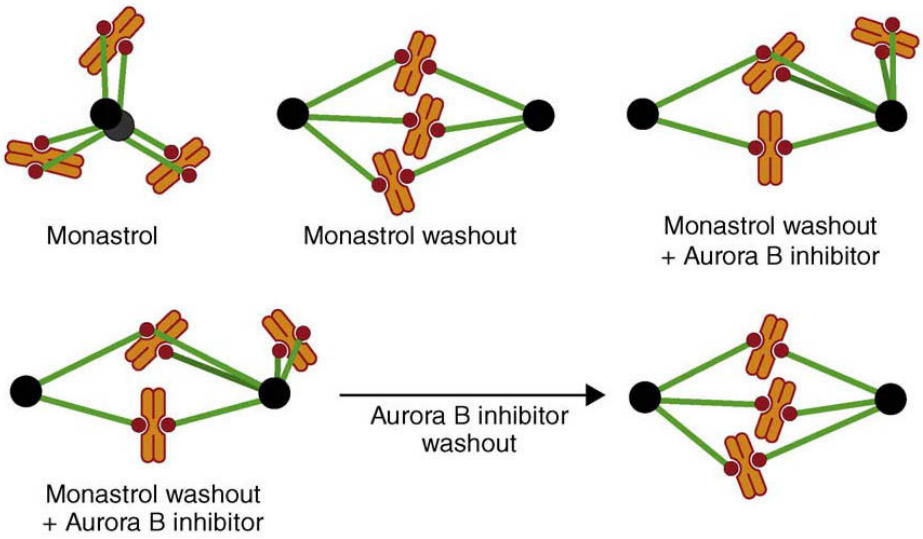

Figure 15. Correction of syntelic attachments by Aurora B. Monastrol induces monopolar spindle, when the drug is washed-out, biorientation of most of the chromosomes can be achieved. However, inhibition of Aurora B prevents the correction of syntelic attachment. *Illustration adapted from Nezi and Musacchio, Curr Opin in Cell Biology, 2009*

Several components of the KMN network, namely Hec1, Mis13 and KNL-1 have been shown to be phosphorylated by Aurora B, leading to the reduction of the MT binding affinity (Biggins et al., 1999; Cheeseman et al., 2006; Ciferri et al., 2008; DeLuca et al., 2006; DeLuca et al., 2011b; Guimaraes et al., 2008; Welburn et al., 2009). Other molecular targets of Aurora B

include MCAK and CENP-E. MCAK is a MT-depolymerizing enzyme, which promotes KT-MT turnover. Phosphorylation of MCAK by Aurora B regulates both its centromeric localization and depolymerizing activity (Andrews et al., 2004b; Lan et al., 2004b). CENP-E is proposed to be involved in the initial capture of MTs at KTs and partly contributes to inappropriate MT attachments. Phosphorylation of CENP-E by Aurora B reduces MT affinity of CENP-E, facilitating biorientation of chromosomes (Kim et al., 2010). As Aurora B is active throughout mitosis, this raises the question of how Aurora B is able to sense lack of tension (which in turn indicates erroneous attachment) and mediates MT detachment. A study using a well characterized Aurora B activity FRET (Fuller et al., 2008) sensor has shown that substrate phosphorylation by Aurora B depends on the physical distance between Aurora B (at inner centromere) and its substrates (at KT) (Liu et al., 2009). When sister chromatids are under tension (i.e. biorientation), the distance between the substrates and the inner centromere increases, thus Aurora B cannot phosphorylate its substrates efficiently, leading to stabilization of attachment. When improper attachments occur, the reduced spatial separation between Aurora B and its substrates allows efficient phosphorylation and subsequent destabilization (Figure 16).

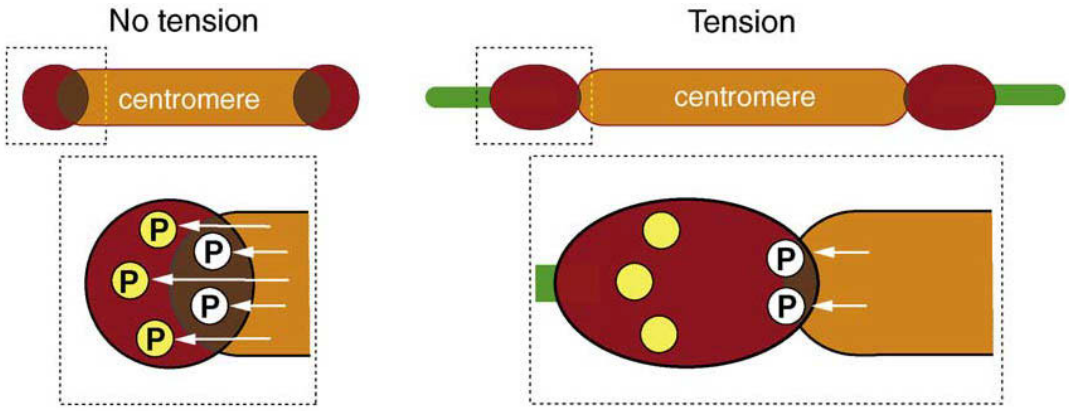

Figure 16. Tension across sister KTs controls Aurora B-mediated phosphorylation. When there is no tension, Aurora B phosphorylates its KT substrates. Once tension is build up, the increased centromere-KT distance leads to dephosphorylation of KT substrates. *Illustration adapted from Nezi and Musacchio, Curr Opin in Cell Biology, 2009*

7. The spindle assembly checkpoint

The Spindle assembly checkpoint (SAC) is a surveillance mechanism evolved in eukaryotes to ensure proper segregation of chromosome during mitosis. It prevents the onset of

anaphase until all chromosomes are properly attached to the spindle MTs. The essential SAC components were identified in yeast genetic screens looking for genes that when mutated, bypassed the ability for the cells to arrest in mitosis in response to spindle poisons (Hoyt et al., 1991; Li and Murray, 1991). Two classes of gene were identified in these screens: *MAD* (mitotic arrest deficient) and *BUB* (budding uninhibited by benimidazole) genes. *MAD* genes include Mad1, Mad2 and Mad3 (BubR1 in human) while *BUB* genes include Bub1 and Bub3. They are all evolutionarily conserved in eukaryotes and involved in the activation of the SAC. In addition to the MAD and BUB proteins, a mitotic kinase Mps1 (originally called TTK) and the Rod/Zw10/Zwilch (RZZ) complex are also involved in the checkpoint signaling and are considered also key SAC components (Abrieu et al., 2001; Karess, 2005; Kops et al., 2005; Stucke et al., 2002; Weiss and Winey, 1996).

As all SAC proteins localize to KTs during prometaphase, it would be plausible that the SAC monitors KT-MT interactions. Various evidences, including the behavior of checkpoint proteins at KTs, support this idea. For example, Mad2 is highly enriched at unattached KTs and the attachment to MTs leads to the loss of Mad2 from KTs, suggesting that SAC could monitor MT attachments (Howell et al., 2001; Waters et al., 1998). Importantly, a single unattached KT is sufficient to activate the SAC and delay anaphase. Cells can enter anaphase shortly after a single unattached KT is destroyed by laser ablation (Rieder et al., 1995). Also the checkpoint proteins Mad2, BubR1 and Bub3 are highly dynamics at KTs (Howell et al., 2004). Altogether, these results indicate that KTs serve as a catalytic platform to generate the SAC activation signal. Although, the lack of MT attachments is clearly the defect sensed by the SAC machinery, the amount of tension generated across sister KTs has also been proposed to be monitored by the checkpoint (Pinsky and Biggins, 2005; Zhou et al., 2002). This idea was first suggested by the study in meiosis I of grasshopper spermatocytes. In these cells, the unpaired mono-oriented chromosome X prevents onset of anaphase. Tension applied on this chromosome with a micro-needle pulls the chromosome away from the nearby pole and anaphase can begin (Li and Nicklas, 1995). The “tension sensitive model” is also supported by the observation that some checkpoint proteins (e.g. BubR1 and Bub1) are recruited to attached but tensionless KTs (Skoufias et al., 2001). However, these results do not directly imply that tension has directly effect on SAC, as tension can both stabilize and increase the number of MTs attached to KTs (King and Nicklas, 2000; Nicklas and Ward, 1994). Also, as mentioned in the previous section, lack of tension can

lead to destabilization of MT attachment by an Aurora B-mediated correction mechanism. Therefore, tension may activate SAC indirectly by modulating MT attachments.

The target of the SAC is Cdc20, a cofactor of the anaphase-promoting complex/cyclosome (APC/C). The current model of SAC signaling is that unattached KTs catalyze the formation of an inhibitory complex called MCC (mitotic checkpoint complex), which inhibits the ability of Cdc20 to activate the APC/C. MCC consists of Mad2, BubR1, Bub3 and Cdc20 (Fraschini et al., 2001; Sudakin et al., 2001). Both BubR1 and Mad2 can directly interact with Cdc20 and can inhibit APC/C activity *in vitro*. In addition to the MCC *per se*, distinct Cdc20 complexes, BubR1-Bub3-Cdc20 and Mad2-Cdc20, have also been described (Fang, 2002; Fang et al., 1998; Tang et al., 2001). It has been recently suggested that the Mad2-Cdc20 complex is formed first by a KT-dependent mechanism. Mad2-bound Cdc20 is then primed for subsequent binding to BubR1-Bub3 to form a complex in which Mad2 is substoichiometric (Kulukian et al., 2009; Nilsson et al., 2008). As the checkpoint function of BubR1 does not require its KT localization (Malureanu et al., 2009), the mechanism of how unattached KTs catalyze the generation of MCC should mainly depend on Mad2 KT recruitment. It has been suggested that unattached KTs recruit and induce a conformational change of Mad2, releasing it to bind Cdc20. Structural studies revealed that Mad2 adopts two conformational states, the open (O-Mad2) and closed (C-Mad2) forms (Luo et al., 2002; Sironi et al., 2002). When bound to Mad1 or Cdc20, Mad2 adopts a closed form in which its C-terminal region wraps around a polypeptide chain of the ligand, resembling a safety belt. In contrast, the ligand-free Mad2 adopts an open from. Importantly, Mad2 is able to dimerize asymmetrically, i.e., forming a C-Mad2:O-Mad2 dimer. *In vitro* reconstitution studies have shown that C-Mad2:Mad1 complex can enhance the ability of O-Mad2 to bind Cdc20 (De Antoni et al., 2005; Mapelli et al., 2006; Mapelli et al., 2007). Based on all known properties of Mad2, the "template model" was proposed to explain how the checkpoint signaling is generated at KTs. The "template model" proposes that Mad1 recruits Mad2 to unattached KT and the resulting C-Mad2:Mad1 complex acts as an "enzyme" to catalyze the formation of C-Mad2:Cdcd20 complexes, through a C-Mad2:O-Mad2 intermediate. The resulting C-Mad2:Cdc20 complex diffuses away from KTs, releasing the dimerization interface of C-Mad2:Mad1 to repeat the cycle. The C-Mad2:Cdc20 in the cytosol may be able to convert more O-Mad2 into C-Mad2:Cdc20, amplifying the signal (De Antoni et al., 2005; Mapelli et al., 2006; Mapelli et al., 2007) (Figure 17A).

Immediately after all chromosomes achieve bi-orientation, the SAC needs to be silenced to allow anaphase onset. Among others, two crucial pathways have been described to inactivate the SAC. First, the dynein/dynactin complex has been implicated in the removal of SAC proteins from attached KTs. Inhibition of dynein or preventing dynein to localize to KTs compromises the transport of SAC proteins from KTs to spindle poles, leading to prolonged SAC activation (Basto et al., 2004; Griffis et al., 2007; Howell et al., 2001; Mische et al., 2008; Varma et al., 2008; Wojcik et al., 2001). A second mechanism is based on a C-Mad2-specific binding protein, called p31^{comet}, which localizes to KTs in a Mad2-dependent manner, acting as a competitive inhibitor of O-Mad2:C-Mad2 dimer formation (Figure 17B). Depletion of p31^{comet} leads to prolonged metaphase arrest while overexpression of p31^{comet} overrides the SAC (Fava et al., 2011; Habu et al., 2002; Mapelli et al., 2007; Xia et al., 2004; Yang et al., 2007a).

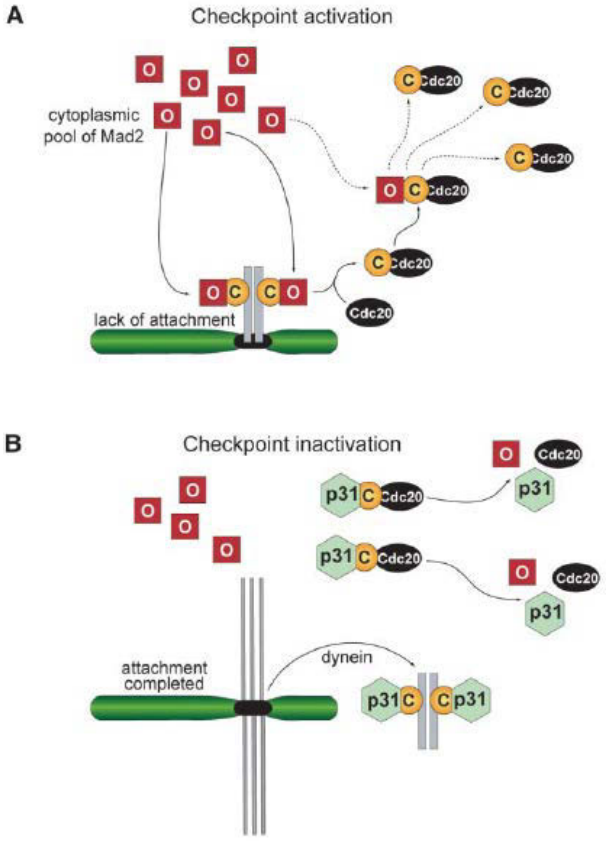

Figure 17. The template model explaining how the SAC is activated and silenced. (A) How KT C-Mad2:Mad1 converts cytosolic O-Mad2 into C-Mad2:Cdc20. See text for details. (B) Dynein-mediated stripping of C-Mad2:Mad1 and p31-dependent inhibition of C-Mad2:Cdc20 generation. See text for detail. *Illustration adapted from De Antoni et. al., Curr Biol, 2005*

Upon inactivation of the SAC, APC/C-Cdc20 becomes active and poly-ubiquitinylates cyclin B and securin promoting their degradation. Securin is an inhibitory binding protein of separase, a protease which cleaves sister chromatid cohesin. Therefore, degradation of cyclin B and securin leads to inactivation of CDK1 and activation of separase, respectively, resulting into the onset of anaphase (Figure 18) (Bharadwaj and Yu, 2004; Musacchio and Salmon, 2007; Pines, 2006).

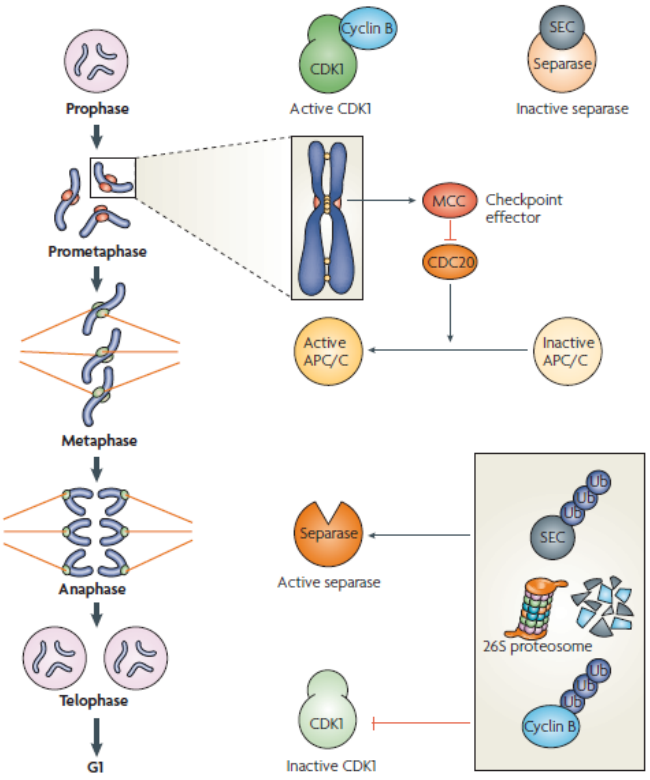

Figure 18. SAC control of anaphase onset. Activation of SAC leads to formation of the MCC, inhibiting the APC/C-Cdc20. APC/C-Cdc20 activity is required for the degradation of securin and cyclin B. The degradation of securin and cyclin B is required for the activation of separase and the inactivation of Cdk1, respectively. *Illustration adapted from Musacchio and Salmon, Nature Reviews Mol Cell Biol, 2007*

Aim of this work

In the curse of this thesis I have studied aspects related to two important protein complexes at KTs. In part I the work related to hSpindly is presented. The dynein/dynactin complex is implicated in many mitotic functions and shows various sub-cellular localizations during mitosis, namely at KT, spindle and cell cortex. Therefore, detailed understanding of the functions of KT dynein requires identification of specific dynein KT recruiters. Spindly was first identified in *Drosophila* as a specific KT recruiter of dynein. To extend our knowledge of KT dynein in human cells, we carried out detailed characterization of the human homolog of Spindly (CCDC99, later named hSpindly). We aimed at understanding the requirements for hSpindly KT localization, identifying its interacting partners and describing the consequences of hSpindly depletion in human cells. Altogether this will help to reveal the functions of KT dynein during mitosis.

In part II of this thesis the work related to the Ska complex is presented. The Ska complex, composed of Ska1-3, has been identified as an important regulator of KT-MT interaction. siRNA-mediated depletion studies reveal that the KMN network cannot maintain stable MT attachment without the Ska complex. As the KT localization of Ska depends both on the MT occupancy and the presence of the KMN network at KTs, this prompted us to investigate the molecular regulation of Ska localization. As Aurora B is also an important regulator of KT-MT interactions, we aimed at studying if and how Aurora B kinase regulates the Ska complex and its interaction with the KMN network.

Part I. Mitotic control of kinetochore-associated dynein and spindle orientation by human Spindly

Introduction I

1.1. The dynein/dynactin complex in mitosis

Error-free chromosome segregation during mitosis depends on the formation of a bipolar spindle and correct attachment of all kinetochores (KTs) to spindle microtubules (MTs) (O'Connell and Khodjakov, 2007; Tanaka and Desai, 2008). To prevent chromosome missegregation, the spindle assembly checkpoint (SAC) delays the onset of anaphase until all chromosomes are properly attached to MTs (Musacchio and Salmon, 2007).

Prominent amongst the MT-dependent motor proteins implicated in various mitotic functions is dynein/dynactin. This minus-end directed motor complex is required for proper spindle formation, plays a role in spindle pole focusing and separation, and controls spindle length (Echeverri et al., 1996; Gaetz and Kapoor, 2004; Goshima et al., 2005; Sharp et al., 2000; Vaisberg et al., 1993). Remarkably, dynein localizes to unattached KTs and disassociates upon MT attachment (King et al., 2000). It is involved in establishing the initial lateral contact between KTs and MTs, which results in rapid poleward movements of chromosomes during early prometaphase (Rieder and Alexander, 1990; Vorozhko et al., 2008; Yang et al., 2007b). Subsequently, these lateral MT interactions mature into stable end-on attachments at the KT that are mediated by the KMN network, a group of evolutionarily conserved proteins comprising KNL-1 and the Mis12 and Ndc80 complexes (Cheeseman and Desai, 2008). Importantly, the dynein/dynactin complex also localizes to the cell cortex where it contributes to spindle orientation and positioning, most likely by providing pulling forces on astral MTs (Busson et al., 1998; O'Connell and Wang, 2000).

1.2. Recruitment and functions of KT dynein/dynactin

The recruitment of dynein/dynactin to KTs is dependent on the conserved Rod/Zw10/Zwilch (RZZ) complex (Karess, 2005), possibly through direct interaction between ZW10 and the dynactin subunit p50-dynamitin (Starr et al., 1998). Additional proteins, notably Nde1 and Ndel1, are also required for targeting dynein/dynactin to KTs (Liang et al., 2007; Stehman et al., 2007; Vergnolle and Taylor, 2007). In recent years, manipulation of the RZZ complex has been extensively used to study the roles of KT-associated dynein. In fact, inhibition of the RZZ complex suppressed the rapid poleward movement of chromosomes and reduced KT tension (Savoian et al., 2000; Yang et al., 2007b), consistent with results obtained upon direct

disruption of dynein function (Howell et al., 2001; Vorozhko et al., 2008). However, the role of KT dynein in chromosome congression remains controversial. While inhibition of dynein/dynactin during prometaphase did not impair metaphase plate formation in vertebrate cells (Howell et al., 2001; Vorozhko et al., 2008), depletion of ZW10 from human cells induced chromosome misalignment, suggesting that KT dynein is required for efficient congression (Li et al., 2007; Yang et al., 2007b). Similarly, depletion of Rod from *Drosophila* S2 cells delayed chromosome alignment (Griffis et al., 2007), but *Drosophila* embryos and larval neuroblasts depleted of ZW10 showed no obvious defect in metaphase plate formation (Williams and Goldberg, 1994).

More recently, the dynein/dynactin complex has been implicated in the removal of SAC proteins from the outer KT and this in turn has been proposed to play an important role in SAC silencing (Basto et al., 2004; Griffis et al., 2007; Howell et al., 2001; Mische et al., 2008; Sivaram et al., 2009; Varma et al., 2008; Whyte et al., 2008; Wojcik et al., 2001). However, studies on the role of dynein/dynactin in SAC silencing through interference with the RZZ complex are confounded by the fact that the RZZ is also essential for SAC activation (Basto et al., 2000; Chan et al., 2000), particularly for recruiting MAD1/MAD2 to KTs (Buffin et al., 2005; Kops et al., 2005). Therefore, the discovery of a specific KT recruiting factor of the dynein/dynactin complex would be useful to study the proposed functions of this multi-tasking MT motor.

Results I

1.1 Identification of CCDC99 (hSpindly) and its orthologs

CCDC99 (accession number: Q96EA4) was one of the unknown proteins identified when a human spindle survey was carried out in our laboratory (Sauer et al., 2005). Later, in the context of a collaboration that was established with several bioinformatic laboratories (ENFIN consortium), CCDC99 was predicted to be a spindle protein (manuscript under review). Independently, CCDC99 had been suggested as the potential human homologue of *Drosophila* Spindly (Griffis et al., 2007). Subsequently, the *C. elegans* homolog of Spindly (called SPDL-1) was also identified (Gassmann et al., 2008b; Yamamoto et al., 2008). Thus, hereafter we refer to CCDC99 as hSpindly (human Spindly). Despite low primary sequence similarity, Spindly proteins share similar secondary structure organization among species i.e. the N-terminus of all Spindly homologs is predicted to consist of mainly coiled-coil domains. In contrast, the C-termini do not contain any predicted secondary structure but multiple putative CDK1 phosphorylation sites (S/TP) (see Figure 19A for hSpindly as example of the overall protein structure). Importantly, within the N-termini, a highly conserved region (so called Spindly box, with a conserved motif: GNS[L,M]F[S,A]EV) has been recently identified (Figure 19B) (Gassmann et al., 2008b; Gassmann et al., 2010). All proposed Spindly homologs recruit dynein to KTs (Gassmann et al., 2008b; Griffis et al., 2007; Yamamoto et al., 2008). Therefore, we carried out a detailed characterization of hSpindly to bring new insight into the functions of KT dynein.

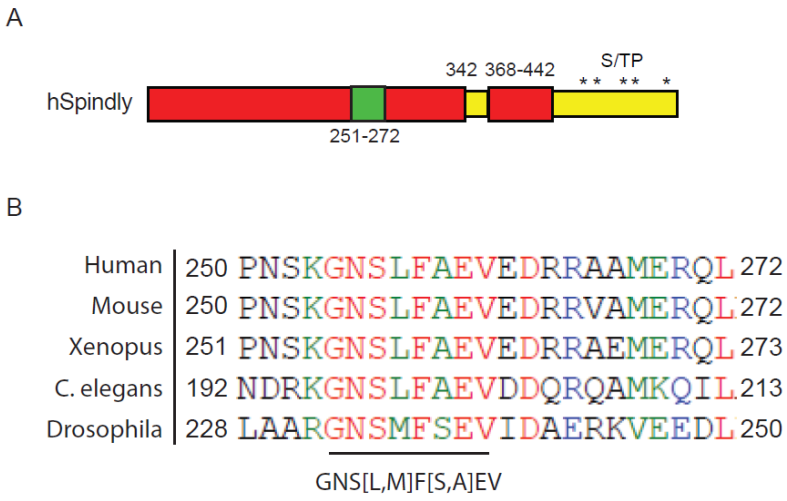

Figure 19. hSpindly protein organization (A) General secondary structure organization of hSpindly. The red box represents the predicted coiled-coil domain, the green box represents the conserved Spindly box, asterisks represent putative CDK1 sites (T509, S515, T552, S555 and T597). **(B)** Alignment of the Spindly box in the indicated species. The highly conserved motif (GNS[L,M]F[S,A]EV) is underlined. The alignment was performed with CLUSTALW (http://npsa-pbil.ibcp.fr).

1.2 Generation of polyclonal antibodies against CCDC99

To characterize hSpindly, we raised two specific antibodies. An antibody generated against the N terminus (1-444 aa) of hSpindly recognizes a single band of 70 kDa, the predicted molecular weight of hSpindly (Figure 20A). This antibody also detects clear KT signals (Figure 20B). No specific signal could be detected with the pre-immune serum or after depletion of hSpindly by siRNA (Figures 20A-C), confirming antibody specificity. Another hSpindly-specific antibody raised against the C-terminus (443-605 aa) also detected specific KT signals, further proving the KT localization of endogenous hSpindly (Figure 20D). As the antibody against the C-terminus could not detect any signal in Western blotting (data not shown), the antibody raised against the N terminus of hSpindly was used throughout this study.

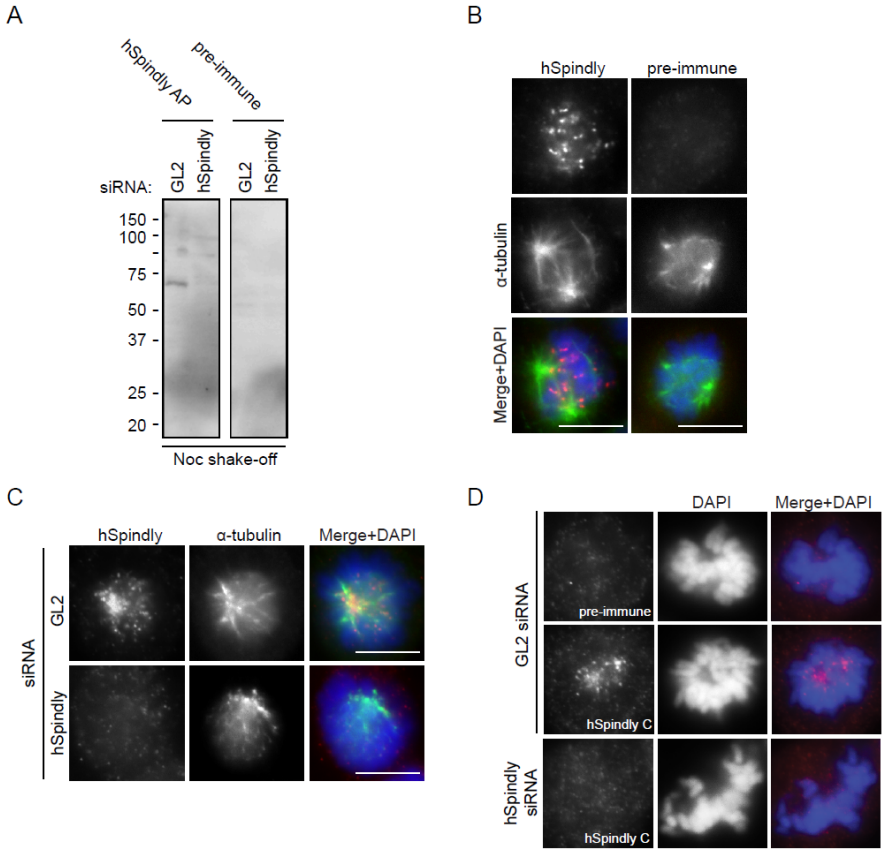

Figure 20. Characterization of hSpindly antibodies. (A) Mitotic HeLa S3 cells (nocodazole shake-off) treated with GL2 or hSpindly siRNAs for 48 h were collected, and equal amounts of cell extracts were separated by SDS-PAGE. Then, proteins were probed by Western blotting with either affinity-purified anti-hSpindly antibody (AP) (left) or pre-immune serum (right). **(B)** Cells were stained with either anti-hSpindly antibody or pre-immune serum (red), together with anti–α-tubulin antibody (green) and DAPI (blue). **(C)** Cells were treated with GL2 or hSpindly siRNAs for 48 h and stained with anti-hSpindly (red) and anti–α-tubulin antibodies (green) and DAPI (blue). **(D)** GL2 or hSpindly siRNA treated (48 h) cells were stained with either anti-hSpindly antibody (raised against C terminus, referred as hSpindly C) or pre-immune serum (red), together with DAPI (blue). Bars = 10 µm.

1.3 hSpindly localizes to KTs and spindle poles

Analysis of Hela S3 cells overexpressing myc-tagged hSpindly by immunofluorescence microscopy revealed KT and spindle pole localization in mitosis (Figure 21), identifying this protein as a *bona fide* spindle component. Interphase localization of both endogenous and myc-tagged hSpindly was mainly nuclear (Figures 21 and 22A). This contrast with *Drosophila* Spindly, which localized to MT plus-end tips (Griffis et al., 2007). In mitosis, hSpindly decorated KTs in early prometaphase before it relocalized to the spindle poles prior to metaphase (Figures 21 and 22B). Colocalization with BubR1, adjacent to the CREST signal, indicated that hSpindly is an outer KT protein (Figure 22C). After all chromosomes achieved perfect alignment, no obvious staining on the spindle poles could be seen (Figure 22D), suggesting that hSpindly diffuses to the cytosol after moving to the poles. At later stages of mitosis (anaphase and telophase), no specific association of hSpindly with any spindle structures could be detected (Figure 22B). A parallel biochemical analysis revealed that hSpindly protein levels were reduced after release from nocodazole arrest (Figure 22E) but this degradation was blocked by addition of the proteasome inhibitor MG132 (Figure 22F), indicating that hSpindly is degraded upon mitotic exit. Furthermore, an upshift could be detected in nocodazole-treated cells, suggesting that hSpindly is modified during M phase (Figures 22E-G). This modification appeared to be phosphorylation-dependent, since the slower migrating form of hSpindly was not detected in lysates from nocodazole-arrested cells treated with λ-phosphatase (Figure 22G).

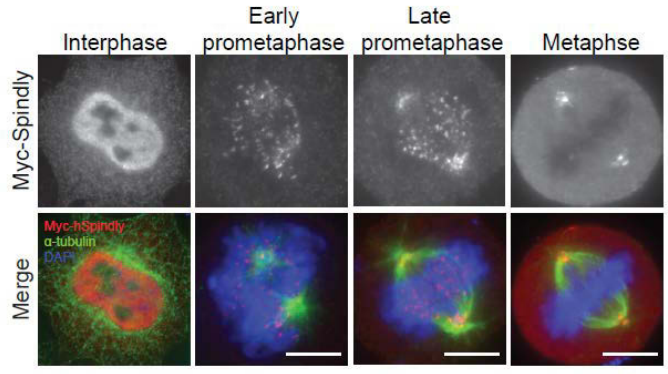

Figure 21. Localization of Myc-tagged hSpindly. HeLa S3 cells were transfected with myc-tagged hSpindly construct for 48 h and stained with anti-myc 9E10 serum (red), anti–α-tubulin antibody (green), and DAPI (blue).

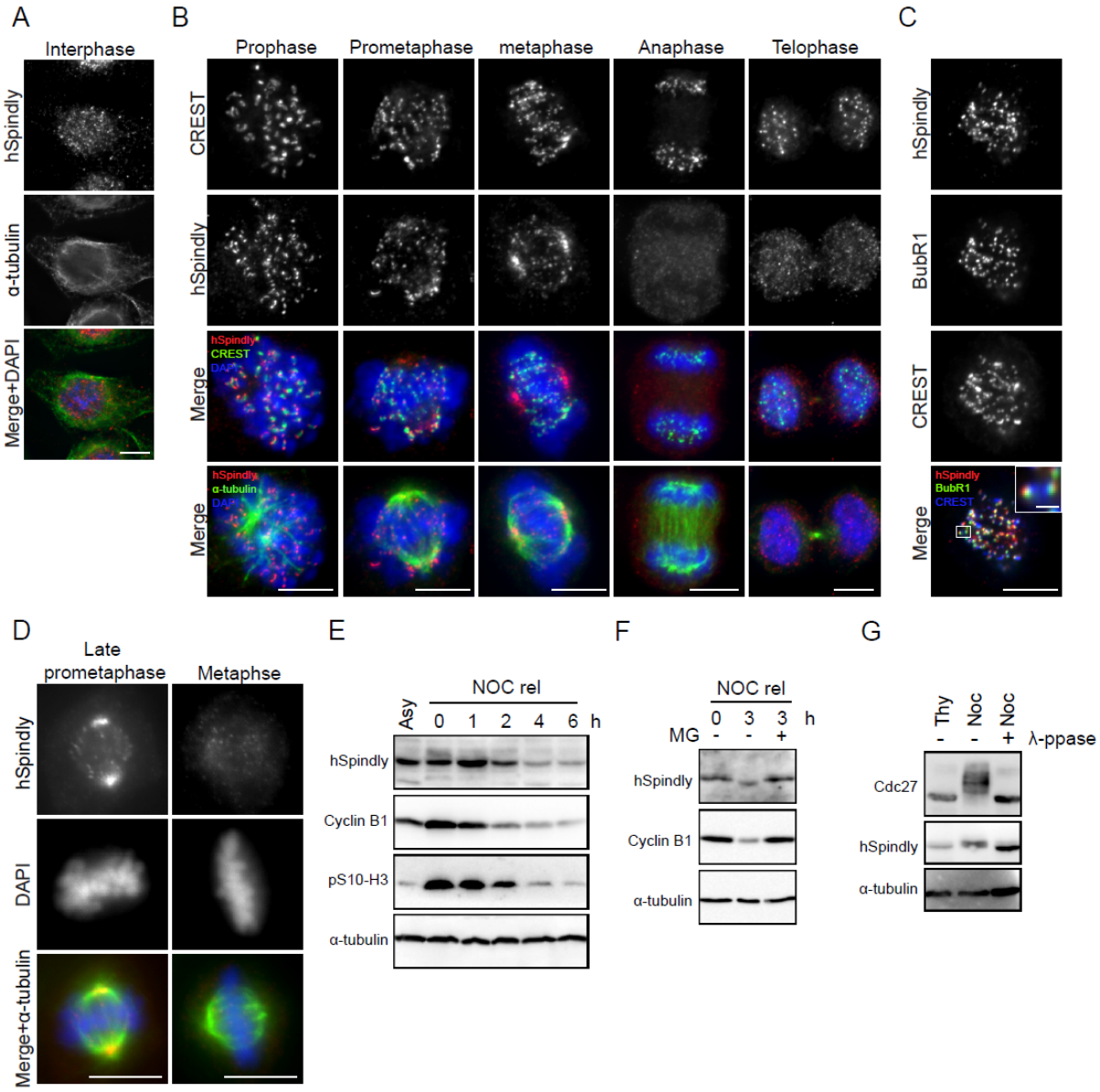

Figure 22. Localization, degradation and phosphorylation of endogenous hSpindly. **(A)** HeLa S3 cells in interphase were stained with anti-hSpindly (red) and anti-α-tubulin antibodies (green) and DAPI (blue). **(B)** Cells at different mitotic stages were stained with anti-hSpindly antibody (red), CREST serum or α-tubulin antibody (green) and DAPI (blue). **(C)** Prometaphase cell stained with anti-hSpindly (red) and anti-BubR1 (green) antibodies and CREST serum (blue). The inset shows a magnification of the selected area (scale bar = 1 µm). **(D)** Cells were stained with anti-hSpindly (red) and anti–α-tubulin antibodies (green) and DAPI (blue). **(E)** Mitotic cells (nocodazole shake-off) were washed with PBS, released into fresh medium, and collected at indicated time points. Lysates were prepared and separated by SDS-PAGE and probed by Western blotting with indicated antibodies. Asynchronous cells were used as control. **(F)** Mitotic cells (nocodazole shake-off) were washed with PBS, released into fresh medium in the presence or absence of MG132, and collected after 3 h. Lysates were prepared and separated by SDS-PAGE and probed by Western blotting with indicated antibodies. **(G)** Cells were treated with thymidine or nocodazole overnight. Lysates were prepared and treated with λ-phosphatase as indicated, before proteins were separated by SDS-PAGE and probed by Western blotting with indicated antibodies. Bars = 10 µm.

1.4 hSpindly acts downstream of the RZZ and Ndc80 complexes

The *Drosophila* and *C. elegans* homologues of hSpindly require the RZZ complex to localize to the KT (Gassmann et al., 2008b; Griffis et al., 2007; Yamamoto et al., 2008). In the case of hSpindly we found that siRNA-mediated depletion of ZW10 (ZW10-1; (Kops et al., 2005) and ZW10-2, respectively) not only abolished KT localization (Figure 23A) but also caused a reduction in hSpindly protein levels (Figure 23B). Conversely, hSpindly depletion did not affect either localization or stability of ZW10 (Figures 23C and 30C). The observed effect of RZZ depletion on the stability of hSpindly appears to reflect a new level of regulation, as no such effect had been seen in either *Drosophila* (Griffis et al., 2007) or *C.elegans* (Gassmann et al., 2008a). In agreement with the results observed in *C.elegans* (Gassmann et al., 2008), RZZ members (ZW10 and Rod), but not dynein, could be coimmunoprecipitated with hSpindly (Figure 23D) from mitotic HeLa S3 cells lysates. However, this interaction could only be observed under detergent-free conditions. In addition, glycerol gradient centrifugation revealed that a fraction of ZW10 co-migrated with hSpindly and hSpindly depletion caused a slight shift in the sedimentation behaviour of ZW10 (Figure 23E). Thus, our results are consistent with an interaction between hSpindly and the RZZ complex, albeit weak and likely dynamic.

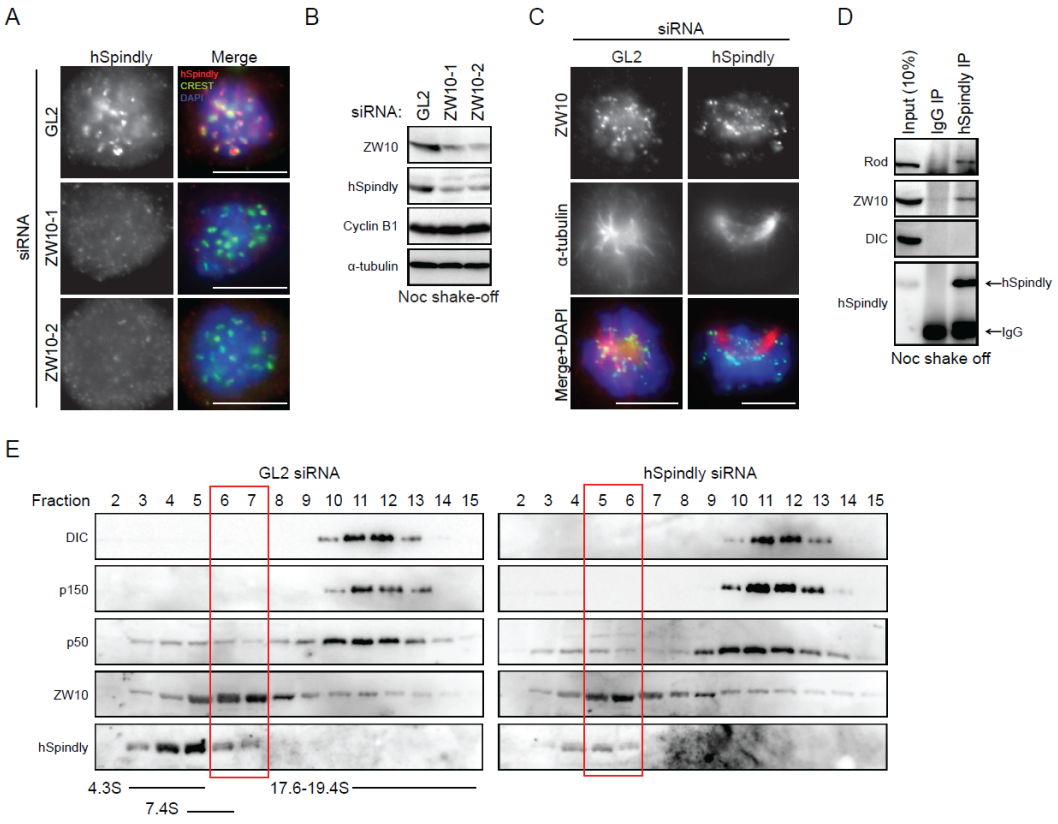

Figure 23. KT localization of hSpindly is dependent on the RZZ complex. (A) Cells treated for 72 h with GL2 (control) or two independent siRNAs targeting ZW10 (ZW10-1 or ZW10-2 siRNA, respectively) were stained with anti-hSpindly antibody (red), CREST serum (green) and DAPI (blue). **(B)** Western blotting of mitotic (nocodazole shake-off) cells treated for 72 h with GL2 (control), ZW10-1 or ZW10-2 siRNAs. Membranes were probed for the indicated antibodies and α-tubulin is shown as loading control. **(C)** HeLa S3 cells were treated with GL2 or hSpindly siRNAs for 48 h and stained with anti-ZW10 (red) and anti–α-tubulin antibodies (green) and DAPI (blue). **(D)** Mitotic cells were collected by nocodazole shake-off. Cells were resuspended in Hepes buffer and opened by nitrogen cavitation. Immunoprecipitation was performed with either IgGs as control or the anti-hSpindly antibody. **(E)** GL2- or hSpindly siRNA–treated mitotic cells (nocodazole shake-off) were analyzed by glycerol gradient centrifugation (10–25%). Each sample was separated into 27 equal fractions. Fractions 2–15 were resolved by SDS-PAGE and probed by Western blotting with indicated antibodies. Sedimentation coefficients were determined using standard proteins. Red rectangles indicate fractions containing maximum amounts of ZW10.

Next we asked whether KT localization was important for the stability of hSpindly. Upon depletion of Hec1/Ndc80 we found that both ZW10 and hSpindly were displaced from KTs (Figures 24A and 24C; see also (Lin et al., 2006)), and yet, levels of hSpindly were unaffected (Figure 24B). This clearly demonstrates that hSpindly degradation does not result from its dissociation from KTs and instead suggests that the interaction with the RZZ stabilizes the protein.

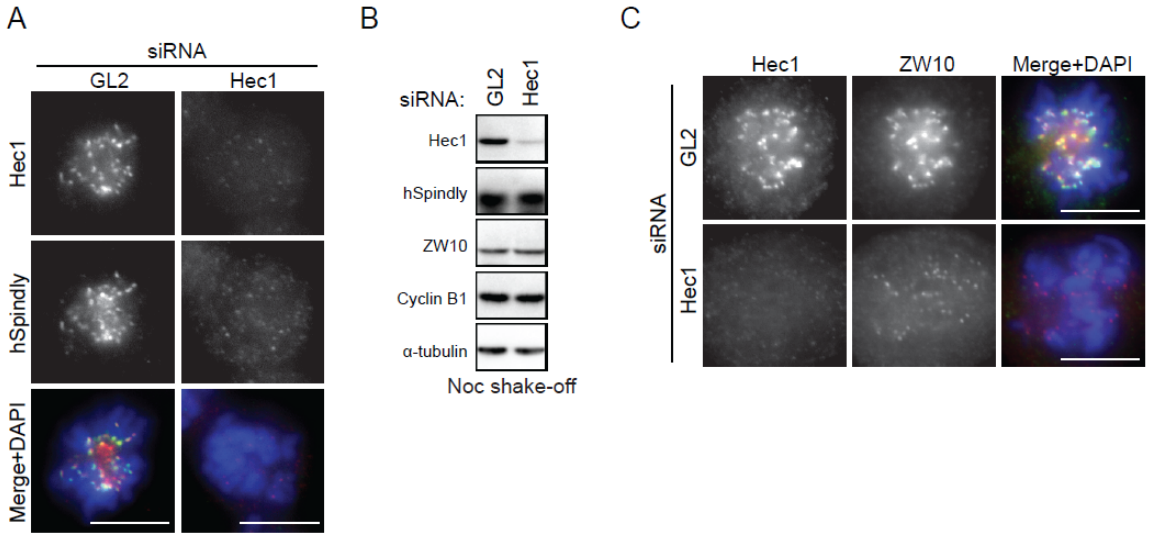

Figure 24. Hec1 controls hSpindly localization but not its expression level. (A) Cells treated with GL2 (control) or Hec1 siRNAs for 48 h were stained with anti-Hec1 (green) and anti-hSpindly (red) antibodies and DAPI (blue). **(B)** Western blotting of mitotic (nocodazole shake-off) cells treated with GL2 (control), or Hec1 siRNAs for 40 h. Membranes were probed for the indicated antibodies and α-tubulin is shown as loading control. **(C)** Cells were treated with GL2 or Hec1 siRNAs for 48 h and stained with anti-Hec1 (green), anti-ZW10 antibodies (red), and DAPI (blue). Bars = 10 μm.

1.5 Aurora B controls KT localization of hSpindly

Aurora B has been shown to promote the recruitment of the RZZ complex to the KT until the establishment of tension (Famulski and Chan, 2007). Thus, we asked whether the KT

association of hSpindly is also regulated by Aurora B. First, we analyzed hSpindly localization after depletion of Aurora B or inhibition of the kinase by the small molecule inhibitor ZM447439 (Ditchfield et al., 2003b). In both cases, hSpindly KT and spindle pole localization was lost (Figures 25A and 25B), as expected considering the dependency of the RZZ on Aurora B. Furthermore, the stability of hSpindly was clearly reduced (Figure 25C). We also observed a slight decrease in ZW10 protein levels, further pointing to an influence of Aurora B on both the RZZ and hSpindly.

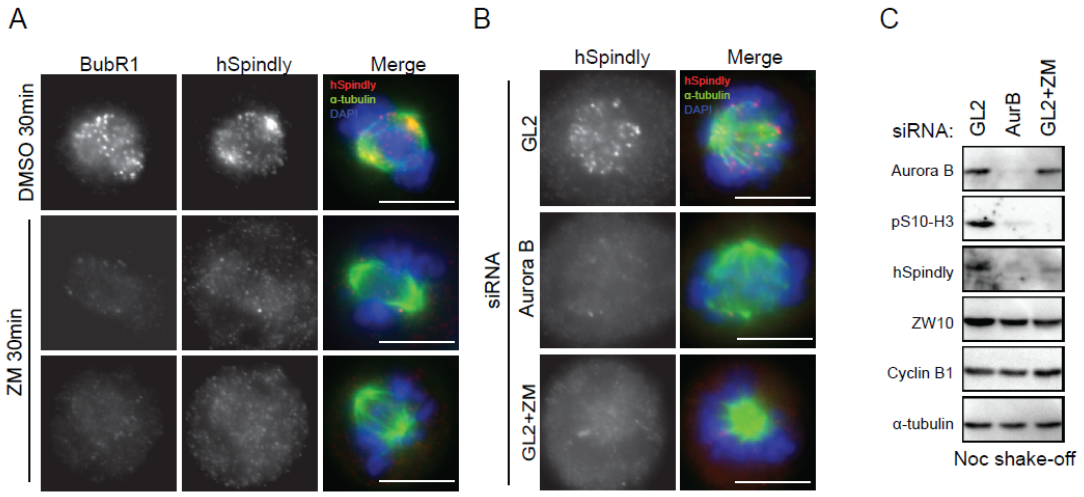

Figure 25. Inhibition of Aurora B abolishes the KT localization of hSpindly. (A) Cells were treated with either DMSO or ZM447439 (ZM) for 30 min and stained with anti-BubR1, anti hSpindly (red), and anti–α-tubulin antibodies (green), and DAPI (blue). **(B)** HeLa S3 cells were treated with GL2 (control) or Aurora B siRNAs for 40 h, or with ZM447439 (ZM) for 16 h before being stained with anti-hSpindly (red) and anti-α-tubulin (green) antibodies and DAPI (blue). **(C)** Cells were treated with GL2 (control) or Aurora B siRNAs for 40 h. DMSO (control) or ZM447439 (ZM) was added to GL2-treated cells for the last 16 h. Mitotic cells (nocodazole shake-off) were collected and equal amounts of cell extracts were separated by SDS-PAGE and probed by Western blotting with the indicated antibodies; α-tubulin is shown as loading control. Bars = 10 μm.

To examine the localization of hSpindly in response to lack of tension, MG132-treated metaphase cells were treated with taxol (1 μM). On most KTs of taxol-treated cells, hSpindly colocalized with BubR1 (Figures 26A-C), which had previously been reported to be enriched at tensionless KTs (Skoufias et al., 2001). While this treatment resulted in few MAD2 (and hSpindly)-positive KTs, likely to be unattached (Hauf et al., 2003), many KTs were hSpindly-positive but MAD2-negative (Figures 26D and 26E; see Figure 27A and 27B for MAD2 antibody characterization). Inhibition of Aurora B kinase by a short treatment with ZM447439, sufficiently short as to not reduce hSpindly levels (Figure 26F), inhibited the recruitment of both hSpindly and MAD2 in cells treated with taxol, but not nocodazole (Figures 26D, 26E and 26G).

Thus, Aurora B controls hSpindly recruitment to KTs in response to taxol, presumably through the RZZ complex.

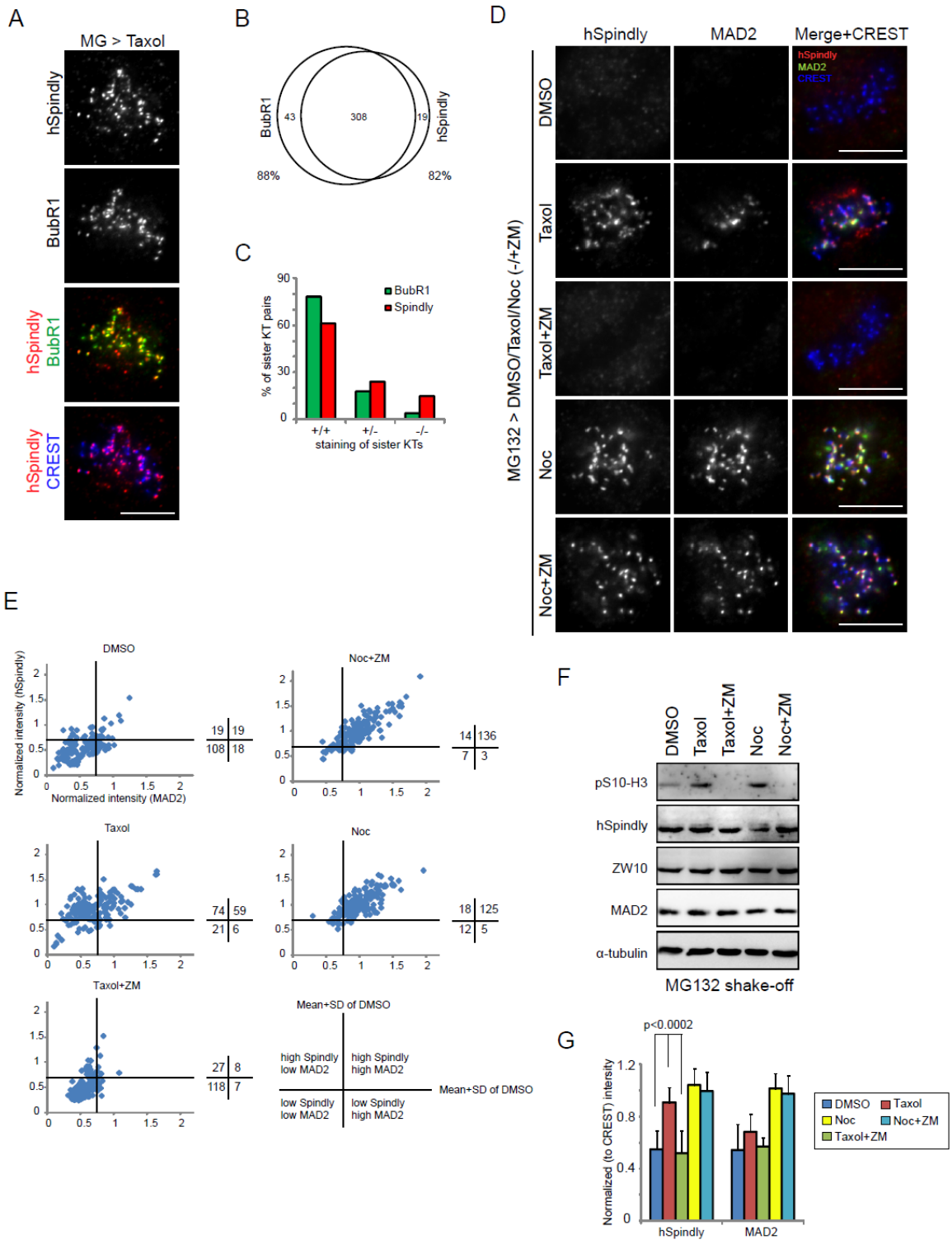

Figure 26. Aurora B regulates the localization of hSpindly in response to taxol. (A) Cells were treated with MG132 for 2 h. During the second hour, taxol was added. Cells were then stained with anti-hSpindly (red) and anti-

BubR1 (green) antibodies and CREST serum (blue). **(B)** Graph showing the numbers of KTs from 10 cells treated as in (A) (399 KTs in total) that were positive for BubR1 (left circle) or hSpindly (right circle). The overlapping region represents the number of KTs that were positive for both BubR1 and hSpindly. Percentages of KTs positive for BubR1 or hSpindly are shown. **(C)** Graph showing the percentages of sister KT pairs with both KTs positive (+/+), only one sister KT positive (+/-) or both negative (-/-), for BubR1 and hSpindly, respectively (>90 sister KT pairs from 10 cells were counted). **(D)** Cells were treated with MG132 for 2 h. During the second hour, DMSO or nocodazole (Noc) or taxol with or without ZM447439 (ZM) were added. Cells were then stained with anti-hSpindly (red) and anti-MAD2 (green) antibodies and CREST serum (blue). **(E)** The normalized intensities of hSpindly and MAD2 staining of cells in (D) were plotted in X-Y graphs. The horizontal and vertical lines in the graphs represent the mean + SD of control cells treated only with MG132 and DMSO. The number of KTs in corresponding categories is shown to the right. **(F)** Cells were synchonized by sequential thymidine arrest (overnight) and release (9 h) before being treated as in (D). Mitotic cells were collected by shake-off. Equal amounts of cell extracts were separated by SDS-PAGE and probed by Western blotting with the indicated antibodies; α-tubulin is shown as loading control. **(G)** Bar graph showing the quantification of hSpindly and MAD2 staining intensities at KTs (normalized against CREST) of cells in (F) (20 KTs were counted per cell and error bars indicate the standard deviation (s.d) of measurements from 8 cells). Scale bars = 10 μm.

To further investigate the possible tension responsiveness of hSpindly, we analyzed hSpindly localization in cells treated with monastrol. Similar to taxol-treated cells, hSpindly was found on many MAD2-negative KTs (Figures 27C and 27D), suggesting that KT-MT attachment is not sufficient to remove hSpindly from KTs. However, a significant fraction of sister KT pairs clearly displayed asymmetric hSpindly localization (Figure 27E), and similar observations were made, albeit less frequently, in taxol-treated cells (Figure 26C). This suggests that hSpindly localization to KTs is not regulated by tension but, presumably, by some structural or dynamic aspect of KT-MT interaction. Interestingly, though, hSpindly can be retained at KTs under some conditions of MT attachment that still allow MAD2 removal.

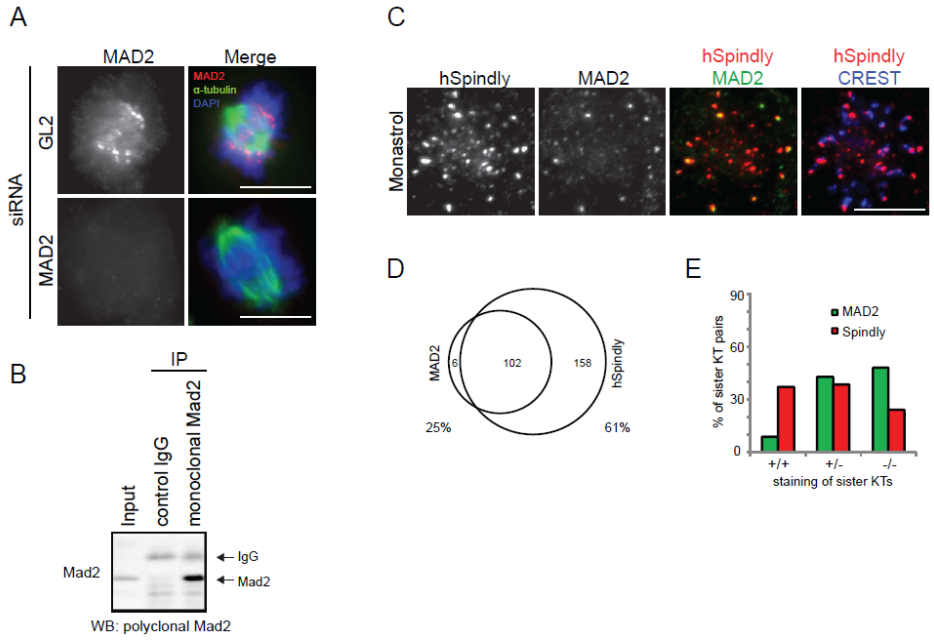

Figure 27. KT localization of hSpindly in monastrol-treated cells. (A) HeLa S3 cells were treated with GL2 or MAD2 siRNAs for 48 h and stained with anti-MAD2 serum (red), anti–α-tubulin antibody (green), and DAPI (blue). **(B)** Mitotic cells (nocodazole shake-off) were lysed and immunoprecipitation was performed with either IgGs as control or the newly generated

monoclonal MAD2 antibody. Membranes were probed with a polyclonal MAD2 antibody. Note that the newly generated monoclonal antibody can be used for immunofluorescence and immunoprecipitation but not for Western blotting **(C–E)** Cells were treated with monastrol for 16 h and analyzed as in Figure 26A–C, except that they were stained with anti-MAD2 antibody (green) instead of anti-BubR1 antibody. In (E), 428 KTs from 10 cells were counted in total. Percentages of KTs positive for MAD2 or hSpindly are shown. Bars = 10 μm.

1.6 hSpindly is essential for mitotic progression

To determine the function of hSpindly, we analyzed the depletion phenotype in HeLa S3 cells. Depletion of hSpindly with either one of two siRNAs (hSpindly-1 and hSpindly-2 siRNA) resulted in an increased mitotic index when compared to GL2-treated cells (Figure 28A). Immunofluorescence analysis of hSpindly-depleted cells revealed elongated spindles and severe chromosome misalignments (Figures 28B and 28C). Strikingly, a significant proportion of hSpindly-depleted cells (~25% and 32%; hSpindly-1 and 2, respectively, ~10% GL2) showed a monopolar-like spindle with chromosomes arranged in a circle (Figure 28B, discussed in detail later).

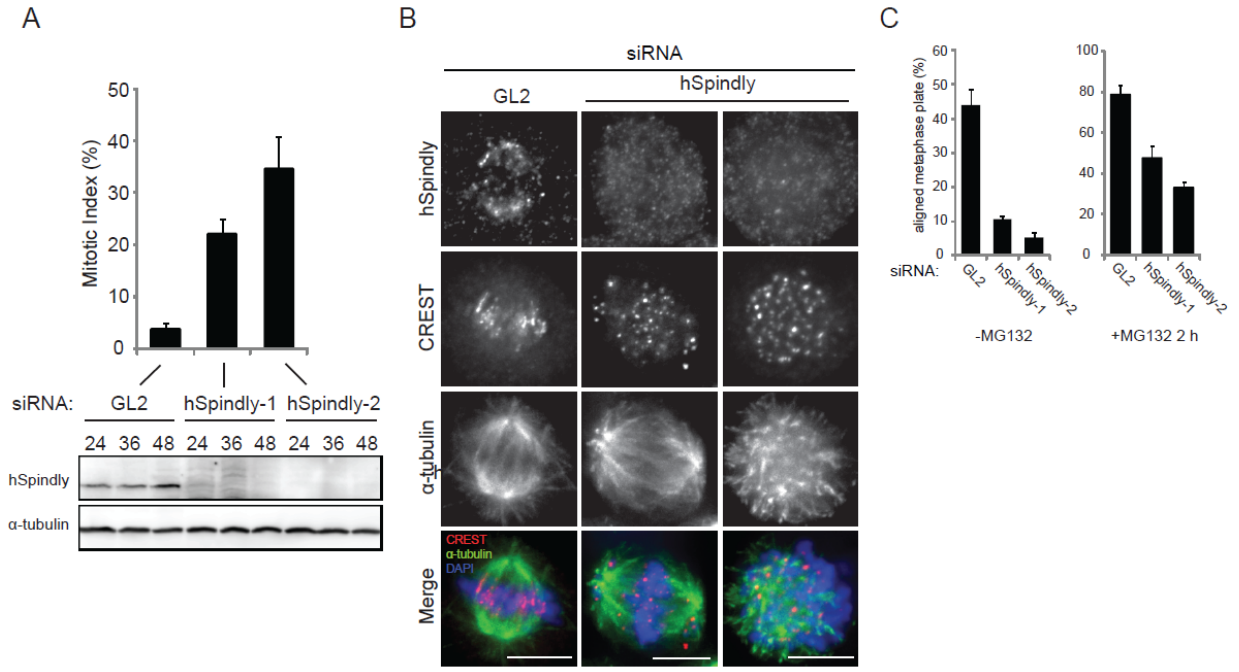

Figure 28. Depletion of hSpindly induces chromosome misalignment. (A) Mitotic indices were determined for HeLa S3 cells after treatment for 48 h with GL2 (control) or two independent siRNAs targeting hSpindly (hSpindly-1 and hSpindly-2, respectively). Bar graphs show the results of 3 independent experiments (>100 cells each) and error bars indicate s.d. The lower panel shows Western blotting of cells treated for the indicated times with the abovementioned siRNAs. Membranes were probed with anti-hSpindly antibody and α-tubulin is shown as loading control. **(B)** Cells treated with GL2 or hSpindly-2 siRNA for 48 h were stained with anti-hSpindly and anti-α-tubulin antibodies (green), and CREST serum (red) and DAPI (blue). **(C)** Cells were treated with GL2, hSpindly-1 or hSpindly-2 siRNAs for 48 h (and treated with or without MG132 for 2 h) and the percentage of mitotic cells with all

chromosomes aligned was determined. Bar graphs represent the results of 3 independent experiments (>100 cells each, only prometaphase and metaphase cells were counted) and error bars indicate s.d.

To examine the hSpindly depletion phenotype in real time we carried out live cell imaging experiments using HeLa S3 cells stably expressing histone H2B-GFP. hSpindly-depleted cells spent an increased time in mitosis from nuclear envelope breakdown to anaphase onset (mean of 92 min and 148 min for hSpindly-1 and 2 siRNAs, respectively), when compared to GL2-treated cells as control (mean of 36 min; Figures 29A and 29B). When the mitotic arrest caused by hSpindly depletion exceeded 4 hours, we often observed cell death (data not shown). hSpindly depleted cells also showed many unaligned chromosomes, similar to the phenotype seen upon ZW10 depletion (Figure 29A). However, in agreement with reported functions for ZW10 (Kops et al., 2005; Yang et al., 2007b), depletion of the latter protein produced no significant effect on overall mitotic timing, although it caused premature anaphase and chromosome missegregation (Figures 29A and 29B). Thus, whereas depletion of either hSpindly or ZW10 results in a chromosome congression defect, only depletion of hSpindly causes a substantial mitotic delay.

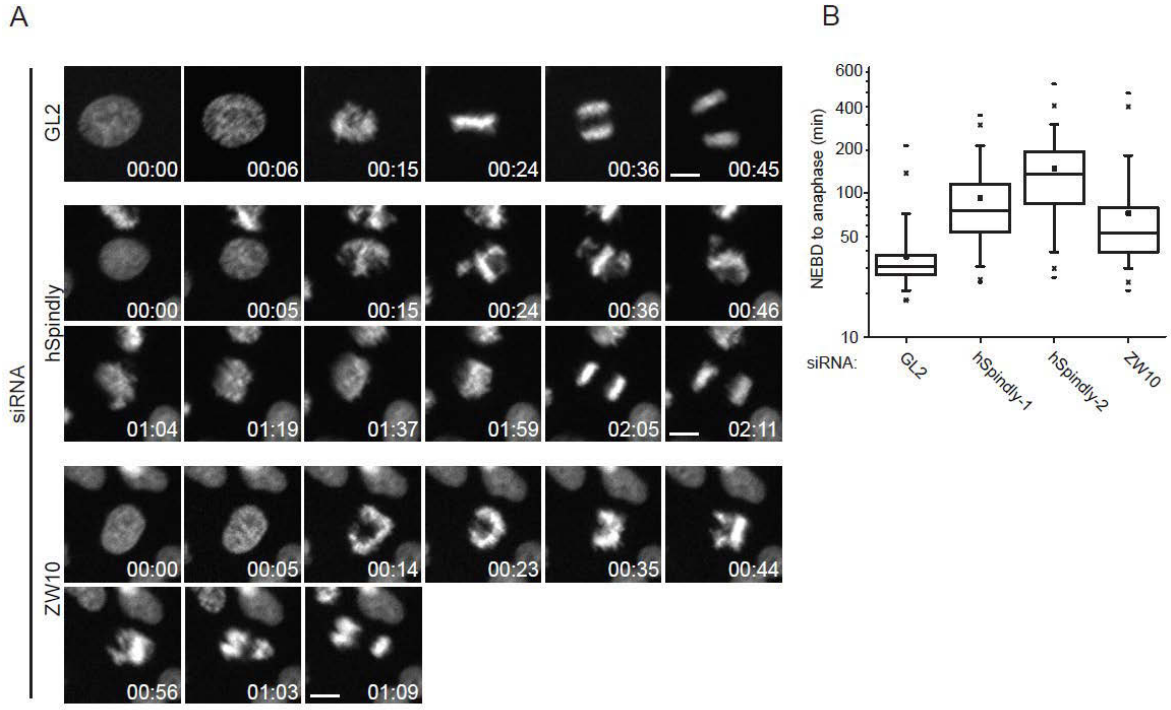

Figure 29. Depletion of hSpindly induces mitotic defects. (A) Representative stills from movies of H2B-GFP expressing HeLa S3 cells treated with GL2, hSpindly-2 and ZW10 siRNAs for 48 h before filming. Time is shown in hh: mm. t = 0 was defined as the time point one frame before chromosome condensation became evident. **(B)** Box-and-whisker plot showing the time cells spent in mitosis from nuclear envelope breakdown (NEBD) to

anaphase after treatment with GL2 (control), hSpindly-1 and hSpindly-2 siRNA (3 experiments, >80 cells per experiment, $p<0.0001$) or ZW10 siRNAs (2 experiments, >80 cells per experiment, $p<0.0001$). Scale bars = 10 μm.

1.7 hSpindly recruits both dynein and dynactin to KTs but is dispensable for removal of checkpoint proteins

Whereas *Drosophila* Spindly was reported to recruit dynein to KTs independently of dynactin (Griffis et al., 2007), *C. elegans* SPDL-1 targets both dynein and dynactin to unattached KTs (Gassmann et al., 2008b). In view of these conflicting data, we asked what role hSpindly plays in the KT recruitment of dynein and dynactin in human cells. Although depletion of hSpindly did not affect the normal localization of either dynein or dynactin on the spindle (see Figure 37H below), it clearly abolished the KT association of both dynein intermediate chain (DIC) and the dynactin subunit $p150^{Glued}$ in nocodazole-treated cells (Figures 30A and 30B), without affecting their protein levels (Figure 30C). This localization could be restored by overexpressing a siRNA-resistant myc-hSpindly construct (Figures 30D and 30E). Thus, hSpindly is clearly required for KT loading of both dynein and dynactin, as reported for *C. elegans* (Gassmann et al., 2008a), but unlike the situation in *Drosophila* (Griffis et al., 2007). Importantly, no other KT protein examined (except dynein/dynactin) was mislocalized after hSpindly depletion, strongly arguing against a general disruption of KT/centromere structure (Figures 31A-D). Of particular interest, hSpindly depletion did not affect Nde1, another protein implicated in the KT recruitment of dynein (Stehman et al., 2007; Vergnolle and Taylor, 2007), nor did Nde1 depletion affect hSpindly (Figures 31E and 31F), indicating that the two proteins cooperate in localizing dynein to the KT.

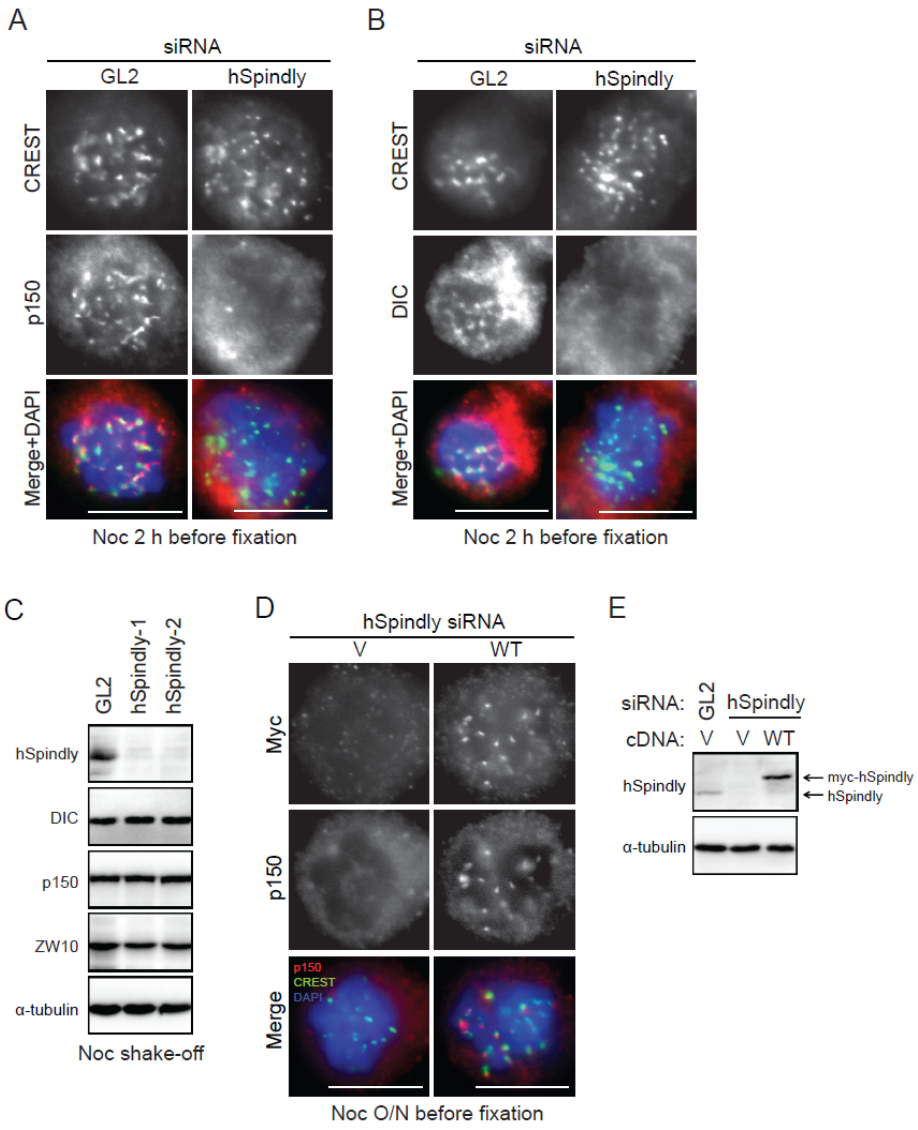

Figure 30. hSpindly targets both dynein and dynactin to KTs. (A) HeLa S3 cells were treated with GL2 or hSpindly siRNAs for 48 h. Nocodazole was added to the cells 2 h before they were stained with CREST serum (green), anti-p150^{Glued} antibody (red) and DNA (blue). **(B)** Cells treated as in (A) were stained with CREST serum (green) and anti-dynein intermediate chain (DIC) antibody (red) and DNA (blue). **(C)** Cells were treated with GL2, hSpindly-1 or hSpindly-2 siRNAs for 48 h. Lysates from mitotic cells (nocodazole shake-off) were prepared and equal amounts of cell extracts were separated by SDS-PAGE and probed by Western blotting with the indicated antibodies. **(D)** Cells were transfected with hSpindly-2 siRNA together with either a myc-vector construct (V) or a myc-tagged hSpindly (siRNA-resistant) construct (WT) for 48 h. Cells were stained with anti-myc, anti-p150^{Glued} antibodies (red), CREST serum (green) and DAPI (blue). **(E)** Cells were treated as in (D). Lysates were prepared and equal amounts of cell extracts were separated by SDS-PAGE and probed by Western blotting with the indicated antibodies.

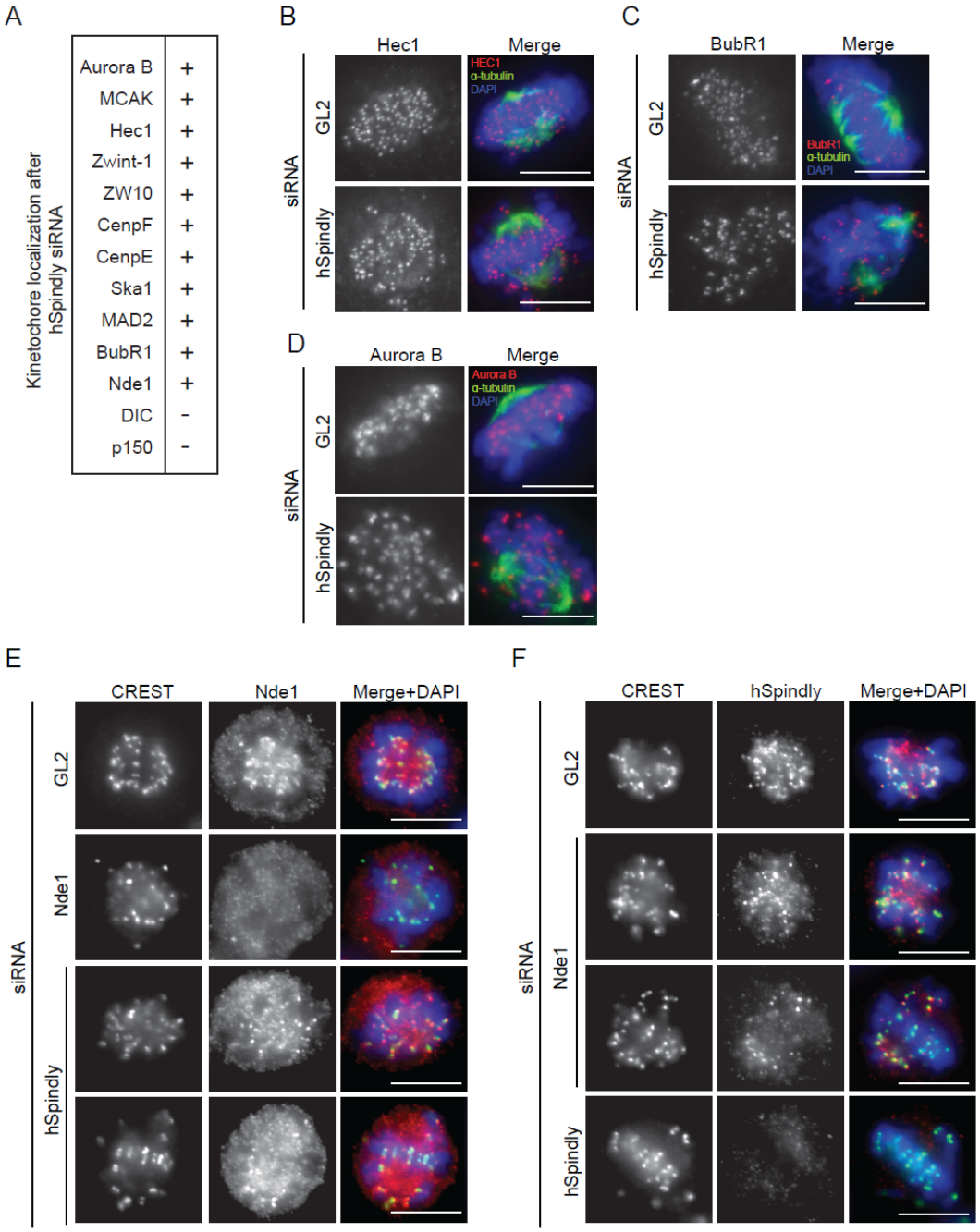

Figure 31. Localization of KT/centromere proteins upon hSpindly depletion. (A) Table showing positive/negative localization of the indicated KT/centromere proteins after hSpindly-depletion for 48 h (-, lost from KT; +, indistinguishable from control). For DIC and p150, experiments were repeated with treatment of nocodazole (2 h) to confirm their dependency on hSpindly. Scale bars = 10 μm. HeLa S3 cells were treated with GL2 or hSpindly siRNAs for 48 h and then stained with anti-Hec1 antibody **(B)**, anti-BubR1 serum **(C)**, or anti-Aurora B antibody (**D**, red), together with anti–α-tubulin (green) antibody and DAPI (blue). **(E)** Cells were treated with GL2, hSpindly, or Nde1 siRNAs for 48 h and stained with CREST serum (green), anti-Nde1 antibody (red), and DAPI (blue). **(F)** Cells treated as in D, but stained with anti-hSpindly antibody (red) instead of anti-Nde1 antibody. Bars = 10 μm.

Although the role of Spindly in recruiting dynein to KTs is apparently conserved amongst species, *Drosophila* Spindly and *C. elegans* SPDL-1 were described to impact differently on the SAC. Whereas SPDL-1 is required for MAD1/MAD2 recruitment to unattached KTs, Spindly is not required for this process, but instead is subsequently required for removal of MAD2 from aligned KTs (Gassmann et al., 2008b; Griffis et al., 2007; Yamamoto et al., 2008). We therefore asked which of these roles is shared by hSpindly. In HeLa S3 cells, depletion of hSpindly did not affect the recruitment of MAD2 to prometaphase KTs (Figure 32A). Moreover, checkpoint proteins including MAD2, MAD1 and ZW10 were detected only on unaligned KTs (Figures 32B-D), arguing that SAC proteins were normally displaced from KTs upon MT attachment. We conclude that hSpindly is not required for the initial recruitment nor the subsequent removal of SAC components. So, the persistent SAC activation seen in hSpindly-depleted cells cannot be explained by impaired removal of SAC proteins.

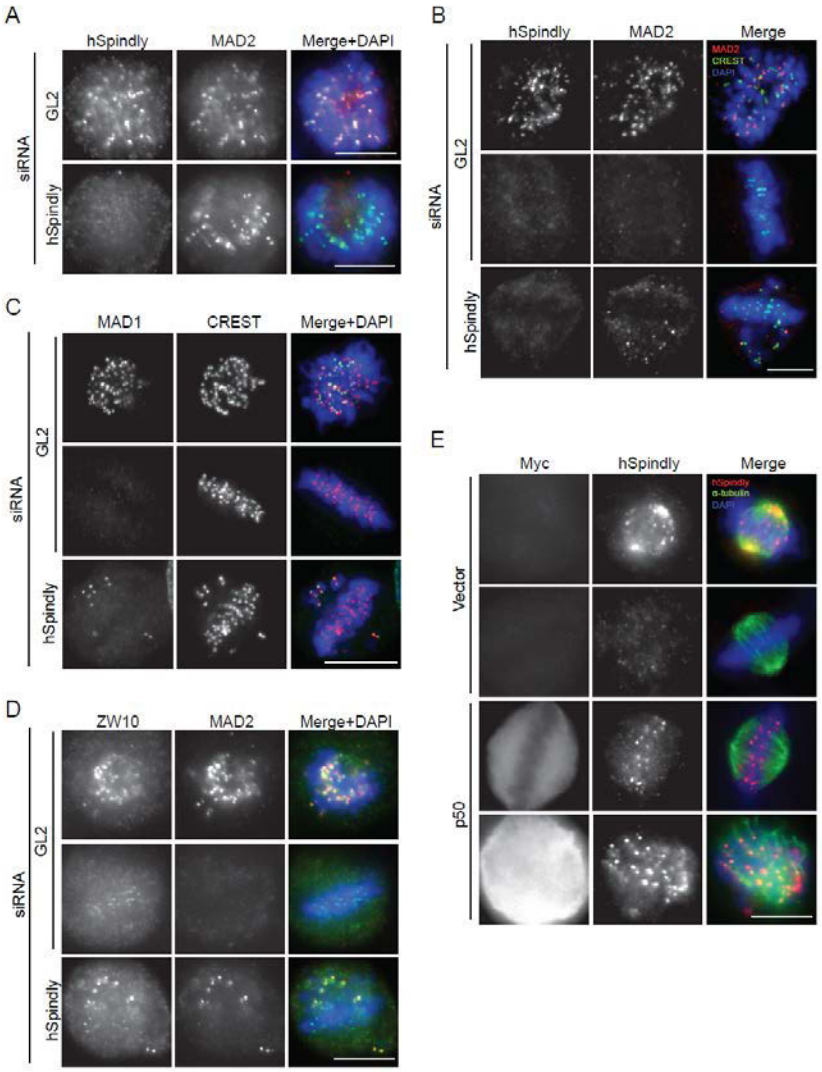

Figure 32. hSpindly is dispensable for removal of MAD2 and ZW10 from KTs. HeLa S3 cells were treated with GL2 or hSpindly siRNAs for 48 h and stained with anti-hSpindly (red) and anti-MAD2 antibodies (green) **(A)** or anti-hSpindly, anti-MAD2 antibodies (red) and CREST serum (green) **(B)**, and DAPI (blue). **(C)** Cells were treated with GL2 or hSpindly siRNAs for 48 h and stained with anti-ZW10 (green), anti-MAD2 (red) antibodies and DAPI (blue). (D) Cells were treated as in (C) except stained with anti-Mad1 antibody (green) and CREST (red). **(E)** Cells were transfected with either a myc-vector construct or a myc-tagged p50-dynamitin construct for 48 h and treated with MG132 for 1 h. Cells are then stained with anti-myc 9E10 serum, anti-hSpindly (red) and anti-α-tubulin antibodies (green) and DAPI (blue). Bars = 10 μm.

It has been previously shown that Spindly and SAC components are removed from KTs in a dynein-dependent manner (Griffis et al., 2007; Howell et al., 2001; Wojcik et al., 2001). To confirm that this also occurs in HeLa S3 cells, we overexpressed p50-dynamitin, a protein known to disrupt the dynein/dynactin complex (Echeverri et al., 1996). Indeed, we found that a much higher proportion of p50-overexpressing metaphase cells retained hSpindly and MAD2 on at least some KTs, when compared to cells transfected with an empty vector (Figures 32E, 33A and 33B), indicating that the removal of these proteins from KTs is inefficient upon disruption of the dynein/dynactin complex. In addition, the adoption of an ATP reduction assay that had previously been used to study dynein-dependent transport (Howell et al., 2001), revealed that hSpindly and SAC components relocalized from KTs to the spindle poles (Figure 33C), but were retained at KTs when cells were additionally treated with nocodazole (Figure 33D). Together, these results suggest that removal of SAC proteins from KTs occurs in a MT- and dynein-dependent manner but does not require hSpindly-mediated accumulation of KT dynein.

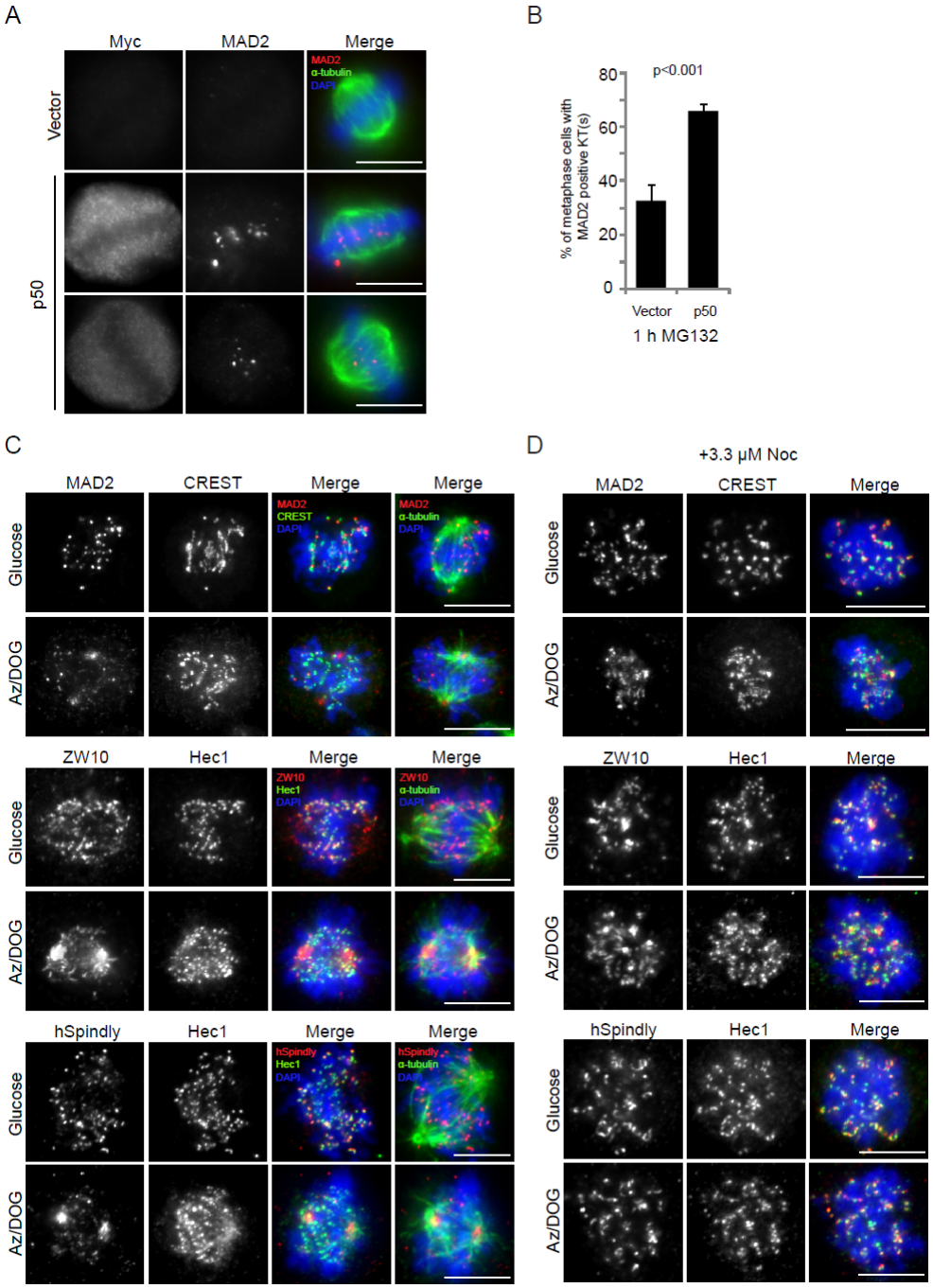

Figure 33. Efficient removal of checkpoint proteins from KTs requires dynein/dynactin. **(A)** HeLa S3 cells were treated as in Figure 32E but stained with anti-MAD2 antibody instead of anti-hSpindly antibody. **(B)** The percentage of metaphase cells treated as in (A) with MAD2-positive KT(s) was determined. Bar graph showing the results of 3 independent experiments (>30 cells each), with error bars indicating s.d. **(C)** To perform an ATP reduction assay, cells were rinsed once with isotonic salt solution and then incubated with either isotonic salt solution with glucose or with sodium azide (Az) and 2-deoxyglucose (DOG). Cells were stained with anti-MAD2 antibody and CREST serum (top panel), anti-ZW10 and anti-Hec1 antibodies (middle panel) and anti-hSpindly and anti-Hec1 antibodies (bottom panel). All cells were simultaneously stained also with anti-α-tubulin antibody and DAPI (blue). **(D)** Cells were treated as in (C), except that nocodazole (3.3 μM) was added to the isotonic salt solution. Bars = 10 μm.

1.8 hSpindly contributes to the establishment of tension and K-fiber stabilization

KT-associated dynein has been suggested to be required for the generation of inter-KT tension on metaphase chromosomes (Howell et al., 2001; Yang et al., 2007b). To test whether

depletion of hSpindly leads to a reduction of tension, we measured the inter-KT distance between Hec1 positive KT pairs in cells treated for 30 min with MG132. Inter-KT distances at unaligned chromosomes in hSpindly-depleted cells were similar to those seen in GL2-depleted cells treated with nocodazole (0.790±0.124 µm, n=58 KT pairs from 10 cells and 0.767±0.111 µm, n=100 KT pairs from 10 cells, respectively). On fully aligned chromosomes, however, the inter-KT distance in hSpindly-depleted cells was about 26 % shorter than in GL2-treated metaphase cells (1.167±0.188 µm (n=70 KT pairs from 10 cells), as compared to 1.306±0.178 µm (n=94 KT pairs from 10 cells). These data are statistically significant ($p < 10^{-5}$) and show that hSpindly depletion leads to reduced KT tension, consistent with the notion that KT dynein contributes to tension establishment (Yang et al., 2007b).

As shown recently, antibody-mediated inhibition of Nde1/Ndel, depletion of ZW10 (Stehman et al., 2007; Yang et al., 2007b), or overexpression of a dynein tail fragment (Varma et al., 2008) all affect K-fiber stability. Therefore, we assessed whether hSpindly is also required for K-fiber stability. Cells were exposed to 4 °C for 20 min, a procedure known to test the stability of K-fibers (Rieder, 1981). Whereas Hec1/Ndc80-depletion, known to impair KT-MT attachments, resulted in cells devoid of cold-stable MTs, hSpindly-depletion caused only a partial reduction of K-fiber stability (Figures 34A and 34B). This indicates that K-fibers could form in the absence of hSpindly, although they were less stable.

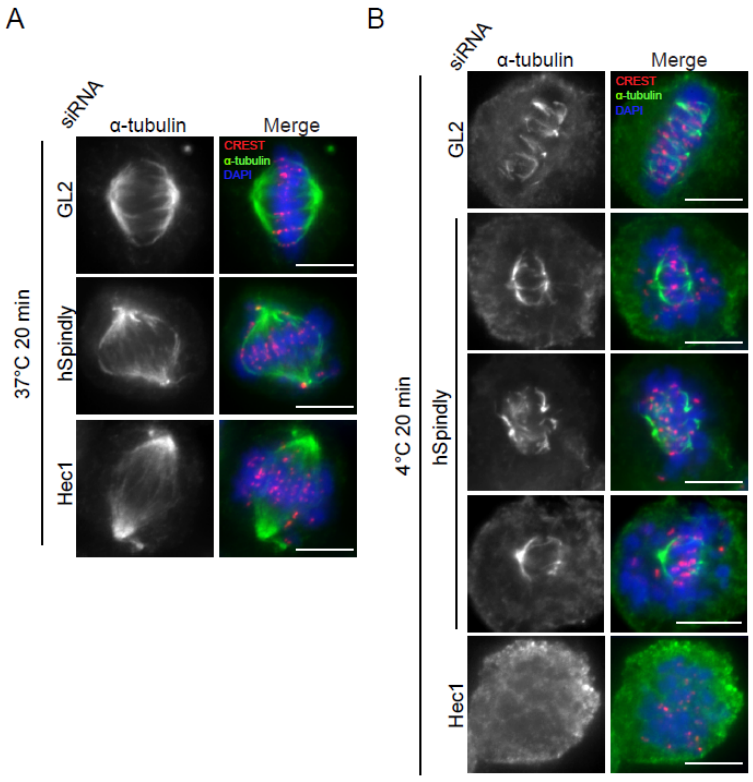

Figure 34. K-fiber stability after hSpindly depletion. HeLa S3 cells were treated with GL2, hSpindly or Hec1 siRNAs for 48 h and left at 37 °C **(A)** or placed at 4 °C **(B)** for 20 min, before they were stained with anti-α-tubulin antibody (green), CREST serum (red) and DAPI (blue). Bars = 10 µm.

1.9 hSpindly inhibition causes spindle misorientation in a dynein-dependent manner

As described above, we frequently observed spindles with an apparently monopolar morphology in hSpindly-depleted cells (Figure 28B). However, closer examination of such spindles, through staining for the centrosomal protein centrin-3 and analysis of the z-dimension, revealed two well-separated spindle poles (Figure 35A). The x-z projection of the centrosomal signal obtained from hSpindly, ZW10 and Nde1-depleted cells seeded on fibronectin-coated coverslips indicated that spindles had frequently rotated, when compared to either GL2-treated or CenpE-depleted cells, although similar to hSpindly depleted cells, the latter showed prominent chromosome misalignments (Tanudji et al., 2004) (Figure 35B; the efficiency of CenpE siRNA is shown in Figure 35C). To quantify these observations, the angle between the axis of each metaphase spindle and the substrate plane (Figure 35D, upper panel, α) was measured, showing a clear increase in hSpindly, ZW10 and Nde1-depleted cells (means of 28, 24 and 26 degrees, respectively), as compared to GL2 or CenpE-depleted cells (means of 12 and 17 degrees, respectively) (Figures 35D). Similar results were obtained also when seeding cells on non-coated coverslips (Figure 36A). Considering that depletion of hSpindly, ZW10 or Nde1 all affect the subcellular localization of dynein, we conclude that the observed spindle rotation most likely reflects the impairment of dynein/dynactin function, rather than chromosome misalignment, mitotic delay, or cell adhesion conditions.

Compared to GL2-treated or CenpE-depleted cells, we also noticed that the average spindle length of hSpindly, ZW10, or Nde1-depleted cells was increased, although to a variable extent (Figure 35E and Figure 36B). One plausible explanation is that KT dynein facilitates the formation of load-bearing KT-MT attachments which counteract the forces pulling on astral MTs, as in the case of dynein controlled by SPDL-1 in *C.elegans* (Gassmann et al., 2008a). Alternatively, hSpindly may be involved in regulating MT polymerization/depolymerization, although our results do not favor the latter hypothesis, since spindle pole accumulation of NuMA and Kif2a were not noticeably affected in hSpindly-depleted cells (data not shown).

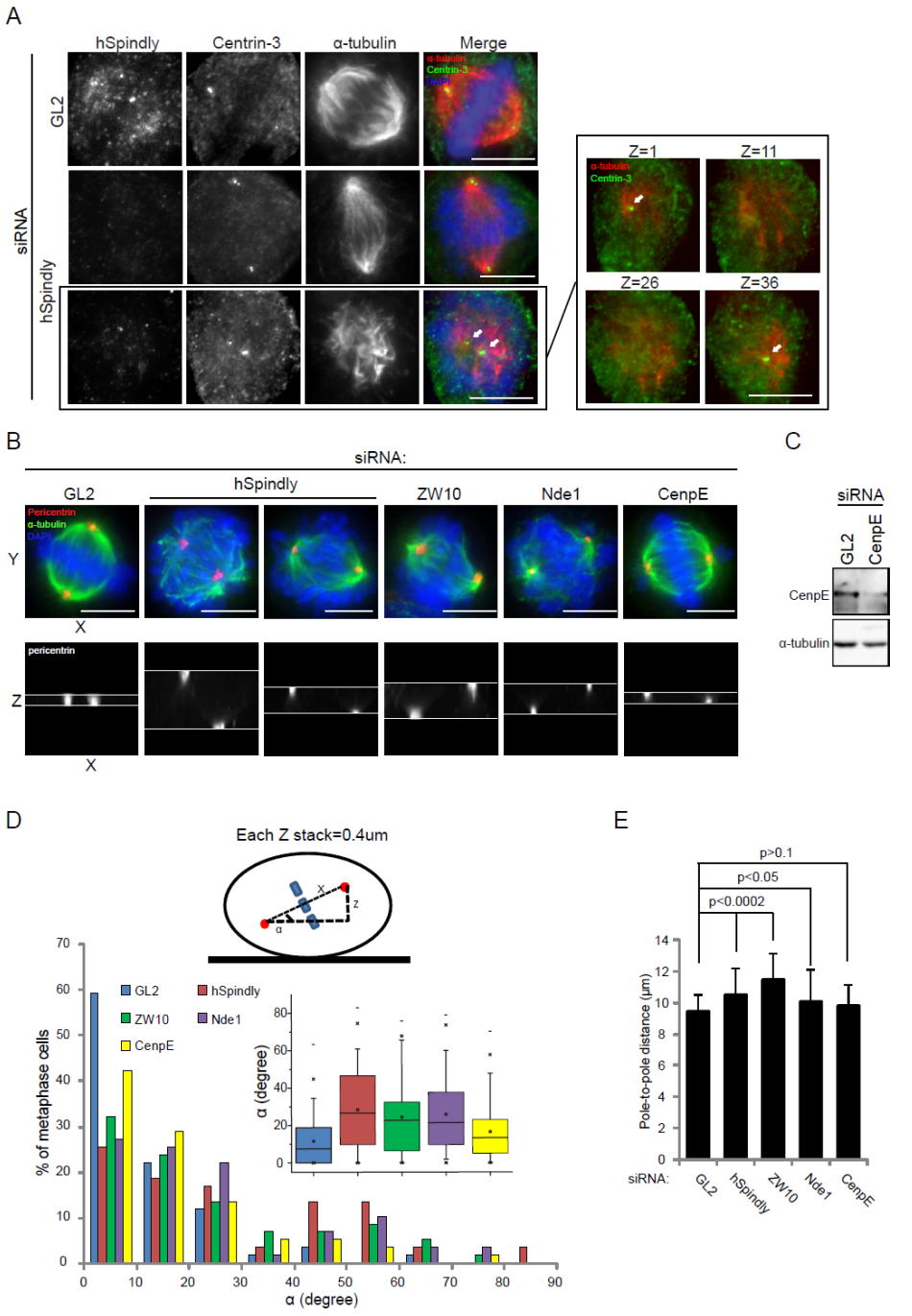

Figure 35. Spindle misorientation and increased spindle length after hSpindly depletion. (A) HeLa S3 cells were treated with GL2 and hSpindly siRNAs for 48 h and stained with anti-hSpindly, anti-centrin-3 (green), and anti-α-tubulin (red) antibodies and DNA (blue). Panels on the right show 4 representative sections along the z-axis (section numbers are indicated). **(B)** Cells were seeded onto fibronectin-coated coverslips, treated with the indicated siRNAs for 48 h and synchronized by a thymidine block (overnight) and release (9 h). MG132 was added to the cells 1 h before they were stained with anti-pericentrin (red) and anti-α-tubulin antibodies (green) and DAPI (blue). Lower panels show the X-Z projection of the pericentrin signal. **(C)** HeLa S3 cells were treated with GL2 or CenpE siRNAs for 48 h. Lysates were separated by SDS-PAGE and probed by Western blotting with anti-CenpE antibody; α-tubulin is shown as loading control. **(D)** Box-and-whisker blot showing the spindle angles (α) of cells treated as in (B), calculated by measuring the pole-to-pole distance (x) and the vertical distance (z) between two poles after taking Z-stacks every 0.4 μm (illustrated in upper panel). Only cells with well separated spindle poles (x > 7 μm) were counted (> 50 cells) (GL2 vs hSpindly/ZW10/Nde1, $p < 0.0002$; GL2 vs CenpE, $p > 0.05$). **(E)** Bar graph showing the pole-to-pole distances (x) of the cells in (B). Error bars show the s.d after measuring distances from > 50 cells. Bars = 10 μm.

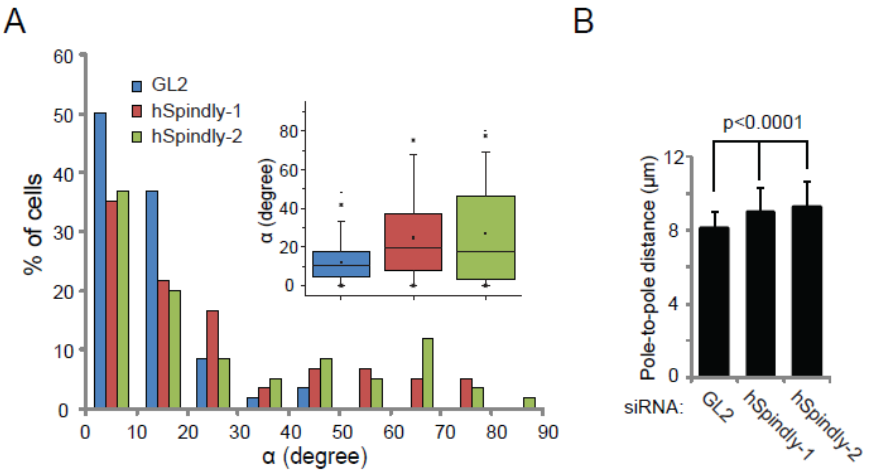

Figure 36. hSpindly depletion induces spindle misorientation and spindle elongation. (A) Cells were treated with GL2, hSpindly-1, or hSpindly-2 siRNAs for 48 h. MG132 was added for 2 h before fixation. Spindle angles were calculated by the same method as used in Figure 35D, except that centrin-3 was used as a centriolar marker and Z-stacks were taken every 0.2 μm. Only bipolar mitotic cells with well-separated spindle poles (x > 6 μm) were counted (60 cells, P < 0.0002). **(B)** Bar graph showing the pole-to-pole distances (x) of the cells in B. Error bars show the s.d after performing measurements on 60 cells.

Next, we analyzed both astral MTs and the actin cytoskeleton, previously shown to be required for proper spindle orientation in HeLa S3 cells (Toyoshima and Nishida, 2007). We did not observe defects in astral MT formation or cortical actin pattern in hSpindly-depleted cells (Figures 37A and 37B). EB1-depletion and cytochalasin B treatment were used as positive controls, respectively.

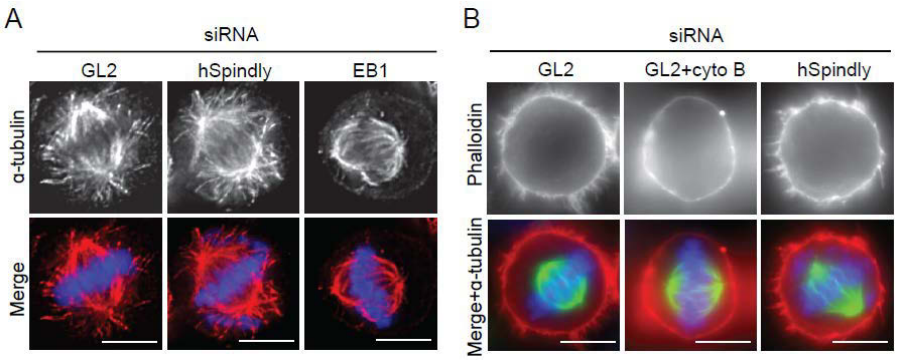

Figure 37. Depletion of hSpindly does not affect astral MTs and cortical actin. (A) Cells were treated with GL2, hSpindly, or EB1 siRNAs for 48 hand stained with anti–α-tubulin (red) and DAPI (blue). **(B)** Cells were treated with GL2 or hSpindly siRNAs for 48 h. Cytochalasin B (cyto B) or DMSO was added to the cells 1 h before they were stained with anti–α-tubulin (red) and DAPI (blue).

To examine whether hSpindly regulates spindle orientation through dynein, we analyzed the spindle rotation in HeLa Kyoto cells stably expressing GFP-α-tubulin/cherry-H2B, by imaging metaphase (MG132-treated) cells for 2 h. More than 60% of hSpindly-depleted cells, but only ~ 30% of GL2-treated cells, showed misoriented chromosomes and spindles. Strikingly, co-depletion of dynein heavy chain 1 (DHC) (Toyoshima et al., 2008) partially rescued the

orientation defects induced by hSpindly depletion (~ 40% of cells) (Figures 38A and 38B). As depletion of DHC affects spindle assembly (an example of a DHC-depleted cell that never forms a bipolar spindle is shown in Figure 38C), we selected only metaphase cells for analysis. Co-depletion of hSpindly and DHC effectively decreased the levels of both proteins (Figure 38D). Finally, we failed to detect cortical hSpindly (Figure 38E) and hSpindly depletion did not noticeably alter dynein/dynactin localization to the cell cortex (Figure 38F), suggesting that hSpindly does not regulate cortical dynein.

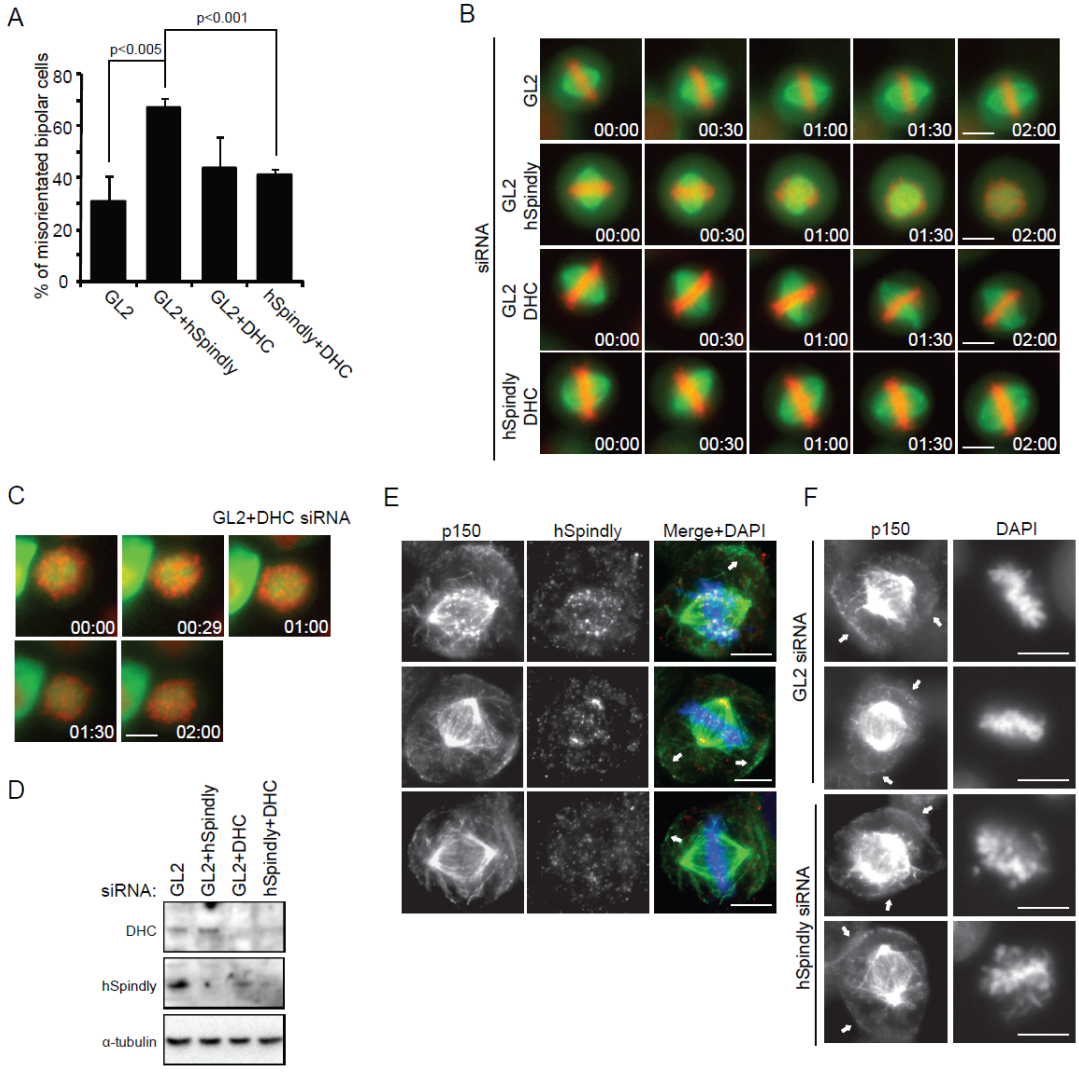

Figure 38. hSpindly depletion induces spindle misorientation in a dynein-dependent manner. (A) GFP-α-tubulin/cherry-H2B expressing HeLa Kyoto cells were treated with the indicated combinations of siRNAs for 54 h and synchonized by double thymidine block and release. 9 h after the second release MG132 was added for 1 h before filming. Bar graph shows the percentages of cells with spindle rotation defects. Error bars show the s.d from 3 experiments (>15 cells per experiment). **(B)** Representative stills from movies of cells treated as in (A). Time is shown in hh: mm. t = 0 was defined as the time point were chromosomes aligned in the metaphase plate. **(C)** Stills of a DHC-depleted cell displaying defects in bipolar spindle formation. Time is shown in hh: mm. **(D)** HeLa Kyoto

cells stably expressing GFP-α-tubulin/cherry-H2B were treated with different combinations of siRNAs as indicated for 48 h. Lysates were prepared and equal amounts of cell extracts were separated by SDS-PAGE and probed by Western blotting with indicated antibodies. **(E)** Cells stained with anti-p150^{Glued} (green) and anti-hSpindy antibodies (red) and DAPI (blue). Arrows indicate p150^{Glued} cortical staining. **(F)** Cells were treated with GL2 or hSpindly siRNAs for 48 h and stained with anti-p150^{Glued} antibody and DAPI. Arrows show p150^{Glued} cortical staining. Bars = 10 μm.

The above results suggested that it is the KT pool of dynein that contributes to control spindle orientation. According to this notion, depletion of *bona fide* KTs core components should result in a similar rotation phenotype as the depletion of hSpindly. Indeed, clear spindle misorientation (comparable to hSpindly depletion) and spindle elongation were observed upon Hec1 or CenpA depletion (Figures 39A and 39B; the efficiency of CenpA siRNA is shown in Figure 39C). Collectively, our results suggest that spindle misorientation induced by hSpindly depletion is due primarily to mislocalization of KT dynein.

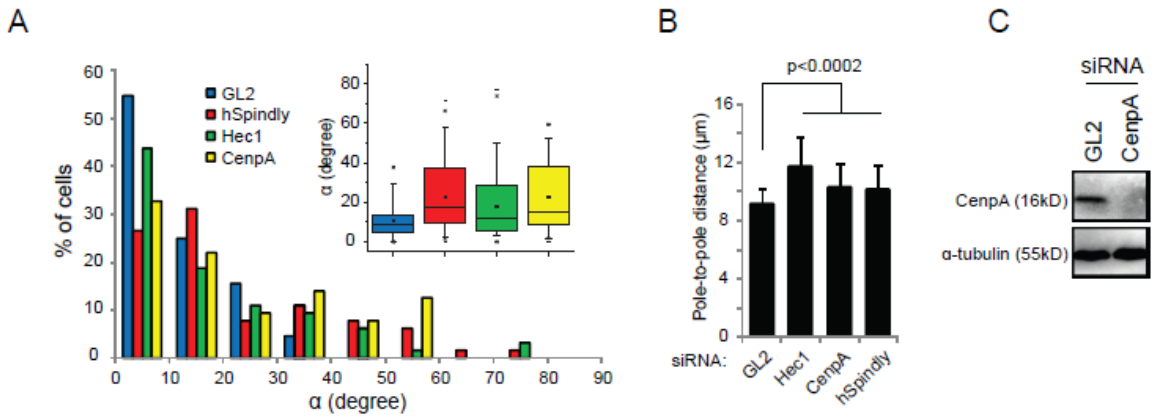

Figure 39. Requirement of general KT structure for proper spindle orientation. (A) Cells were treated with GL2, hSpindly, Hec1, or CenpA siRNAs for 48 h and MG132 was added for 1 h before fixation. Spindle angles were calculated by the same method as used in Figure 31D. ≥60 cells were measured ($P < 0.0002$). **(B)** Bar graph shows the pole-to-pole distances (x) of the cells as in (A). Error bars show the s.d after performing measurements on ≥60 cells. **(C)** Cells were treated with GL2 or CenpA siRNAs for 48 h. Western blotting was performed with anti-CenpA antibody; α-tubulin is shown as loading control.

1.10 CDK1 phosphorylation of hSpindly C-terminus does not affect its localization

Finally, to understand how hSpindly is targeted to KTs, we devoted efforts to map the region responsible for its KT localization. The N-terminus of hSpindly contains mainly a coiled-coil domain, while the C-terminus does not contain any predicted secondary structure but five conserved putative CDK1 sites (T509, S515, T552, S555 and T597) (Figure 19A). To test which region of hSpindly is responsible for its KT localization, we generated and tested two truncations of the protein: the N-terminus comprising amino acids 1-444 (1-444) and the C-terminus

comprising amino acids 443-605 (443-605). Cells were treated with hSpindly siRNA and complemented with full length, 1-444 or 443-605 hSpindly constructs. Only the full length protein localized to KTs, suggesting that both the N- and C-terminus are required for proper KT localization of hSpindly (Figure 40A).

Next, we investigated whether CDK1-mediated phosphorylation of hSpindly controls its localization. We confirmed that hSpindly can be phosphorylated by cyclin B-CDK1 *in vitro* and mutating five putative CDK1 sites to alanine (generating a non-phosphorylatable 5A mutant) abolished Cdk1 phosphorylation (Figure 40B). To examine the effect of CDK1-mediated phosphorylation, we also generated the phosphomimetic mutant by substituting the CDK1 sites to aspartate (5D mutant) and investigated hSpindly-depleted cells expressing either WT hSpindly or the phospho-mutants (5A and 5D). Similar to WT, both the 5A and 5D mutants could localize to unattached KTs and rescued the KT localization of p150 (Figure 40C). In addition, both phospho-mutants were relocalized to the spindle poles in late prometaphase (Figure 40D). Altogether, these data show that CDK1-mediated phosphorylation of hSpindly is not required for both its KT recruitment and subsequence transport to spindle poles.

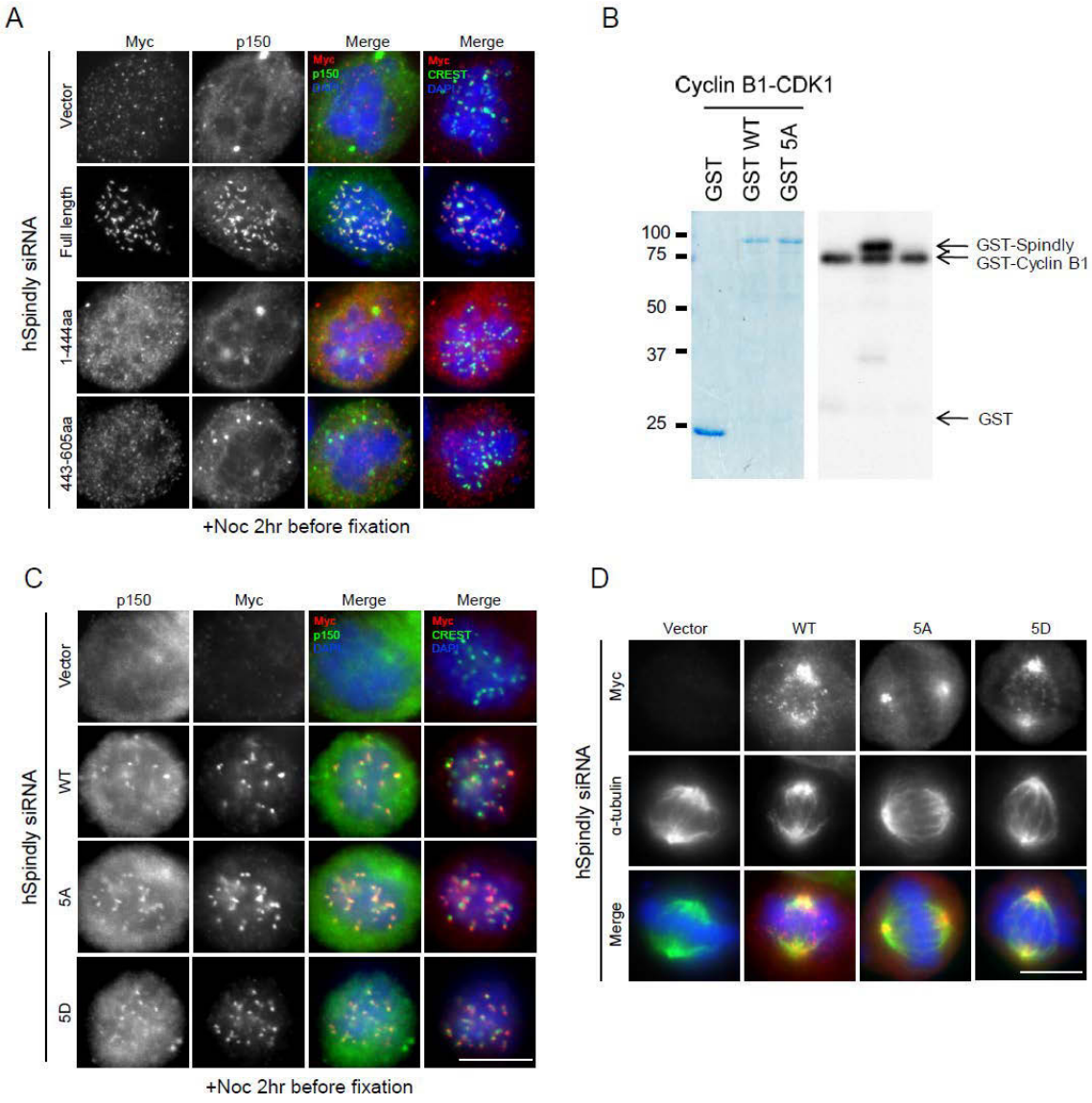

Figure 40. KT localization of hSpindly requires both N- and C-terminus but is not regulated by CDK1 phosphorylation. (A) HeLa S3 cells were transfected with hSpindly siRNA and plasmids expressing full length, 1-444 or 443-605 amino acids of hSpindly. Cells were treated with 2 h nocodazole before stained with 9E10 serum (red), anti-p150 antibody and CREST serum (green), and DAPI (blue). **(B)** *In vitro* Cyclin B1-CDK1 kinase assays of GST-hSpindly^{WT} and GST-hSpindly^{5A}. GST alone serves as negative control. Coomassie-stained gel (left panel) and autoradiogram (right panel) show protein loading and protein phosphorylation, respectively. **(C)** Cells were treated with hSpindly siRNA and plasmids expressing WT, 5A or 5D mutants of hSpindly. Cells were treated with 2 h nocodazole before stained with 9E10 serum (red), anti-p150 antibody and CREST serum (green), and DAPI (blue). **(D)** Cells were treated as in (C) except stained with 9E10 serum (red), anti-α-tubulin (green) and DAPI (blue). Bars = 10 μm.

Discussion I

In the first part of this thesis we have dissected the diverse functions of human Spindly. We show that hSpindly localizes to the outer KTs during prometaphase and relocalizes to the spindle poles prior to metaphase, in a MT- and dynein/dynactin-dependent manner. Similar to *Drosophila* Spindly and *C. elegans* SPDL-1 (Gassmann et al., 2008a; Griffis et al., 2007), the RZZ complex acts as an upstream regulator of hSpindly. However, in human cells, the RZZ complex not only controls localization of hSpindly but also its protein level, suggesting that hSpindly is stabilized through association with the RZZ complex. SPDL-1 could be co-immunoprecipitated with Zwilch from *C. elegans* extracts (Gassmann et al., 2008a). Similarly, we were able to coimmunoprecipitate hSpindly with ZW10 and Rod, provided that detergents were omitted, and our glycerol gradient analysis is also consistent with an interaction between hSpindly and the RZZ complex. We propose that hSpindly forms transient and dynamic interactions with the RZZ complex, rather than being a stable subunit of the complex. The fact that Hec1/Ndc80 depletion mislocalized both ZW10 and hSpindly without affecting the corresponding protein levels indicates that KT localization is not a pre-requisite for the stability of hSpindly. Similar to the RZZ complex (Famulski and Chan, 2007), Aurora B activity controls hSpindly localization in response to taxol. Although this might be interpreted to suggest a tension-sensitive localization of hSpindly, we emphasize that hSpindly occasionally showed an asymmetric localization on sister KTs, especially in monastrol-treated cells, arguing that hSpindly localization responds to a particular state of KT-MT attachment (or MT dynamics) rather than tension across the inner centromeres. Interestingly, inhibition of Aurora B also caused a reduction in hSpindly levels, suggesting a regulatory relationship between the two proteins, likely through the RZZ complex. We found that hSpindly is phosphorylated by Cdk1 but have so far been unable to phosphorylate the protein by Aurora B. Similarly, we have not been able to phosphorylate ZW10 (data not shown). Thus, if Aurora B regulates the interaction between hSpindly and the RZZ complex by direct phosphorylation of one of the subunits, this most likely involves other members of the RZZ complex.

The role of Spindly in the KT recruitment of dynein is apparently well conserved amongst species. In contrast, whereas *Drosophila* Spindly recruits dynein but not dynactin (Griffis et al., 2007), both hSpindly and *C. elegans* SPDL-1 recruit both complexes to KTs

(Gassmann et al., 2008a). KT dynein is believed to control the initial lateral interaction between KTs and MTs and facilitate the subsequent formation of end-on attachments mediated by the Ndc80 complex (Gassmann et al., 2008a; Rieder and Alexander, 1990; Vorozhko et al., 2008). Consistent with this notion, chromosome misalignment was induced by either depletion of hSpindly or ZW10 ((Li et al., 2007; Yang et al., 2007b); this study). Remarkably, however, only cells depleted of hSpindly showed an overall lengthening in the duration of M phase, likely because cells depleted of ZW10 compensate a prolonged prometaphase with a premature onset of anaphase (Yang et al., 2007b), due to SAC defects (Buffin et al., 2005; Kops et al., 2005). Thus, the specific defects resulting from the impaired recruitment of dynein to KTs can more readily be visualized in hSpindly-depleted cells, as this protein is not required for SAC activity.

KT dynein was suggested to be required for the generation of tension across sister KTs (Howell et al., 2001; Yang et al., 2007b). The decreased inter-KT distance observed upon hSpindly depletion clearly supports this notion. Furthermore, the increase in spindle length upon hSpindly knock-down is in agreement with the idea that KT dynein facilitates the formation of load-bearing attachment, as is the case for SPDL-1 (Gassmann et al., 2008a). For *C.elegans* it was further proposed that the RZZ complex negatively regulates the MT-binding activity of the Ndc80 complex at tensionless KTs (Gassmann et al., 2008b). The data obtained here for HeLa S3 cells suggest that the functions of hSpindly and ZW10 differ significantly between species. First, in human cells the RZZ complex controls not only the localization but also the stability of hSpindly, whereas in invertebrates it apparently controls only localization. Second, the depletion of Hec1/Ndc80 abolished KT localization of both ZW10 and hSpindly in human cells, but not in *C. elegans* (Gassmann et al., 2008b; Yamamoto et al., 2008). Third, KNL-1 in *C. elegans* is required for KT targeting of both Ndc80 and RZZ complexes (Desai et al., 2003; Gassmann et al., 2008b), whereas Blinkin, its human homologue, is not required for the KT localization of Hec1/Ndc80 (Kiyomitsu et al., 2007). Together with data from the literature, our present results suggest that in human cells hSpindly and the RZZ complex act downstream of the Ndc80 complex to recruit dynein/dynactin.

Interference with Spindly function in different species also revealed fundamental differences with regard to the role of KT dynein during SAC inactivation. Several studies have implicated dynein/dynactin in the silencing of the SAC through the removal of checkpoint proteins, such as MAD2 and the RZZ complex, from KTs and their transport along MTs to

spindle poles (Basto et al., 2004; Griffis et al., 2007; Howell et al., 2001; Mische et al., 2008; Sivaram et al., 2009; Varma et al., 2008; Whyte et al., 2008; Wojcik et al., 2001). In contrast, hSpindly depletion did not block the removal of MAD2 and ZW10 from aligned chromosomes. Furthermore, we seldom observed a complete inhibition of SAC protein removal upon overexpression of p50-dynamitin in metaphase cells. These could either reflect an incomplete depletion/disruption of hSpindly/the dynein/dynactin complex, respectively, or alternatively, the existence of a dynein-independent removal mechanism that is able to compensate for the loss of dynein. Two recent studies provide evidences to support the existence of a dynein-independent mechanism (Barisic et al., 2010; Gassmann et al., 2010). Consistent with our data, these studies also reported that depletion of hSpindly does not impair the removal of KT proteins (Mad1/2, the RZZ, etc.) from aligned KTs. However, when cellular ATP levels were reduced, KT proteins were retained at KTs in hSpindly-depleted cells, in contrast to control cells in which those proteins showed clear pole accumulation (Gassmann et al., 2010). This suggests the presence of a compensatory mechanism for removal of KT components. Interestingly, mutating or deleting the conserved Spindly box domain still allowed hSpindly to localize to KTs but prevented dynein KT recruitment. These mutants persisted even at aligned KTs. Expression of the Spindly box-mutants leaded to the retention of Mad1/2 at aligned KTs. These results indicate that the dynein-independent mechanism is suppressed when hSpindly cannot be removed from KTs (Barisic et al., 2010; Gassmann et al., 2010).

Importantly, we also found that depletion of hSpindly or ZW10 induced frequent spindle rotation, similar to what had previously been observed upon depletion of the dynein regulator Nde1 (Feng and Walsh, 2004) and depletion or overexpression of LIS1 (Faulkner et al., 2000; Yingling et al., 2008). These proteins are well known to determine the stability of astral MTs, the cortical localization of dynein and proper spindle assembly (Faulkner et al., 2000; Feng et al., 2000; Feng and Walsh, 2004; Yingling et al., 2008). In addition, ZW10, Nde1 and dynein are also required for the integrity of the Golgi apparatus (Hirose et al., 2004; Liang et al., 2004), but this is not the case for hSpindly (data not shown). These studies thus suggest that ZW10, Nde1/Ndel1 and LIS1 regulate dynein activity both at the KT and elsewhere, whereas hSpindly exclusively controls the function of dynein at KTs.

So, how could hSpindly depletion lead to spindle misorientation? hSpindly was undetectable at the cortex or on astral MTs. Furthermore, neither the actin cytoskeleton nor the

cortical localization of dynein was detectably impaired in hSpindly-depleted cells. Yet, remarkably, the spindle rotation phenotype could be rescued by co-depletion of dynein. The observation that a comparable spindle orientation defect could also be induced by depletion of Hec1 or CenpA highlights a role of KTs in spindle orientation and supports the notion that spindle misorientation induced by hSpindly depletion is due to interference with KT-associated but not cortical dynein. It seems plausible, therefore, that KT forces cooperate with cortical forces essential for spindle orientation.

In summary, our characterization of hSpindly helps to understand which dynein-mediated processes require dynein accumulation at the kinetochore (notably chromosome congression) and which processes do not (notably SAC silencing). Both chromosome alignment and KT tension are now confirmed to be regulated by KT-associated dynein/dynactin complexes, which in turn are regulated by Spindly and the RZZ complex in all metazoans. In contrast, the mechanism by which hSpindly and KT dynein control spindle orientation awaits to be elucidated.

Part II. Aurora B controls kinetochore-microtubule attachments by modulating the interaction between the Ska complex and the KMN network.

Introduction II

2.1 The KT-MT interphase

Chromosome alignment and segregation requires that all KTs establish stable bioriented attachments to the spindle MTs. Central to this process and providing the core KT-MT attachment interface at outer KTs is the conserved KMN network, composed of the KNL1 protein, the four-subunit Mis12 complex (Mis12, Mis13, Mis14 and Nnf1) and the four-subunit Ndc80 complex (Hec1, Nuf2, Spc24 and Spc25) (Santaguida and Musacchio, 2009). Both the Ndc80 complex and KNL1, but not the Mis12 complex, bind directly to MTs *in vitro* (Cheeseman et al., 2006). The Mis12 complex instead serves as a scaffold to form the KMN network and it synergistically enhances the MT binding activity of KNL1 and the Ndc80 complex (Cheeseman et al., 2006). Furthermore, the Mis12 complex provides the connection to the inner KT/centromere by directly interacting with CENP-C (Przewloka et al., 2011; Screpanti et al., 2011) and HP1 (Kiyomitsu et al., 2010).

2.2 Identification of the Ska complex

Other proteins localize to the KT-MT interface during mitosis and are likely to contribute to the formation of functional connections such that chromosome biorientation can be achieved. Prominent among these is the Ska complex, composed of Ska1, 2 and 3. Ska1, originally C18orf24, was first identified as a novel spindle component in a proteomic survey conducted in our laboratory (Sauer et al., 2005). Subsequently, Ska2 (Fam33a) was shown to interact with Ska1 in a yeast two-hybrid screen (Hanisch et al., 2006). Finally, Ska3 (C13orf3, also Rama1) was identified as a subunit of the Ska complex by co-immunoprecipitation with Ska1 and Ska2 in two independent studies (Gaitanos et al., 2009; Welburn et al., 2009). The formation of the Ska complex was confirmed by the *in vitro* reconstitution with recombinant proteins (they form a ternary complex comprising two copies of each subunit) and also by directed yeast two-hybrid interactions (Gaitanos et al., 2009; Theis et al., 2009; Welburn et al., 2009). *In vivo*, all three Ska members colocalize at outer KTs and siRNA-mediated depletion of any of them reduces the expression levels of the others, demonstrating that they function as an entity (Gaitanos et al., 2009; Hanisch et al., 2006; Welburn et al., 2009).

2.3. The function of the Ska complex

The Ska complex is required to generate stable KT-MT attachment during mitosis in human cells (Gaitanos et al., 2009; Hanisch et al., 2006; Raaijmakers et al., 2009; Theis et al., 2009; Welburn et al., 2009). The Ska complex can directly bind to MTs *in vitro* (Welburn et al., 2009). Efficient depletion of the Ska complex leads to a severe attachment phenotype and unstable K-fibers, reminiscent of the KT-null phenotype observed upon Ndc80 depletion (Gaitanos et al., 2009; Raaijmakers et al., 2009; Welburn et al., 2009) (see however (Daum et al., 2009)). As the Ska complex is recruited to KTs through the Ndc80 complex, the phenotype observed in Ndc80-depleted cells might reflect the loss of both the Ncd80 complex and the Ska complex. The available evidence thus suggests that the Ska complex acts in concert with the KMN network and that both complexes are essential for generating stable end-on attachments. Therefore, key to understanding how functional KT-MT attachments are stabilized in mitosis, is to determine if and how the Ska complex interacts with members of the KMN network and how this is regulated in time and space (Figure 41).

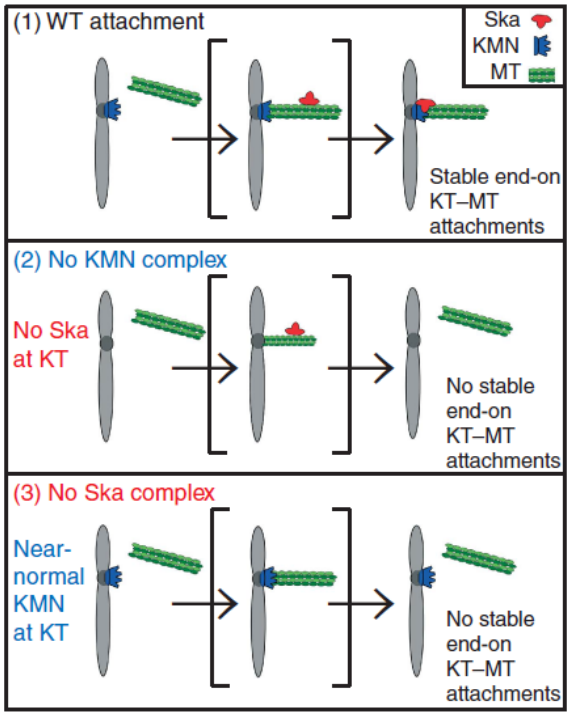

Figure 41. The proposed model for the requirement of the Ska complex for KT-MT attachments. The KMN network alone is not sufficient to form stable attachment. It requires subsequent recruitment of the Ska complex. Depletion of either the KMN or the Ska impairs the ability of KT to form stable attachments. Thus, the KMN and Ska co-operate to mediate stable KT-MT interactions. *Illustration adapted from Gaitanos et al., EMBO J, 2009*

Results II

2.1 Negative regulation of Ska KT localization by Aurora B activity

We have previously observed that the localization of the Ska complex depends on MT occupancy at KTs, as nocodazole or vinblastine-induced MT depolymerization led to a strong reduction of Ska1 and Ska3 KT recruitment (Gaitanos et al., 2009; Hanisch et al., 2006). To obtain insight into the regulation of KT-MT attachment by the Ska complex, we first investigated how the KT localization of this complex is controlled. In agreement with our previous observations, Ska3 staining intensity at metaphase KTs was about twofold higher than that at prometaphase KTs (Figures 42A and 42B). In addition, Ska levels were clearly reduced at misaligned KTs when compared to aligned KTs (Figure 42C), indicating that the Ska complex preferentially accumulates at fully attached and bioriented KTs.

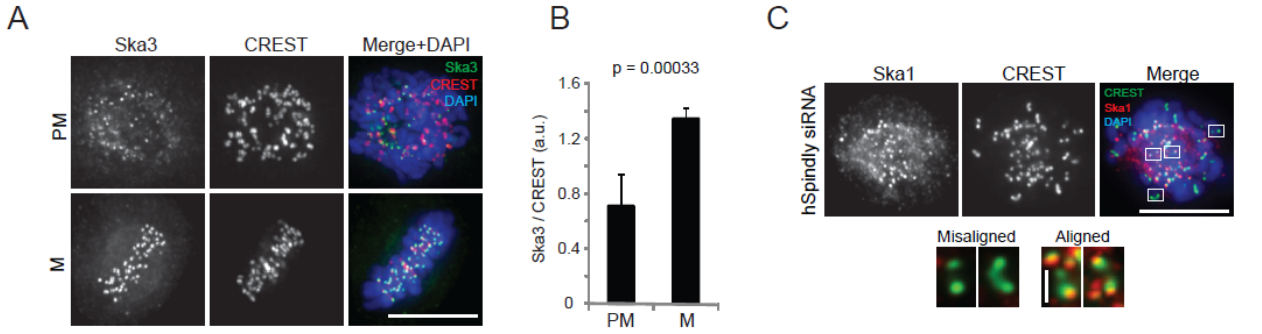

Figure 42. The Ska complex preferentially accumulates at aligned KTs. (A) HeLa S3 cells in prometaphase (PM) or metaphase (M) were fixed with PTEMF and stained with anti-Ska3 antibody (green), CREST serum (red) and DAPI (blue). **(B)** Bar graph showing the quantification of Ska3 staining intensity at KTs (normalized against CREST) of cells as in (A) (>100 KTs from 5 cells, error bars indicate the standard derivation (s.d) of 5 cells), a.u. = arbitrary units. **(C)** HeLa S3 cells were treated with hSpindly siRNA for 48 h before staining with anti-Ska1 antibody (red), CREST serum (green) and DAPI (blue). Insets at the bottom right side show examples of misaligned and aligned KTs (scale bar, 1 µm).

It has been recently shown that phosphorylation of Aurora B substrates at outer KTs decreases as KTs become bioriented and tension is established (Liu et al., 2009; Welburn et al., 2010). Therefore, we asked whether Aurora B might be responsible for removing Ska from unattached KTs. For this purpose, Ska3 localization was monitored in nocodazole-treated cells that had been incubated with the small molecule inhibitor of Aurora B ZM447439 (Ditchfield et al., 2003b). In parallel, we also tested the effects of inhibiting other prominent mitotic kinases such as Mps1 (by using Mps1-IN-1 (Kwiatkowski et al., 2010) or reversine (Santaguida et al., 2010)) or Plk1 (by using TAL (Santamaria et al., 2007)). Cold treated-cells were included to

serve as a positive control, as we have previously observed that exposure to low temperature is able to rescue the KT localization of Ska proteins in nocodazole-treated cells by a yet unknown mechanism (Gaitanos et al., 2009; Hanisch et al., 2006). Indeed, inhibition of Aurora B, but not Mps1 or Plk1, restored the KT staining of Ska3 (Figures 43A and 43B). Similar results were obtained when exogenous GFP^{LAP}-Ska2 and endogenous Ska1 were examined (Figures 43C and 43D), indicating that inhibition of Aurora B produces a change in the localization of the entire Ska complex. To further strengthen the notion that Aurora B negatively regulates Ska localization at KTs, we took a reciprocal approach. We expressed a Mis12-INCENP-GFP fusion protein, which has been shown to increase phosphorylation of Aurora B substrates by recruiting additional Aurora B to outer KTs (Liu et al., 2009). Expression of Mis12-INCENP-GFP resulted in a clear twofold reduction of Ska3 staining at KTs (Figures 43E and 43F). In contrast, a Mis12-INCENP (TAA)-GFP mutant, which is unable to activate Aurora B (Sessa et al., 2005), had no effect on Ska3 levels at KTs (Figures 43E and 43F). Taken together, we conclude that Aurora B activity counteracts Ska localization at KTs.

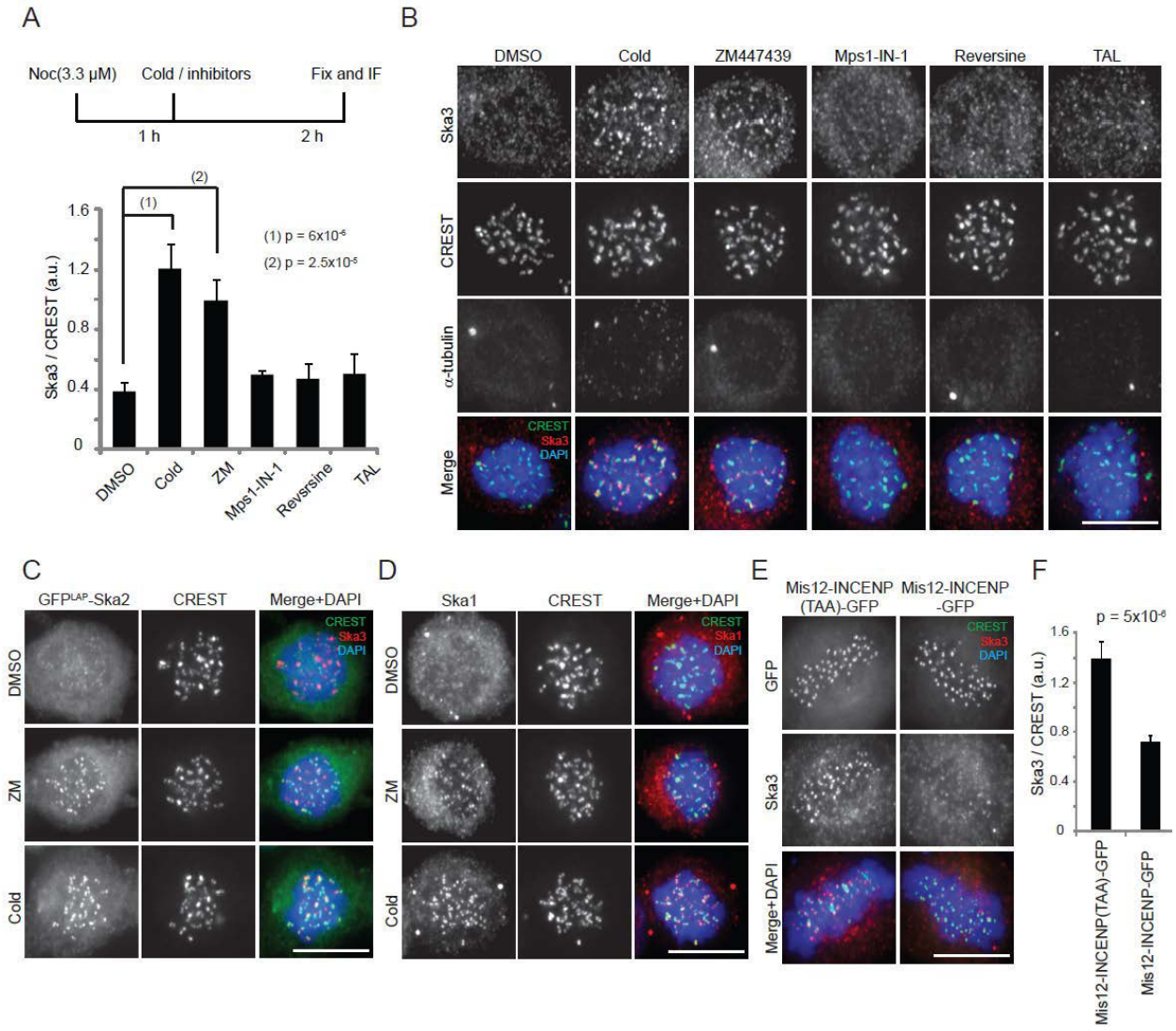

Figure 43. Aurora B antagonizes Ska complex localization to KTs. (A) Upper panel: Schematic representation of the protocol employed in (B). Lower panel: Bar graph showing the quantification of Ska3 staining intensity at KTs (normalized against CREST) of cells as in (B) (>100 KTs from 5 cells, error bars indicate the s.d of 5 cells). **(B)** HeLa S3 cells treated as in (A) were fixed with PTEMF and stained with anti-α-tubulin and anti-Ska3 antibodies (red), CREST serum (green) and DAPI (blue). **(C)** GFP^{LAP}-Ska2 expressing HeLa cells were treated with 3.3 µM nocodazole (Noc) for 1 h followed by 2 h treatment with DMSO, TAL, ZM447439 (ZM) or cold exposure. Cells were then stained with CREST serum (red) and DAPI (blue), GFP signal is shown in green. **(D)** HeLa S3 cells were treated with nocodazole for 1 h followed by 2 h treatment with DMSO, ZM or exposure to cold. Cells were then stained with anti-Ska1 antibody (red), CREST serum (green) and DAPI (blue). **(E)** HeLa S3 cells were transfected with plasmids encoding either Mis12-INCENP-GFP or Mis12-INCENP (TAA)-GFP. Cells were then stained with anti-Ska3 antibody (red), CREST serum (green) and DAPI (blue). GFP signal is shown in green. **(F)** Bar graph showing the quantification of Ska3 staining intensity at KTs (normalized against CREST) of cells as in (E) (>100 KTs from 5 cells, error bars indicate the s.d of 5 cells). Bars = 10 µm.

2.2 Aurora B-dependent interaction between Ska and KNM complexes

Next, we investigated how Aurora B influences the KT recruitment of the Ska complex. It has been previously shown that the KT localization of Ska proteins depends on the Ndc80 complex (Gaitanos et al., 2009; Hanisch et al., 2006; Raaijmakers et al., 2009; Welburn et al., 2009). We thus asked whether the other KMN components, namely KNL1 and the Mis12 complex, are also required for Ska localization to KTs. Indeed, depletion of not only Hec1, but also KNL1 or Mis13 abolished the KT localization of Ska3 without affecting Ska protein levels (Figures 44A-C).

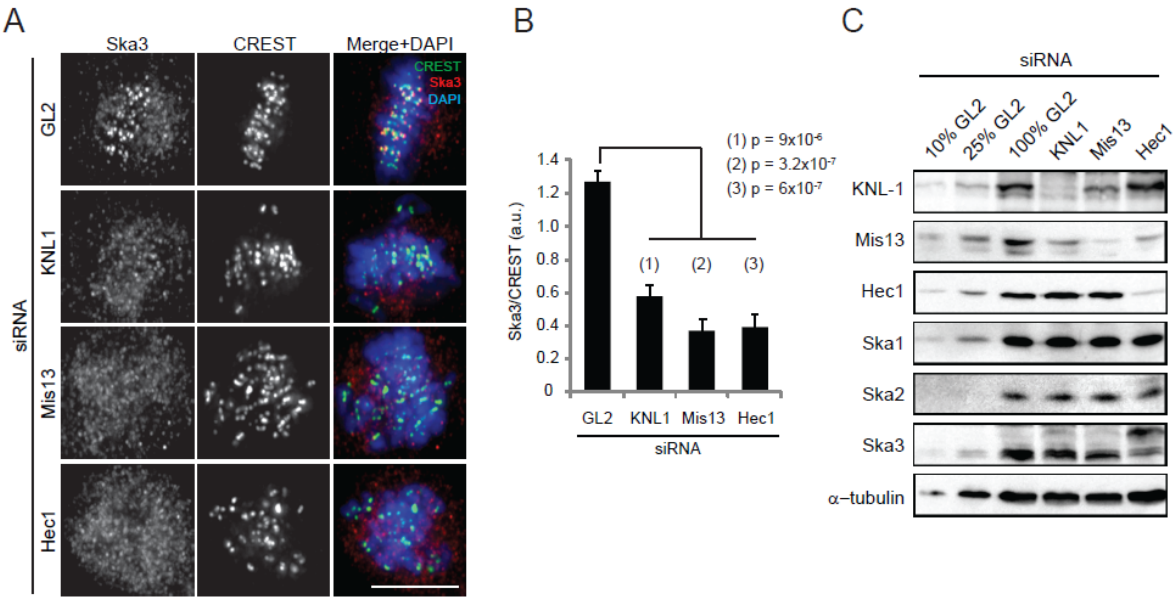

Figure 44. The KMN network is required for the KT recruitment of Ska. (A) Cells were treated for 48 h with GL2, KNL1, or Hec1 siRNAs or for 72 h with Mis13 siRNA before staining with anti-Ska3 antibody (red), CREST serum (green) and DAPI (blue). **(B)** Bar graph showing the quantification of Ska3 staining intensity at KTs (normalized against CREST) from cells as in (A) (>100 KTs from 5 cells, error bars indicate the s.d of 5 cells). **(C)** Cells were treated for 48 h with GL2, KNL1, or Hec1 siRNAs or for 72 h with Mis13 siRNA. Lysates were obtained and analyzed by Western blotting with indicated antibodies. Different amounts of GL2 siRNA-treated lysate were loaded to allow rough estimation of the depletion efficiency. Bars = 10 μm.

To see if Aurora B plays a role in the KMN-dependent localization of the Ska complex at KTs, we tested whether Aurora B inhibition can still rescue the KT localization of Ska3 in cells that were depleted of the KMN network. When cells depleted of KNL1, Mis13, Hec1 or GL2 (as control) were treated with nocodazole or nocodazole followed by ZM447439, Aurora B inhibition did not restore Ska3 to the KT in KNL1, Mis13 or Hec1-depleted cells, although it did so in control (GL2-treated) cells (Figures 45A and 45B). These results led us to speculate that Aurora B regulates the interaction between the KMN and Ska complexes. To test this possibility,

we investigated whether KMN components could be co-immunoprecipated with Ska proteins and whether Aurora B inhibition might strengthen this interaction. Indeed, Mis12 could readily be co-immunoprecipitated with the Ska complex and the interaction was clearly enhanced when cells were treated with ZM447439 (Figure 45C and 45D). Aurora B inhibition also revealed an interaction between the Ska complex and Hec1, although we failed to detect KNL1 in our Ska1 immunoprecipitates (Figure 45C and 45D).

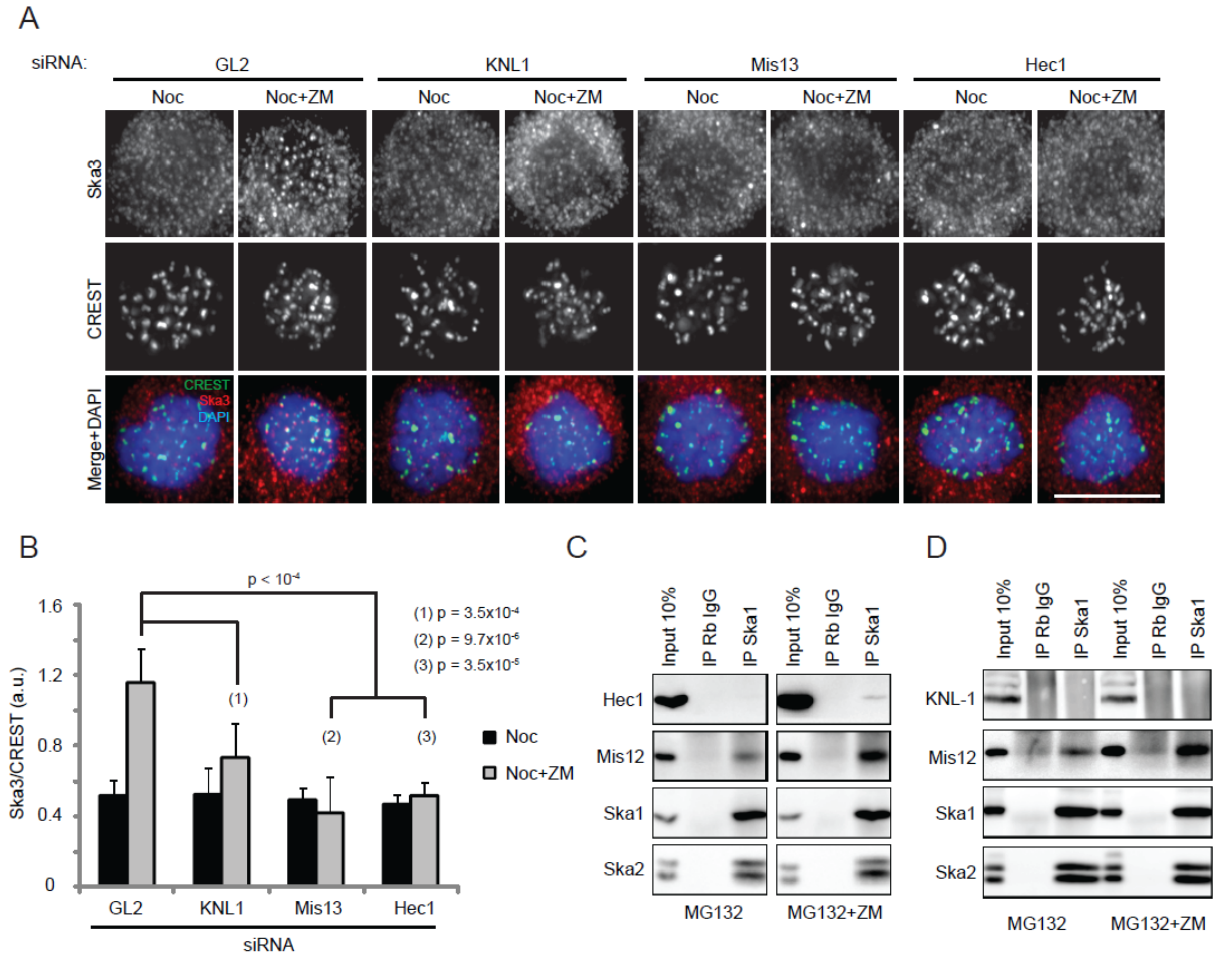

Figure 45. Aurora B regulates the interaction between Ska and KMN. (**A**) HeLa S3 cells were treated for 48 h with GL2, KNL1 or Hec1 siRNAs or for 72 h with Mis13 siRNA prior to treatment with 3.3 µM nocodazole (Noc) for 1 h and a 2 h incubation with DMSO or ZM447439 (ZM). Cells were then fixed with PTEMF and stained with anti-Ska3 antibody (red), CREST serum (green) and DAPI (blue). (**B**) Bar graph showing the quantification of Ska3 staining intensity at KTs (normalized against CREST) of cells treated as in (A) (>100 KTs from 5 cells, error bars indicate the s.d of 5 cells). (**C, D**) Nocodazole (0.33 µM)-arrested mitotic cells were released into medium containing MG132 or MG132 plus ZM. After 2 h, cells were collected and immunoprecipitation was performed with either rabbit IgGs (as control) or anti-Ska1 antibody. Western blotting was performed with the indicated antibodies. Bars = 10 µm.

To see if any of the subunits of the Mis12 and Ndc80 complexes can interact with the Ska proteins, directed yeast two-hybrid experiments were performed. Importantly, we observed multiple interactions between members of the Ndc80 and Mis12 complexes and the Ska complex, namely Hec1 and Ska1, Mis13 and Ska2 and Spc24 and Ska3 (Figures 46A-D). To further map the regions of interaction, we made several truncations of Ska1, Hec1 and Mis13 and tested the interactions by yeast two-hybrid experiments. The N-terminus (aa 1-91) of Ska1 interacted with Hec1 (Figure 46E). However, none of the truncations of Hec1 and Mis13 interacted with Ska1 and Ska2, respectively (Figure 46F and 46G), suggesting that the full length proteins are required for interaction. Together, these results support the requirement of the KMN network to recruit the Ska complex to KTs and reveal the Aurora B-dependent regulation of such recruitment.

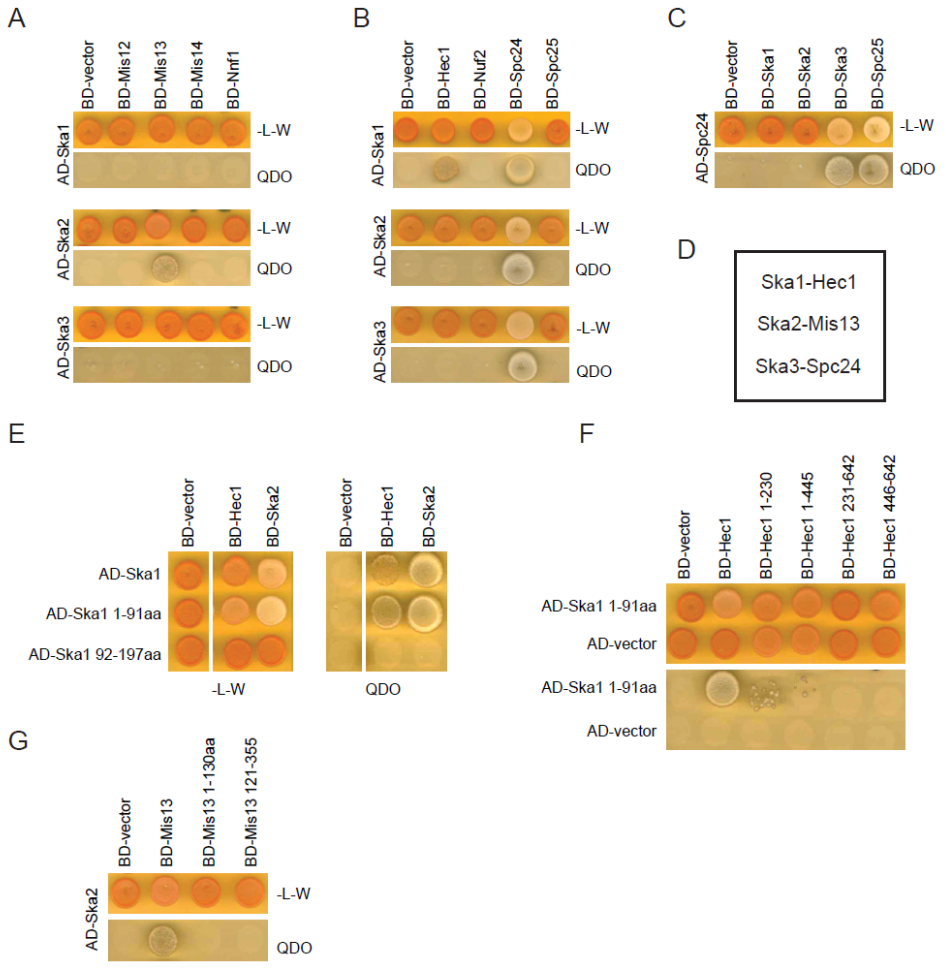

Figure 46. Directed yeast two-hybrid interactions between the KMN and Ska members. (A) Yeast two-hybrid interaction between the three Ska members fused to the activation domain (AD) and the Mis12 complex members fused to the binding domain (BD). Interaction was reflected by the growth on selective medium (QDO: -Leu/-Trp/-Ade/-His). For control, growth on non-selective plates (-L-W) is shown. (**B**) Yeast two-hybrid analysis between the three Ska members fused to the AD and the Ndc80 complex members fused to the BD. BD-Spc24 showed non-specific binding to the AD. (**C**) Yeast two-hybrid interaction between AD-Spc24 and the three Ska members fused to the BD. Only BD-Ska3 showed specific interaction with AD-Spc24. (**D**) Summary of the specific interactions identified in the yeast two-hybrid experiments. **(E)** Yeast two-hybrid analysis between the truncations of Ska1 and Hec1/Ska2. **(F)** Yeast two-hybrid analysis between the truncations of Hec1 and Ska1(1-91 aa). **(G)** Yeast two-hybrid analysis between the truncations of Mis13 and Ska2.

2.3 Phosphorylation of Ska1 and Ska3 by Aurora B *in vitro*

According to previous work, mitotic phosphorylation of Ska3 is at least partly Aurora B-dependent (Theis et al., 2009). To test whether Aurora B can directly phosphorylate any member of the Ska complex, we assayed the ability of recombinant Aurora B expressed in *E. coli* to phosphorylate a Ska complex reconstituted from recombinant full length proteins. Recombinant MCAK was included as a positive control (Andrews et al., 2004b; Lan et al., 2004b). Under these *in vitro* conditions, Ska1 and Ska3, but not Ska2, were readily phosphorylated by Aurora B (Figure 47A). This phosphorylation was completely abolished when samples were incubated with ZM447439, attesting to its specificity (Figure 47A). Examination of the Ska1 and Ska3 protein sequences revealed four conserved Aurora B consensus sites (K/R-X-T/S) (Cheeseman et al., 2002) in Ska1 (T157, S185, T205, S242), and two in Ska3 (S87 and S110) (Figures 47B and 47C). Furthermore, mass-spectrometry analysis following *in vitro* phosphorylation of the Ska complex by Aurora B identified a highly conserved site in Ska3 (S159). Although this site does not match the canonical Aurora B consensus (Figures 47B and 47C), a peptide spanning S159 of Ska3 was clearly phosphorylated when used as a substrate for Aurora B kinase on cellulose membranes (Figure 47D). In addition, several of the putative Aurora B sites in Ska proteins have been shown to be phosphorylated *in vivo* in phospho-proteomics studies performed on mitotic cells (Nousiainen et al., 2006; Olsen et al., 2010; Santamaria et al., 2011; Sui et al., 2008) (Figure 47C). To examine the physiological relevance of Ska complex phosphorylation, we generated mutants including all potential Aurora B sites in each Ska proteins, namely T157, S185, T205, S242 in Ska1 and S87, S110 and S159 in Ska3. Kinase assays performed on non-phosphorylatable mutants (denoted as $Ska1^{4A}$ and $Ska3^{3A}$) confirmed that these sites represent major targets of Aurora B in Ska1 and Ska3 (Figure 47E).

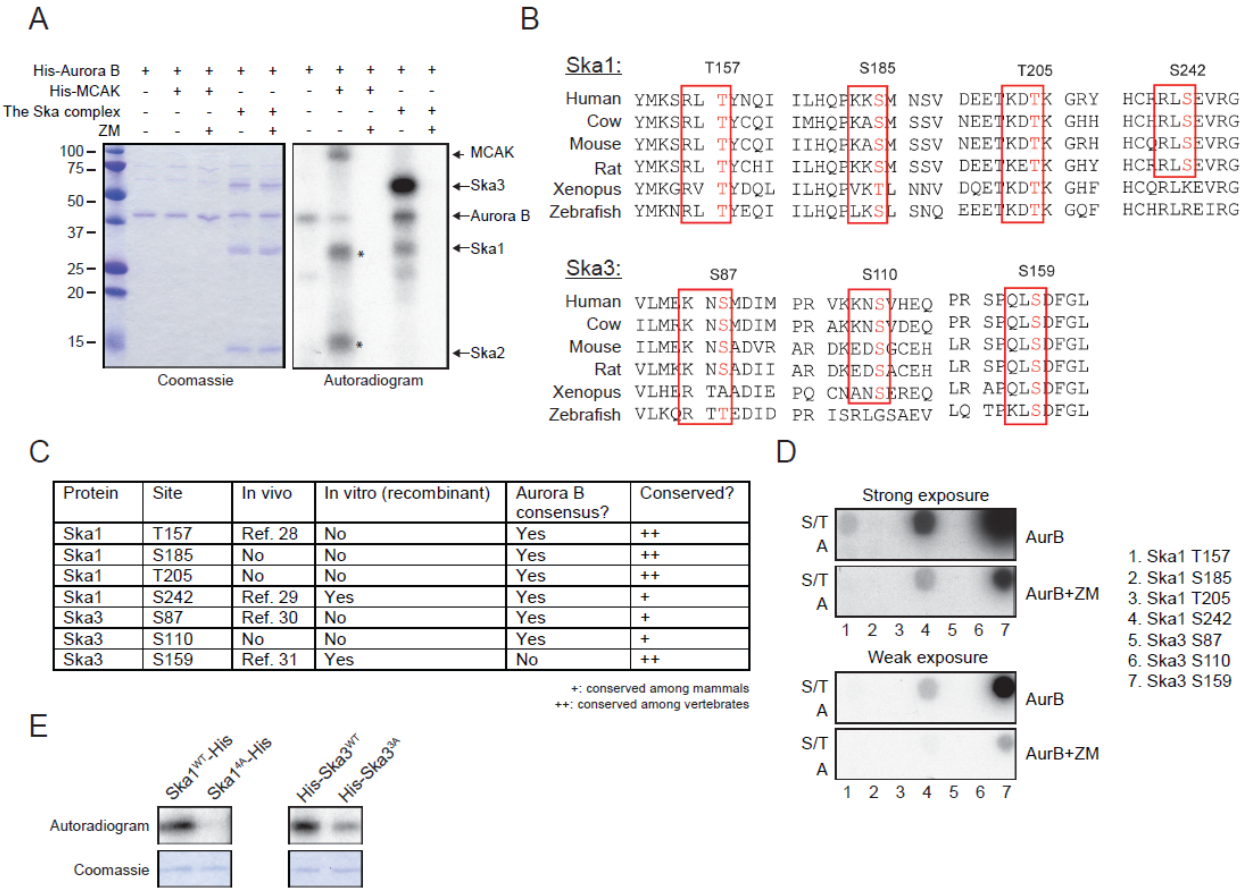

Protein	Site	In vivo	In vitro (recombinant)	Aurora B consensus?	Conserved?
Ska1	T157	Ref. 28	No	Yes	++
Ska1	S185	No	No	Yes	++
Ska1	T205	No	No	Yes	++
Ska1	S242	Ref. 29	Yes	Yes	+
Ska3	S87	Ref. 30	No	Yes	+
Ska3	S110	No	No	Yes	+
Ska3	S159	Ref. 31	Yes	No	++

+: conserved among mammals
++: conserved among vertebrates

Figure 47. Aurora B phosphorylates Ska1 and Ska3 *in vitro*. (A) *In vitro* kinase assay with Aurora B alone or Aurora B plus ZM447439 (ZM) on the Ska complex comprising recombinant full length proteins or His-MCAK (as positive control). Coomassie-stained gel (left panel) and the corresponding autoradiogram (right panel) show protein phosphorylation and equal protein loading, respectively. Asterisks indicate unspecific (likely degradation) bands in the MCAK preparation. **(B)** Sequence alignment of the potential Aurora B sites in Ska1 and Ska3 from the indicated species. The alignments were performed with CLUSTALW (http://npsa-pbil.ibcp.fr). Potential Aurora B sites conserved across species are marked with a rectangle. **(C)** Table summarizing the collected information for the seven potential Aurora B sites mutated in Ska1 and Ska3. **(D)** Immobilized Ska1 and Ska3 peptides (phosphoacceptor S/T or alanine) containing potential Aurora B sites synthesized directly on cellulose membranes were used as substrates for Aurora B *in vitro* kinase assays with or without ZM. Two different exposures are shown **(E)** *In vitro* Aurora B kinase assays of Ska1^{WT}-His and His-Ska3^{WT} and the corresponding non-phosphorylatable mutants. Autoradiogram (upper panel) and Coomassie-stained gel (lower panel) show protein phosphorylation and equal protein loading, respectively.

2.4 Proper mitotic progression requires both phosphorylation and dephosphorylation of Ska proteins

To assess the role of Aurora B phosphorylation on the Ska complex *in vivo*, we first investigated the effect of the phosphomimetic (to aspartate) and non-phosphorylatable (to alanine) mutants of Ska1 and Ska3 using an siRNA-based complementation approach, combined with live-cell imaging performed on HeLa S3 cells stably expressing H2B-GFP (Sillje et al., 2006)

(Figures 48A and 48B). Consistent with previous work (Gaitanos et al., 2009), co-depletion of Ska1 and Ska3 yielded a significant increase in mitotic timing (mean duration of 338 min from nuclear envelope break down (NEBD) to anaphase onset or mitotic cell death) and a significant number of cells died after prolonged arrest in mitosis (47.6%); for comparison, GL2-treated control cells proceeded rapidly from NEBD to anaphase (mean of 42 min) and virtually no mitotic cell death was observed (Figures 48A and 48C). Ska depleted-cells also showed prolonged prometaphase with obvious chromosome congression defects (62% of Ska-depleted cells showed misaligned chromosomes, compared to 3% in GL2 control cells) (Figures 48A and 48C). These defects were largely rescued by co-expressing $Ska1^{WT}$ and $Ska3^{WT}$ (mean of 85 min for mitotic timing, with only 3% cell death and 14% of cells with misaligned chromosomes) (Figures 48A and 48C. In contrast, expression of neither the non-phosphorylatable mutants ($Ska1^{4A}$ +$Ska3^{3A}$), nor the phosphomimetic mutants ($Ska1^{4D}$+ $Ska3^{3D}$) rescued the observed depletion phenotypes (mean of 246 min for mitotic timing, 23% and 38% of cell death and misalignment, respectively for $Ska1^{4A}$+$Ska3^{3A}$; mean of 297 min for mitotic timing, 31% and 40% of cell death and misalignment, respectively for $Ska1^{4D}$+$Ska3^{3D}$) (Figures 48A and 48C). These results show that dynamic control of Ska phosphorylation is essential for mitotic progression, since lack of phosphorylation as well as the prevention of dephosphorylation of Ska1 and Ska3 resulted in severe mitotic delay, chromosome misalignment and cell death.

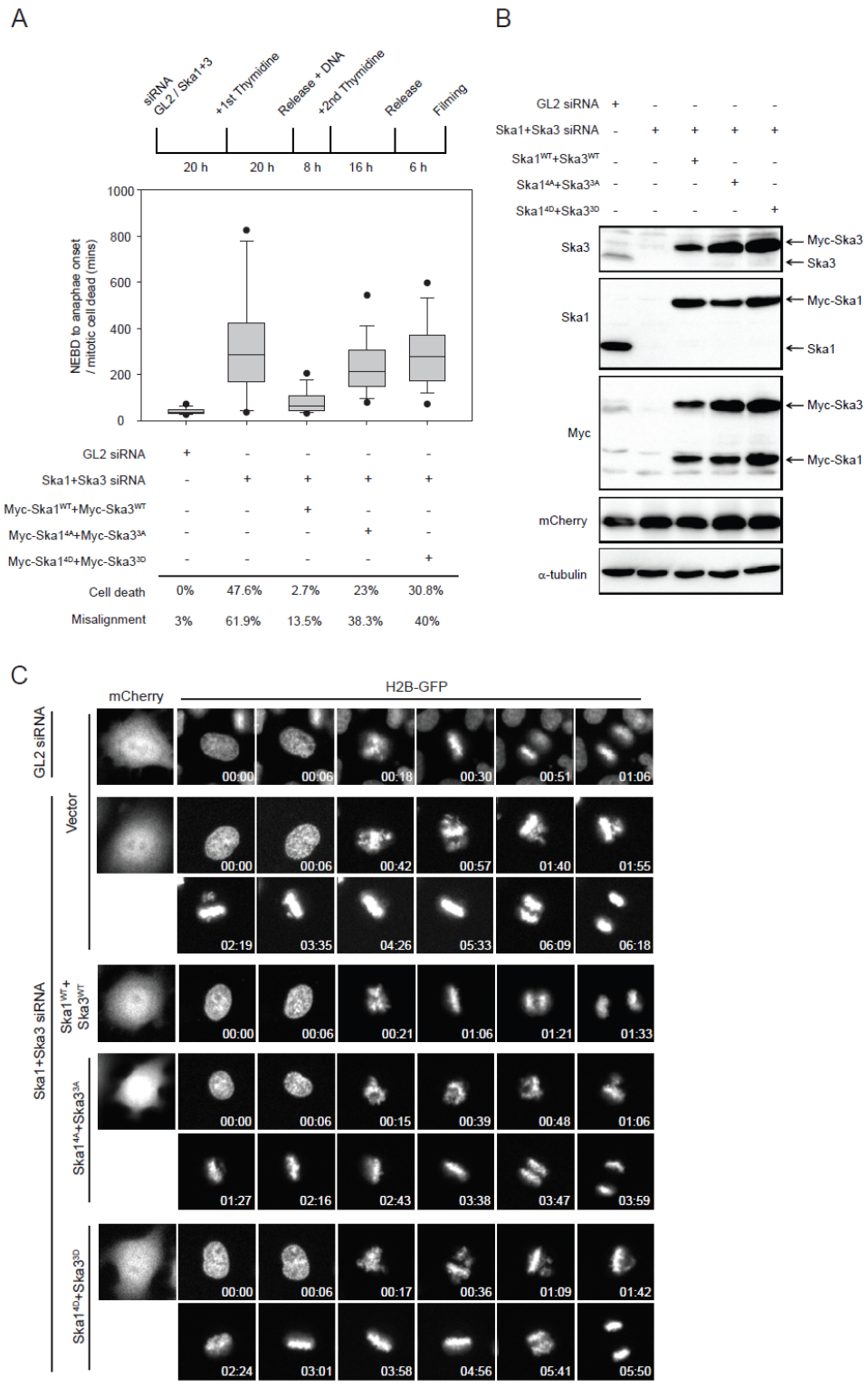

Figure 48. Aurora B phosphorylation regulates the function of the Ska complex. (A) Upper panel: schematic representation of the Ska rescue protocol employed to assess mitotic progression. Lower panel: box-and-whisker plot showing the elapsed time (h:min) that H2B-GFP expressing HeLa S3 cells spent in mitosis from NEBD to anaphase onset or mitotic cell death (≥60 cells from 2 independent experiments). In this box-and-whisker plot, boxes represent 25–75% of the cells, the line within the box indicates the median, lower and upper whiskers represent the 10th and 90th percentiles and dots represent the 5th and 95th percentiles, respectively. Percentages of mitotic cell death and cells with misaligned chromosomes are displayed below the plot. **(B)** Cells treated as in (A) were transfected with the indicated plasmids. Lysates were obtained and analyzed by Western blotting with the indicated antibodies. **(C)** Movie stills from representative cells in (A). Time is indicated in h: min. t=0 was defined as the time point two frames before chromosomes condensation became evident. mCherry signal at time 0 for each cell is shown on the left.

2.5 Aurora B phosphorylation regulates the localization of the Ska complex

As Aurora B activity controls Ska localization at KTs (Figure 43), we next examined the localization of the above mutant proteins. The phosphomimetic mutants ($Ska1^{4D}$+ $Ska3^{3D}$) failed to localize to KTs (Figure 49A). This observation confirms that Aurora B-mediated phosphorylation significantly reduces binding of the Ska complex to KTs. In contrast, the non-phosphorylatable mutants ($Ska1^{4A}$ +$Ska3^{3A}$) localized to KTs identically to their wild-type Ska counterparts. Considering that the association of the Ska complex with KTs is both highly dynamic (Raaijmakers et al., 2009) and maximal during metaphase (Figure 42), we reasoned that hindering Aurora B phosphorylation on Ska1 and Ska3 might induce premature KT recruitment or prevent normal turnover of the Ska complex at KTs. To test if the non-phosphorylatable Ska mutants would resist Aurora B-dependent removal from KTs, Ska1 and Ska3 constructs were co-transfected with either Mis12-INCENP-GFP or Mis12-INCENP (TAA)-GFP plasmids, which recruit Aurora B to outer KTs (Figure 49B). In contrast to the wild-type Ska proteins, which were displaced from KTs in cells expressing Mis12-INCENP-GFP, the non-phosphorylatable mutants persisted at KTs even in the presence of increased Aurora B activity at outer KTs (Figure 49B). This clearly indicates that mutations preventing Aurora B phosphorylation on the Ska complex severely compromise its Aurora B-dependent removal from KTs.

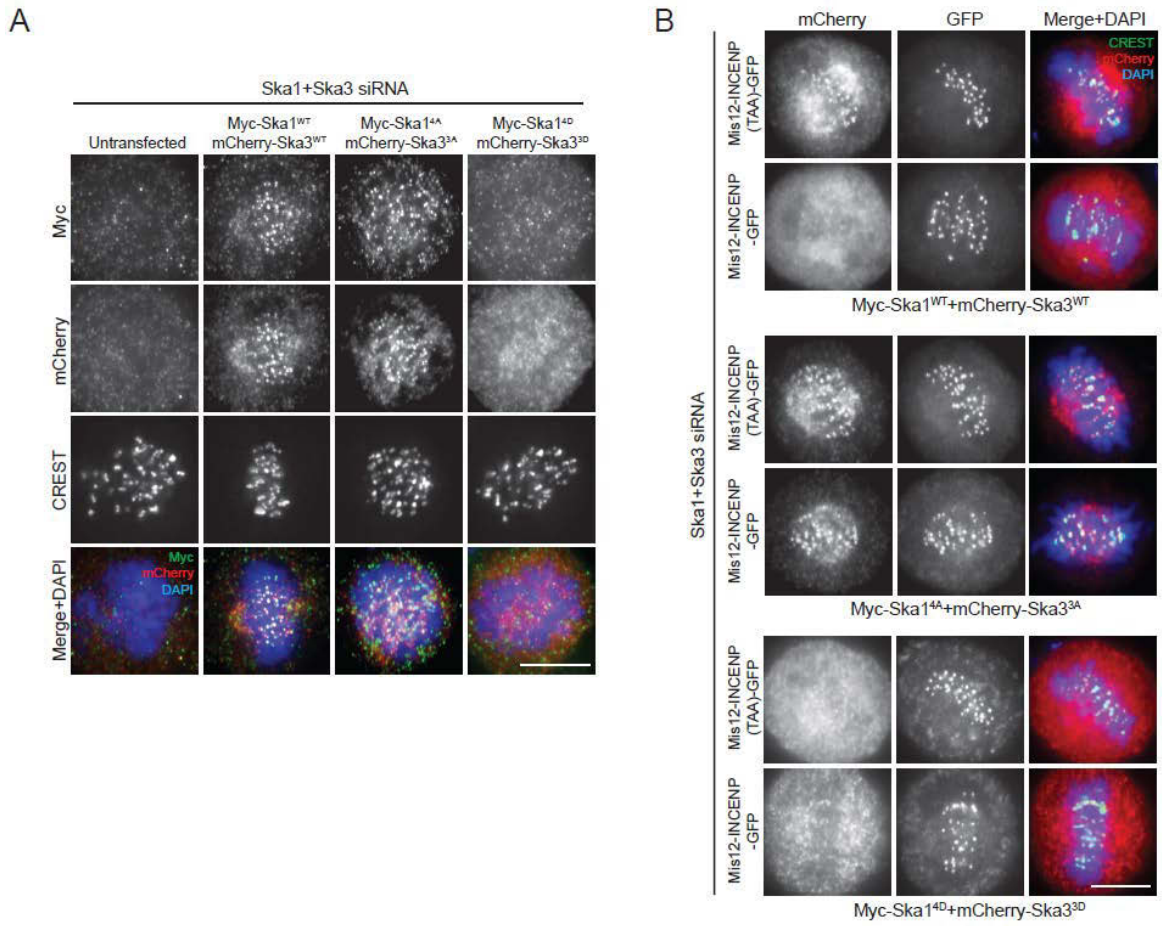

Figure 49. Aurora B phosphorylation regulates the function and localization of the Ska complex. (A) HeLa S3 cells were first co-depleted of Ska1 and Ska3 and subsequently transfected with the indicated plasmids following the protocol shown in Figure 37A, except that cells were fixed after 10 h release from the second thymidine block. Cells were then fixed with PTEMF and stained with anti-Myc serum (green), anti-mCherry antibody (red), CREST serum and DAPI (blue). **(B)** Cells were treated as in (A) but Mis12-INCENP-GFP or Mis12-INCENP (TAA)-GFP plasmids were co-transfected with the Ska plasmids. Cells were fixed with PTEMF and stained with anti-mCherry antibody (red), CREST serum and DAPI (blue). GFP signal is shown in green. Bars = 10 μm.

2.6 Aurora B phosphorylation on the Ska regulates K-fibers stability

As shown previously (Gaitanos et al., 2009), K-fiber stability is lost upon Ska depletion. Thus, we assayed the stability of K-fibers after exposure of Ska siRNA-treated cells expressing either wild-type Ska proteins or non-phosphorylatable or phosphomimetic mutants to low temperature for 20 min. As expected, expression of the KT-localizing Ska^{WT} proteins rescued K-fibers stability (Figures 50A and 50B). In contrast, replacing the endogenous Ska proteins with the phosphomimetic mutants impaired K-fiber stability, in line with the reduced KT recruitment of these Ska proteins. This readily explains the inability of these mutants to rescue the Ska

depletion phenotype (Figures 48A and 48C). Importantly, the non-phosphorylatable mutants supported stable K-fiber formation (Figures 50A and 50B). Similarly, these mutants of Ska were able to generate inter KT tension comparable to that observed in cells expressing Ska^{WT} proteins (inter KT distance of 1.25 µm and 1.21 µm for $Ska1^{4A}$ +$Ska3^{3A}$ and Ska^{WT}, respectively) (Figures 51A and 51B), raising the question of why the expression of these mutants in cells caused severe mitotic defects. Given that the non-phosphorylatable mutants persisted at KTs with high Aurora B-activity (Figure 49B), we explore whether the phenotype observed in cells rescued with $Ska1^{4A}$ +$Ska3^{3A}$ (Figures 48A and 48C) was due to hyper-stable KT-MT attachments. We conducted monastrol wash-out assays to test the efficiency of these cells in correcting syntelic attachments induced by monopolar spindles. One hour after monastrol wash-out, only about 30% of cells expressing the Ska non-phosphorylatable mutants had achieved metaphase, whereas more than 60% of control (GL2-treated) and Ska^{WT} expressing cells had done so (Figures 51C and 51D). These results argue that the observed mitotic defects may well be due to premature and/or excessive stabilization of KT-MT attachments, which would in turn interfere with the error correction process. Taken together, these results demonstrate that Aurora B-mediated regulation of Ska complex recruitment to KTs is crucial to stabilize KT-MT interactions.

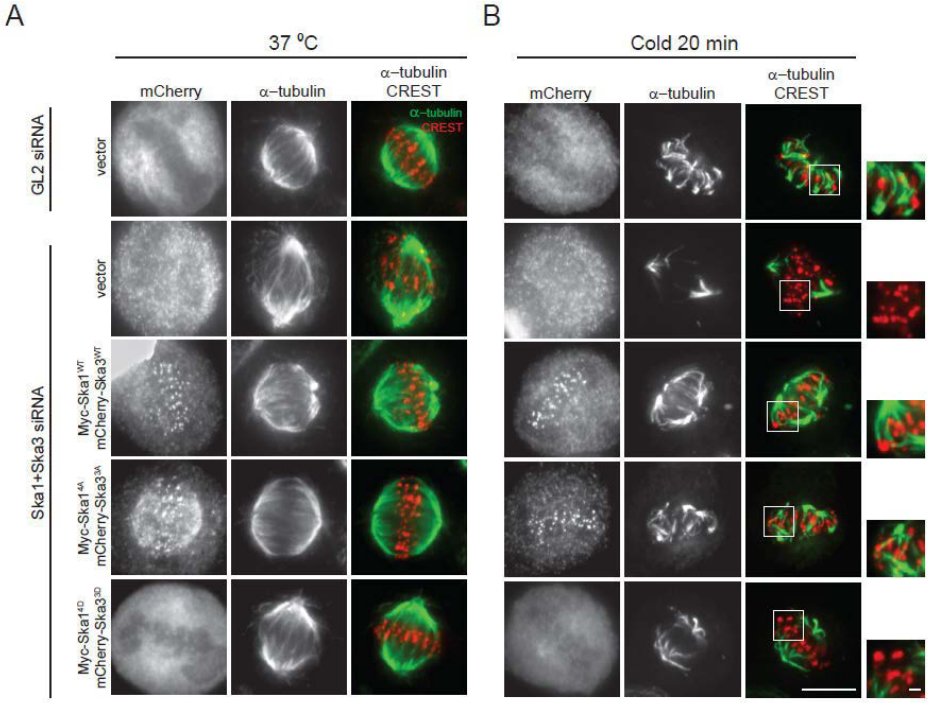

Figure 50. Aurora B phosphorylation on the Ska regulates K-fibers stability. HeLa S3 cells were treated as in Figure 37A. Cells were then left at 37ºC **(A)** or placed at 4ºC **(B)** for 20 min, before being fixed with PTEMF and stained with anti-tubulin antibody (green), anti-mCherry antibody and CREST serum (red). Insets on the right side show magnifications of a few KTs with or without cold-stable K-fibers for each condition (scale bar, 1 µm). Bars = 10 µm.

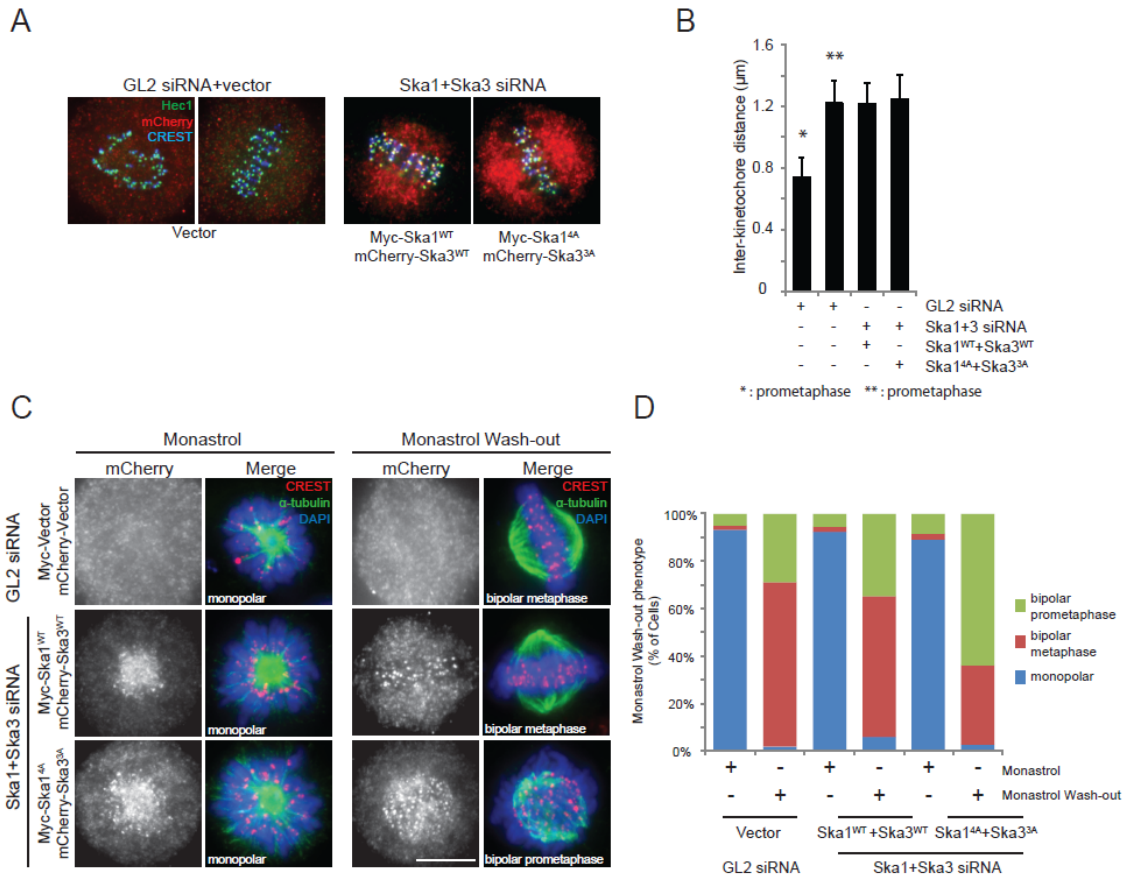

Figure 51. The Ska non-phosphorylatable mutants prevent efficient correction of syntelic attachments. (**A**) Cells were treated as in Figure 40A before stained with anti-mCherry (red) and anti-Hec1 (green) antibodies, and CREST serum (blue). (**B**) Bar graph showing the measurement of inter-KT distances (Hec1-Hec1 distances). Error bars indicate s.d of at least 45 KT pairs) of cells as in (A)). (**C**) Cells were treated as in Figure 40A except that monastrol was added after the second thymidine release. After 10 h, cells were either fixed, or washed and released into fresh medium with MG132 for 1 h before fixation. Cells were then stained with anti-α-tubulin (green) and anti-mCherry antibodies, CREST serum (red) and DAPI (blue). (**D**) Bar graph showing the quantification of cells with monopolar spindles or bipolar spindles in prometaphase or metaphase, more than 60 cells were counted per condition, at least 20 cells were counted in 3 independent experiments. Bars = 10 μm.

2.7 CENP-P controls Ska localization in a distinct manner than the KMN network

Previously, a yeast two-hybrid screen conducted in our laboratory using Ska2 as bait identified CENP-P as a potential interacting partner (Hanisch, Wehner and Sillje unpublished results). Therefore, we investigated whether this CCAN component regulates the localization of the Ska complex. A rabbit polyclonal antibody against CENP-P had been generated in our laboratory. This antibody recognized a band of ~30 kDa, the predicated molecular weight of CENP-P, by Western blotting (Figure 52A). In mitosis, CENP-P decorated KTs from prophase to anaphase (Figure 52B and 52C). No special signal could be detected with the pre-immune serum

(Figure 52A and 52C) or after depletion of CENP-P by siRNA targeting the 3' untranslated region (Figures 52D and 52E).

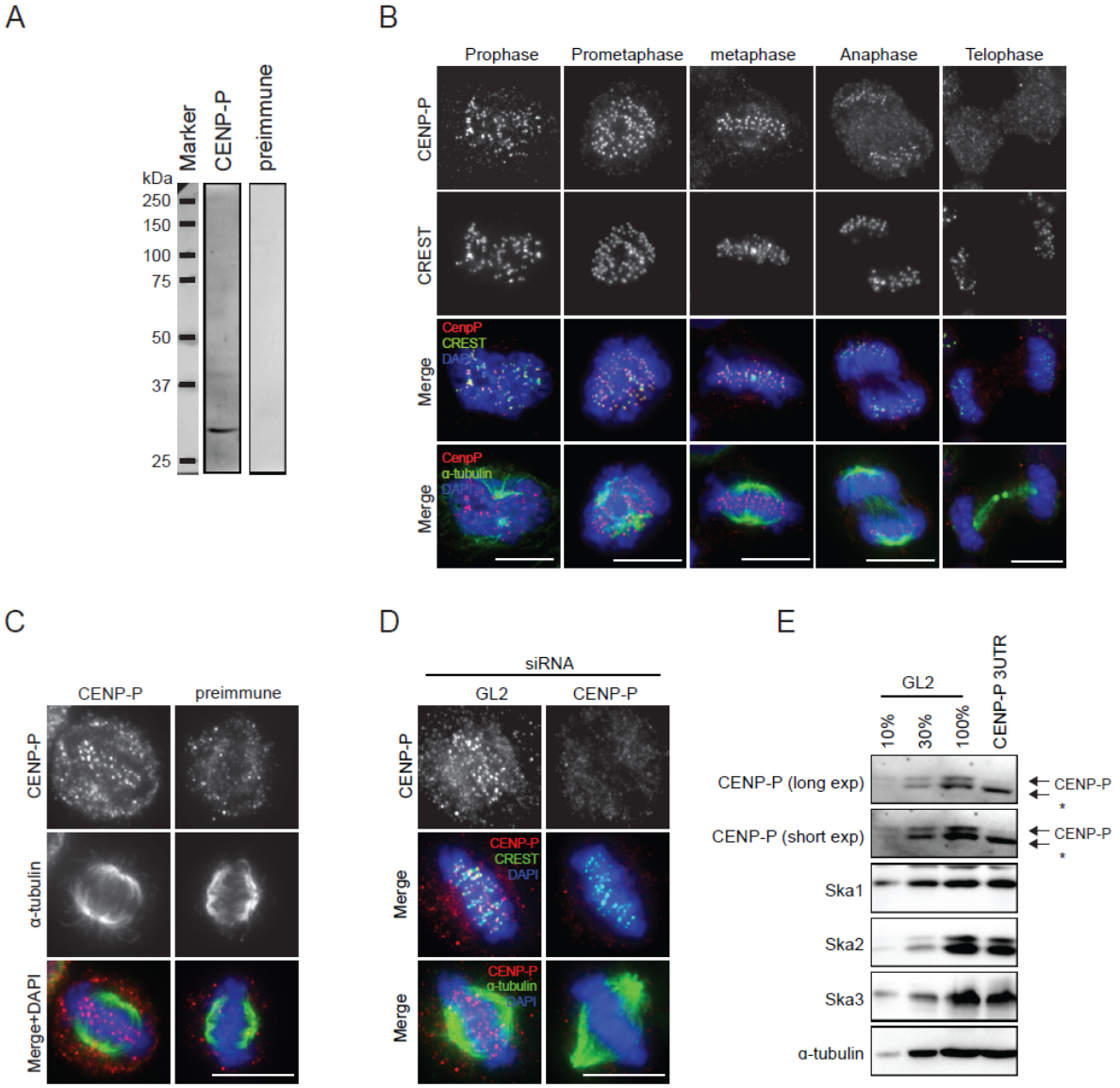

Figure 52. Characterization of the CENP-P antibody. (**A**) HeLa S3 cell extract was separated by SDS-PAGE and probed by Western blotting with either anti-CENP-P antibody or pre-immune serum. **(B)** Cells were stained with anti-CENP-P (red) and anti-α-tubulin antibodies (green), CREST serum (green), and DAPI (blue). (**C**) Cells were stained with anti-CENP-P antibody or pre-immune serum (red), anti-α-tubulin antibody (green) and DAPI (blue). (**D**) Cells were treated with GL2 or CENP-P siRNAs for 72 h before stained with anti-CENP-P (red), anti-α-tubulin antibodies (green) and CREST serum (green), and DAPI (blue). (**E**) Cells were treated with GL2 or CENP-N siRNAs for 72 h. Lysates were obtained and analyzed by Western blotting with indicated antibodies. Different amounts of GL2 siRNA-treated lysate were loaded to allow rough estimation of the depletion efficiency.

Importantly, depletion of CENP-P reduced the KT signal of Ska3 without affecting the protein expression levels of the Ska proteins (Figures 52E and 53A). The reduction of Ska3 KT signal could be rescued by expressing exogenous Myc-tagged CENP-P, confirming the specificity of the depletion (Figures 53A and 53B). To test if CENP-P regulates the Ska localization in a similar manner as the KMN network, we performed the cold treatment assay shown previously. Cells were treated with nocodazole prior to incubation with low temperature. As shown before (Figure 43), cold treatment restored the KT localization of Ska3 in GL2-treated control cells but not in Hec1-depleted cells (Figure 53C). In contrast to Hec1 depletion, cold treatment could restore the KT localization of Ska3 in CENP-P-depleted cells (Figure 53C), arguing that CENP-P regulates the Ska localization in a distinct manner than the KMN network.

In spite of preliminary results from a yeast-two hybrid screen suggesting an interaction between CENP-P and the Ska complex, we failed to confirm this interaction by directed yeast two hybrid between CENP-P and Ska2 or by co-immunoprecipitation (data not shown). Together, these results suggest that CENP-P does control Ska localization but in a different manner to that exerted by the KMN network. CENP-P, and in turn the CCAN complex, could possibly play a fine-tuning role in modulating the KT recruitment of Ska, regulating for instance Ska dynamics at KTs.

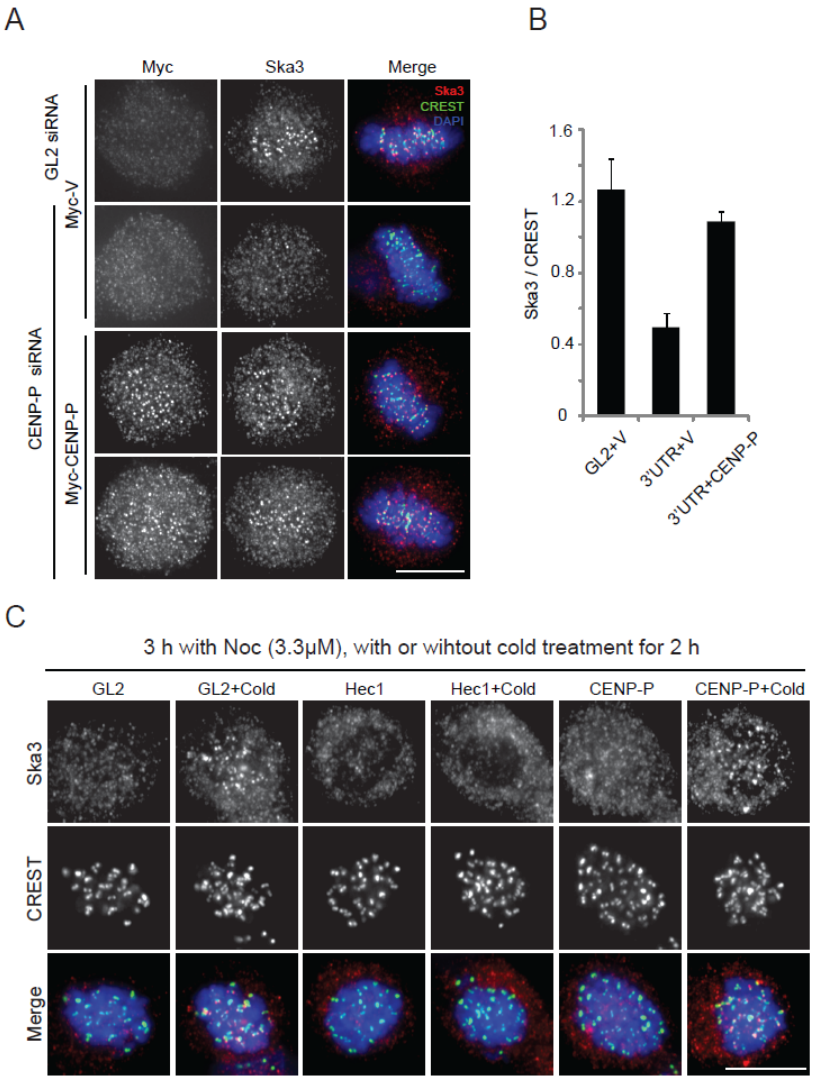

Figure 53. The role of CENP-P in regulating Ska localization. (**E**) HeLa S3 cells were treated with GL2 or CENP-P siRNAs for 72 h, 48 h before fixation, cells were then transfected with Myc-vector or Myc-CENP-P plasmids before stained with Myc 9E10 serum, anti-Ska3 antibody (red), CREST serum (green) and DAPI (blue). (**F**) Bar graph showing the quantification of Ska3 staining intensity at KTs (normalized against CREST) of cells treated as in (E) (>100 KTs from 5 cells, error bars indicate the s.d of 5 cells). (**G**) HeLa S3 cells were treated for 48 h with GL2 or Hec1 siRNAs, or for 72 h with CENP-P siRNA prior to treatment with 3.3 μM nocodazole (Noc) for 1 h and a 2 h incubation at 4°C. Cells were then fixed with PTEMF and stained with anti-Ska3 antibody (red), CREST serum (green) and DAPI (blue). Bars = 10 μm.

Discussion II

KTs need not only to establish and maintain stable connections with spindle MTs, but they should also sense and correct aberrant MT attachments. Aurora B activity is critical for the correction of defective KT-MT attachments by destabilizing them (Lampson et al., 2004; Nezi and Musacchio, 2009). Several KMN subunits, namely Hec1, Mis13 and KNL1, have been shown to be phosphorylated by Aurora B leading to reduction of the KMN's MT binding affinity (Cheeseman et al., 2006; Ciferri et al., 2008; DeLuca et al., 2006; DeLuca et al., 2011a; Guimaraes et al., 2008; Welburn et al., 2010). In addition to controlling the activity of the KMN network, Aurora B also positively regulates the localization of many centromere/KT proteins, such as Shugoshin (Kawashima et al., 2007), MCAK (Andrews et al., 2004a; Lan et al., 2004a), protein phosphatase 1 (Kim et al., 2010), several checkpoint proteins (e.g. Mps1, Bub1 and BubR1) (Ditchfield et al., 2003a; Hauf et al., 2003), the RZZ complex (Famulski and Chan, 2007) and hSpindly (see part I of this thesis). On the other hand, the KT localization of the Astrin-SKAP complex has been shown to be antagonized by Aurora B kinase activity (Schmidt et al., 2010).

In this study, we demonstrate that the Ska KT localization is negatively regulated by Aurora B activity. Furthermore, the KMN network is absolutely required to recruit the Ska complex to KTs. More importantly, the interaction between the KMN and Ska is strenghten when Aurora B activity is inhibited. Together, our study suggests that Aurora B activity antagonizes the interaction between Ska and KMN complexes thereby controlling the Ska localization to KTs.

Based on our results, we propose an additional mechanism (additional to KMN regulation) for how Aurora B can negatively regulate KT-MT attachments. To stabilize the end-on attachments mediated by the KMN network, the Ska complex is subsequently recruited to those attached KTs. At poorly attached and/or tensionless KTs, Ska is spatially closer to Aurora B and is therefore more readily phosphorylated (Liu et al., 2009; Wang et al., 2011). Specifically, Aurora B-mediated phosphorylation of Ska1 and Ska3 reduces the KT recruitment of the Ska complex, by interfering with KMN-Ska interactions. Once sister chromatids are bi-oriented and tension is established, members of the KMN and Ska complexes are dephosphorylated, leading to full stabilization of the KT-MT attachments. Our analysis of the non-phosphorylatable and

phosphomimetic mutants of the Ska members supports this model. While the phosphomimetic mutants cannot be properly recruited to KTs and therefore cannot support stable K-fibers formation, the non-phosphorylatable mutants persist at KTs and do support the formation of stable K-fibers. However, the latter mutants interfere with the process of correcting error attachments, likely due to premature or hyper-stable K-fiber formation. Therefore, we conclude that the dynamic control of both the phosphorylation and dephosphorylation of the Ska complex is required to ensure proper mitotic progression. Whether Aurora B phosphorylation on the KMN subunits (i.e., Hec1, Mis13 and KNL1) also influences the interaction between the KMN and Ska complex, remains to be investigated. However, this possibility may be less likely as the non-phosphorylatable Ska mutants are stably recruited to KTs in cells with high Aurora B activity at outer KTs (i.e., expressing INCENP-Mis12). We also do not exclude that Aurora B phosphorylation on Ska could have additional effects, such as modulating its MT binding or influencing Ndc80 activity and it will be interesting to investigate these possibilities in the future.

The cooperation of the KMN network and the Ska complex in the formation of stable end-on attachments is reminiscent of that of the Ndc80-Dam1 complexes in budding yeast. Thus, the Ska complex has been proposed to be the functional counterpart of the fungal Dam1 complex in metazoan organisms (Gaitanos et al., 2009; Hanisch et al., 2006; Welburn et al., 2009). Although this view is far from being universally accepted, our present results on the regulation of the Ska complex by Aurora B strengthen the view that different organisms employ an evolutionarily conserved mechanism to form and maintain KT-MT attachments. Similar to the results reported here the interaction between Dam1 and Ndc80 is also regulated by Aurora B *in vitro* (Lampert et al., 2010; Tien et al., 2010) and Ndc80 mutants that cannot bind Dam1 show defects in forming end-on attachments in *S.cerevisiae* (Maure et al., 2011). Interestingly, Dam1 in *S. pombe*, and Ska3 in chicken DT40 cells are both non-essential for viability (Ohta et al., 2010; Sanchez-Perez et al., 2005). These results suggest that the Ska and Dam1 complexes act as stabilizing and/or processivity factors for KMN-mediated attachments and that are less critical in certain cell types with regional centromeres. Hopefully, structural information on how the KMN network and the Ska complex interact with each other will provide additional molecular and mechanistic understanding of how these two complexes cooperate to perform their functions at metazoan KTs.

Conclusions and Perspective

In part I, we conducted the detailed characterization of human Spindly. We show that hSpindly is the recruiting factor of KT dynein and it is itself recruited by the RZZ complex. We conclude that hSpindly-mediated accumulation of dynein at KTs is required for proper chromosome congression, stabilization of K-fibers and proper tension establishment. Moreover, we reveal a novel role of KT dynein, i.e., maintaining proper spindle orientation. However, hSpindly is not required of the stripping of checkpoint proteins from KTs upon MT attachment, suggesting that a compensatory mechanism is involved to release checkpoint proteins from KTs in human cells. In the future, it would be important to explore this dynein-independent mechanism.

In part II, we analyzed the regulation of Ska localization by Aurora B-mediated phosphorylation. Aurora B antagonizes the KT recruitment of Ska, probably by inhibiting the interaction between KMN and Ska complex. Indeed, phosphomimetic mutants of Ska cannot localize properly to KTs and cannot support the formation of stable K-fibers. On the other hand, non-phosphorylatable mutants induce hyper-stable MT-KT attachments which interfere with the error correction process mediated by Aurora B. To gain more mechanistic insight about how Ska and KMN work together, it would be important in the future to investigate whether phosphorylation of Ska affects its own MT binding and/or affect the activity of the KMN network. Furthermore, it will also be informative to map the regions or essential residues responsible for the interactions between the KMN and Ska members.

Materials and Methods

1. Cloning procedure

All cloning procedures were performed according to standard techniques, as described in Current Protocols in Molecular Biology, Wiley, 1999 and Molecular Cloning, A Laboratory Manual, 2nd Edition, Sambrook, J., Fritsch, E.F., Maniatis, Cold Spring Harbor Laboratory Press, 1989. Fermantas Fastdigest restriction enzymes were used as specified by the suppliers (Thermo Fisher Scientific) and ligation reactions were carried out using Rapid Ligation Kit (Roche Diagnostics, Indianapolis, IN). DNA extraction from agarose gels and plasmid DNA preparation were performed with Qiagen (Qiagen GmbH, Germany) kits, as recommended by the manufacturer. PCR reactions were carried out in a RoboCycler Gradient 96 by using Pfu DNA polymerase (Stratagene, La Jolla, CA), according to the manufacturer's instructions. All constructs were verified by sequencing service provided by Microsynth Laboratory, Switzerland.

In part I, for cloning of hSpindly (Q96EA4), a cDNA clone (IRAUp969B0653D) was obtained from the Deutsches Ressourcenzentrum für Genomforschung (RZPD), The full length protein was cloned in-frame into a pcDNA3.1 vector (Invitrogen) encoding an N-terminal 3xMyc tag. The siRNA-resistant version of hSpindly containing six silent mutations was produced by mutating the siRNA-corresponding region with the following pair of primers (5'-TTACAGAATCAATTGGACAAGTGCCGCAACGAGATGATGACCATG-3' and its reversed complement) using QuickChange Site-Directed Mutagenesis kit (Stratagene). Underlined letters correspond to the six silent point mutations made. Both the N-terminus hSpindly (1-444 aa) and C-terminus hSpindly (443-605 aa) were PCR cloned in pcDNA3.1 vector encoding an N-terminal 3xMyc tag. For the 5A and 5D mutants, following PCR primers and their reversed complements were used:

T509A: 5'-GTTTCTATACACGCACCAGTAGTCAG-3'
S515A: 5'-GTAGTCAGTCTCGCTCCTCACAAAAAT-3'
T552A: 5'-GAAGTGGAAACGCCCCTAACTCTCC-3'
S555A: 5'-CCCTAACGCTCCCAGGTTAGCTGC-3'
T596A: 5'-GTCTTCTAAATCTGCTCCAGAGACCC-3'
T509D: 5'-GTTTCTATACACGATCCAGTAGTCAG -3'
S515D: 5'-GTAGTCAGTCTCGATCCTCACAAAAAT-3'

T552D: 5’-GAAGTGGAAACGACCCTAACTCTCC-3’
S555D: 5’-CCCTAACGATCCCAGGTTAGCTGC-3’
T596D: 5’-GTCTTCTAAATCTGATCCAGAGACCC-3’

For cloning of p50-dynamitin, a cDNA clone (IMAGE: 3504109) was obtained from Geneservice and cloned into pcDNA3.1 vector encoding an N-terminal 3xMyc tag.

In part II, the cDNAs of Ska1, Ska3 and CENP-P were cloned into pcDNA5/FRT/TO or pcDNA3.1 vectors (Invitrogen, Carlsbad, CA) encoding an N-terminal 3xMyc tag or an N-terminal mCherry tag. An siRNA-resistant version of Ska1 containing six silent mutations and the non-phosphorylatable and phosphomimetic mutants of Ska1 and Ska3 were generated using the QuickChange site-directed mutagenesis Kit (Stratagene, La Jolla, CA), with the following primers and their reversed complements:

Primers to generate an siRNA-resistant version of Ska1:
5’ GAAATCTCGGTTGACATACAACCAAATTAATG 3’

Primers to generate Ska1 and Ska3 phospho-mutants:
Ska1 T157A: 5’ GAAATCTCGGGCATACAACCAAATTAATG 3’
Ska1 T157D: 5’ GAAATCTCGGGACTACAACCAAATTAATG 3’
Ska1 S185A: 5’ CAGCCAAAAAAGGCTATGAATTCTGTGA 3’
Ska1 S185D: 5’ CAGCCAAAAAAGGATATGAATTCTGTGA 3’
Ska1 T205A: 5’ GAAACGAAGGATGCC AAAGGTCGTTATT 3’
Ska1 T205D: 5’ GAAACGAAGGATGAC AAAGGTCGTTATT 3’
Ska1 S242A: 5’ ACTGCCGGAGGCTAGCAGAGGTCCGAGG 3’
Ska1 S242D: 5’ ACTGCCGGAGGCTAGACGAGGTCCGAGG 3’
Ska3 S87A: 5’CTAATGGAAAAAAATGCAATGGATATTATG 3’
Ska3 S87D: 5’CTAATGGAAAAAAATGACATGGATATTATG 3’
Ska3 S110A: 5’CGTGTCAAGAAAAATGCAGTACACGAGCAAG 3’
Ska3 S110D: 5’CGTGTCAAGAAAAATGATGTACACGAGCAAG 3’
Ska3 S159A: 5’CGTAGTCCACAACTTGCAGATTTTGGACTTGA 3’
Ska3 S159D: 5’CGTAGTCCACAACTTGATGATTTTGGACTTGA 3’

2. Production and purification of recombinant proteins and antibodies

For production of recombinant proteins, the respective plasmids were transformed into *Escherichia coli* BL21, grown overnight under ampicillin or kanamycin together with chloramphenicol and diluted with fresh medium in the next morning. The culture was grown further until OD_{600} of ~0.5 before 0.5 mM IPTG was added. The culture was further incubated at 30 ºC for 3-4 hours. Cells were then lysed in corresponding buffer (see below) and opened by EmulsiFex-C5 high pressure homogenizer (Avestin, ON, Canada). The final purified proteins were frozen by liquid nitrogen and stored in -80 ºC for long term storage.

For His_6-hSpindly, 1-444 aa and 443-605 aa were cloned in a pET-28b vector, His_6-Aurora B (Yang et al., 2008) was a gift from X. Yao, University of Science and Technology of China), Ska1-His_6 was cloned in a pET-28b vector and His_6-Ska3 in a pET-28c vector. *E. coli* cells were resuspended with His_6 lysis buffer (20 mM NaH_2PO_4/Na_2HPO_4 pH 7.8, 150 mM NaCl, 0.05% NP40, 0.1 mM ATP (only for His_6-Aurora B), 0.2 mM β-Mercaptoethanol and 10 mM imidazole). Lysates were incubated with Ni-NTA agarose beads in a rotating wheel at 4ºC for 2 h. The beads were spun down and washed with the lysis buffer for 4 times. The proteins were eluted with the His_6 elution buffer (same as the His_6 lysis buffer except with 250 mM imidazole). His_6-Aurora B, purified protein was dialyzed against Tris buffer (50 mM Tris-HCl pH 8, 100 mM NaCl, 1 mM DTT and 10% glycerol). The others were dialyzed against 1X PBS with 1 mM DTT and 5% glycerol.

GST-Spindly was cloned in a pGEX-5x-1 vector, cells were resuspended in TNE lysis buffer (10 mM Tris-HCl pH 8, 50 mM NaCl, 1 mM DTT, 0.05% NP40, 1 mM EDTA). Lysates were incubated with glutathione sepharose 4B beads in a rotating wheel at 4ºC for 2 h. The proteins were eluted with the GST elution buffer (50 mM Tris-HCl pH 8.6, 20 mM glutathione).

For purification of the full length Ska complex, Ska1-His_6 and untagged Ska2 (Gaitanos et al., 2009) (a gift from A. A. Jeyaprakash and E. Conti, Max Planck Institute of Biochemistry) were co-transformed while His_6-Ska3 was transformed alone. Two populations of cells were mixed and co-lysed with buffer containing 20 mM Tris-HCl pH 7.5, 500 mM NaCl and 1 mM DTT, followed with Ni-NTA beads purification. The Ni-NTA beads-purified proteins were then loaded on a Resource Q 6 mL column (GE healthcare) using an ÄKTA Explorer FPLC system (Amersham). The elution was performed with buffer with increasing salt concentration (100mM to 1M NaCl, with 20 mM Tris-HCl pH 7.5 and 1M DTT). The elution from the anion exchange

chromatography containing the Ska complex was then loaded on a Superdex 200 16/60 column (GE Healthcare). The elution was performed with buffer containing 20 mM Tris-HCl pH 7.5, 100 mM NaCl and 1 mM DTT.

The antibody against hSpindly was generated by immunization of rabbits (Charles River Laboratories) with injections of His_6-tagged hSpindly (1–444 aa or 443-605 aa). Antibodies in serum were purified by Affi-Prep protein A Matrix (Bio-Rad Laboratories) and eluted 100 mM Glycine-HCl pH ~2.5. The elution was immediately neutralized by adding suitable amount of 1 M Tris-HCl pH 8.0. The antibody solution was then dialysis against 1X PBS with 5 % glycerol. Finally, 0.02 % of sodium azide was added.

3. Cell culture and synchronization

HeLa S3 cells, HeLa S3 cells stably expressing H2B-GFP (Sillje et al., 2006), HeLa Kyoto cells with a FRT-site and stably expressing GFP-α-tubulin/cherry-H2B cells (a gift from D. Gerlich, ETH Zurich, Switzerland) and HeLa cells stably expressing GFP^{LAP}-Ska2 (Welburn et al., 2009) (a gift from I. M. Cheeseman, MIT Whitehead, Boston) were cultured in a 5% CO_2 atmosphere in Dulbecco's modified Eagle's medium (Invitrogen), supplemented with 10% heat-inactivated fetal calf serum (FCS) and penicillin-streptomycin (100 IU/ml and 100 µg/ml, respectively). Nocodazole (0.33 µM or 3.3 µM), thymidine (2 mM), Taxol (1 µM), monastrol (150 µM), cytochalasin B (4 µM), G418 (0.5 mg/ml), puromycin (0.5 µg/ml), 2-deoxy-d-glucose (1 mM) and sodium azide (5 mM) were obtained from Sigma (St. Louise, MO). ZM447439 (10 µM) was obtained from Tocris (Moorend Farm Avenue, Bristol). MG132 (10 µM) was obtained from Calbiochem (San Diego, CA). Reversine (0.5 µM) was obtained from Cayman Chemical (Ann Arbor, MI). Mps1-IN-1 (Kwiatkowski et al., 2010) (2 µM) was a gift from N.S. Gray (Dana-Farber Cancer Institute, Boston). Fibronectin-coated coverslips were purchased from BD Biosciences. ATP reduction assays were performed as follow: cells were rinsed in saline (140 mM NaCl, 5 mM KCl, 0.6 mM $MgSO_4$, 0.1 mM $CaCl_2$, 1 mM Na_2HPO_4, 1 mM KH_2PO_4 pH 7.3) to remove tissue culture medium and placed in either saline containing glucose (saline with 4.5 g/liter d-glucose) or saline plus 5 mM sodium azide (Az) and 1 mM 2-deoxy-d-glucose (DOG) for 30 min at 37 °C. Cells were then either processed for immunofluorescence. For cold treatment assay, medium was replaced by ice-cold medium, followed by additionally placing the

dishes in a closed box filled with ice. HeLa cells were incubated therein 4 °C for 20 min or 2 h before fixation.

4. Transient transfections of plasmid DNA and siRNA

Plasmid transfections were performed using TransIT®-LT1 reagent (Mirus Bio Corporation, Madison, WI) according to the manufacturer's instructions. For HeLa cells covered with 2 ml medium, 200 µl OptiMEMI (Invitrogen), 3 µl TransIT®-LT1 reagent and ~1 µg plasmid DNA were used. Mis12-INCENP-GFP and Mis12-INCENP (TAA)-GFP plasmids (Liu et al., 2009) were kindly provided by S. M. Lens, University Medical Center, Utrecht. siRNA duplexes were transfected using Oligofectamine (Invitrogen) according to the manufacturer's instructions. For HeLa cells covered with 2 ml medium, 200 µl OptiMEMI (Invitrogen), 3 µl Oligofectamine reagent and 3-6 µl siRNA were used. Cells were usually treated for 48-72 hours. Stock concentration of siRNA is 20 µM. The sequences of the siRNA duplexes (purchased from Dharmacon RNA Technologies or Qiagen) used in this study are listed in Table 1.

Target	Sense sequence	Reference
GL2	CGU ACG CGG AAU ACU UCG AdTdT	(Elbashir et al., 2001)
hSpindly	GGA GAA AUU UAA GAA UUU AdTdT	
hSpindly	GGA UAA AUG UCG UAA UGA AdTdT (used throughout the study unless otherwise stated)	
EB1	UUG CCU UGA AGA AAG UGA AdTdT	
ZW10	UGA UCA AUG UGC UGU UCA AdTdT	(Kops et al., 2005)
Hec1	GUU CAA AAG CUG GAU GAU CdTdT	(Martin-Lluesma et al., 2002)
Mad2	GAG UCG GGA CCA CAG UUU AdTdT	(Martin-Lluesma et al., 2002)
CENP-E	ACU CUU ACU GCU CUC CAG UdTdT	(Martin-Lluesma et al., 2002)
Aurora B	GGA AAG AAG GGA TCC CTA AdTdT	(Klein et al., 2006)
CENP-A	CTC GTG GTG TGG ACT TCA AdTdT	(Klein et al., 2006)
Nde1	SMART pool siRNA from Dharmacon D-020625-01 to D-020605-04	(Vergnolle and Taylor, 2007)
Dynein HC	GGA UGA AUC UAA UGU GUU AdTdT	(Toyoshima et al., 2007)
Ska1	CGC UUA ACC UAU AAU CAA AdTdT	(Hanisch et al., 2006)

Ska3 3'UTR	AGA CAA ACA UGA ACA UUA AdTdT	(Gaitanos et al., 2009)
KNL1	GGA AUC CAA UGC UUU GAG AdTdT	(Liu et al., 2010)
Mis13	CGU UUC AGA GGA AAG AAU UdTdT	(Obuse et al., 2004)
CENP-P 3'UTR	CAG UGA ACG UGG AGG AUG AdTdT	

Table 1. List of siRNA duplexes used in this study, together with their respective references of the published sequences.

5. Cell extracts, Western blotting, and immunoprecipitations

For preparing cell extracts of HeLa S3 cells for Western blotting, the cells were washed once with ice-cold PBS, scraped or shaked off the plate and resuspended in ice-cold HEPES lysis buffer (50 mM Tris, pH 7.4, 150 mM NaCl, 0.5 % Triton-X 100, 1 mM DTT, 30 µg/ml RNase, 30 µg/ml DNase, protease inhibitors cocktail (Roche, 1 tablet for 10 ml lysis buffer) and phosphatase inhibitors cocktail (Sigma)). Lysed cells were centrifuged at 14000 rpm for 30 min at 4°C. Protein concentrations in the cleared lysate were determined with the Dc protein assay (Bio-Rad Laboratories, Hercules, CA). Lysates were then boiled in sample buffer and resolved in SDS-PAGE gels.

For immunoprecipitation of endogenous hSpindly, lysates were prepared using HEPES lysis buffer without Triton-X 100. Resuspended cells were opened by nitrogen cavitation (1000 PSI, 20min; Parr Instrument). ~5 µg anti-hSpindly antibody or control rabbit IgGs (Abcam) were incubated to ~1 mg of clarified cell lysates. After 30 min, ~10 µl of Affi-prep Protein A beads (Bio-Rad Laboratories, Hercules, CA) were added to the mixtures. Incubations were then performed in a rotating wheel, at 4ºC. Immune complexes were spun down and washed four times with the same HEPES lysis buffer and then boiled in SDS-PAGE sample buffer. For immunoprecipitation of endogeneous Ska1, lysates were prepared using HEPES lysis buffer with 0.1 % Triton-X 100. Immunoprecipitations on cell lysates were performed using 5 µl of solid beads Affi-Prep protein A Matrix chemically crosslinked to 3 µg/µl of anti-Ska1 antibody against 1 mg of clarified lysates for 2 h at 4° C. The beads were washed 4 times with the same lysis buffer and bound species were resolved by SDS-PAGE.

For phosphatase assay, 2 µl of λ-phosphatase (Roche) was added to 100 µg of cell extracts and these were incubated at 37°C for 30 min before boiled in sample buffer.

To detect specific proteins by Western blotting, cell lysates or IPs were loaded on SDS-PAGE gels. Separated proteins were transferred to nitrocellulose membranes (Whatman, Dassel,

Germany). Primary antibodies used in this study for Western blotting are listed in Table 2 with respective dilutions and sources. The primary antibodies were then detected by HRP-conjugated goat anti-mouse and anti-rabbit secondary antibodies (1:3000, Bio-Rad). Bound antibodies were detected by ECL Supersignal (Pierce Biotechnology, Rockford, IL), with a digital Fujifilm LAS-1000 camera, which was attached to an Intelligent Darkbox II (Raytest GmbH, Straubenhardt, Germany).

6. Glycerol gradient centrifugation

Cell lysates (10 mg) were applied on a 10–25% glycerol cushion (10 ml) and spun down at 28,000 rpm (SW 40 Ti rotor; Beckman Coulter) for 14 h. 27 fractions of 400 µl each were collected for Western blotting analysis. Albumin, aldolase, ferritin, and thyroglobulin were used as controls to determine the sedimentation coefficient.

7. Immunofluorescence microscopy

For spindle/KT proteins staining, HeLa S3 cells were grown on coverslips and simultaneously fixed and permeabilized for 10 min at RT in PTEMF buffer (20 mM PIPES pH 6.8, 3.7 % formaldehyde, 0.2 % Triton-X 100, 10 mM EGTA and 1 mM $MgCl_2$). For astral MTs detection, cells were fixed with cold methanol for 10 min. For cortical $p150^{Glued}$ detection, cells were first pre-extracted with 0.5% Triton X-100 in PEM (20 mM PIPES, pH 6.8, 10 mM EGTA, and 1 mM $MgCl^2$), followed by cold methanol fixation for 10 min. For phalloidin staining, cells were fixed with 3.7 % formaldehyde for 10 min and permeabilized with 0.5% Triton X-100 in PBS for 10 min, followed by incubation with Alexa Fluor 546–phalloidin (Invitrogen) for 1 h. Primary antibodies used for immunofluorescence in this study are listed in Table 2. DNA was stained with DAPI (2 µg/ml). Primary antibodies were detected with Cy2-, Cy3-, and Cy5-conjugated donkey anti–mouse, anti–rabbit, anti–goat, anti-sheep, or anti–human IgGs (1:1,000; Dianova). Coverslips were mounted in mounting solution (0.5 % *p*-phenylenediamine in 90% glycerol and 50 mM Tris-HCl pH 8.6).

Immunofluorescence microscopy was performed using Zeiss Axioplan II microscope (Zeiss, Jena, Germany) with Apochromat 63x oil immersion objectives. Photographs were taken using a Micromax CCD camera (model CCD-1300-Y, Princeton Instruments, Treton, NJ) and

MetaMorph software (Molecular Devices, Sunnyvale, California). For high resolution images, a Deltavision microscope (Applied Precision, Issaquah, WA) equipped with PlanApo 60x/1.50 oil immersion objective (Olympus) and a CoolSNAP HQ camera (Photomertrics) was used for collecting 0.2 or 0.4 μm-distanced optical sections in the z-axis. Images at single focal planes were processed with a deconvolution algorithm, and optical sections were projected (X-Y or Z-Y projections) into one picture using Softworx software (Applied Precision). The same software was used to measure inter-KT distances (distance between centers of sister Hec1 dots in the same optical section). Quantification of KT intensities was performed with ImageJ (http://rsb.info.nih/gov/iJ/). A circular region with fixed diameter was centered on each kinetochore, and CREST intensity was measured in the same region and used for normalization after subtraction of background intensity measured outside the cell. Statistical significances were verified by 2-tailed Student's *t* test.

Protein	MW (kDa)	Species	IF dilution	WB dilution	Company/Reference
hSpindly (1-444aa)	70	rabbit	1:1000	1:100	
hSpindly (443-605aa)	70	rabbit	1:1000		
CENP-P	30	rabbit	1:1000	1:1000	Generated by Herman Sillje and Anja Wehner
pS10-Histone H3	16	rabbit		1:1000	Millipore
Dynamitin p50	50	mouse	1:1000	1:1000	BD Biosciences
Mad2	23	mouse	1:1000		Generated by Andreas Uldschmid, see also (Fava et al., 2011)
Mad2	23	rabbit		1:1000	Bethyl Laboratories
CENP-E	310	goat		1:200	Santa Cruz Biotechnology
CDC27	97	mouse		1:1000	BD Biosciences
Rod	250	mouse		1:100	Abnova
CENP-A	16	mouse		1:1000	MBL International
α-tubulin	55	mouse	1:1000	1:1000	Sigma-Aldrich
α-tubulin	55	sheep	1:1000		Santa-Cruz Biotechnology
Zw10	88	rabbit	1:400	1:400	Abcam
Dynein IC	70	mouse	1:200	1:1000	Sigma-Aldrich
$p150^{Glued}$	150	mouse	1:1000	1:1000	BD Biosciences
Myc 9E10 serum		mouse	1:5	1:5	Homemade

Myc		rabbit	1:500		Santa-Cruz Biotechnology
Cyclin B1	60	mouse		1:1000	Millipore
Hec1	75	mouse	1:1000	1:1000	GeneTex
Nde1	40		1:1000		Proteintech Group
Aurora B	41	mouse	1:500	1:500	BD Biosciences
Dynein HC	450	rabbit		1:100	Santa-Cruz Biotechnology
CREST serum		human	1:2000		Immunovision
pericentrin	380	rabbit	1:2000		Abcam
Centrin-3	20	goat	1:200		(Thein et al., 2007)
Ska1	30	rabbit	1:1000	1:1000	(Hanisch et al., 2006)
Ska2	14	rabbit		1:1000	(Hanisch et al., 2006)
Ska3	50	rabbit	1:1000	1:1000	(Gaitanos et al., 2009)
mCherry	30	rabbit	1:2000	1:5000	(Hubner et al., 2010)
KNL1	300	rabbit		1:500	Abcam
Mis13	45	rabbit	1:500	1:500	(Yang et al., 2008)

Table 2. List of antibodies used for immunofluorescence and Western blotting in this study. The first column indicates which proteins the antibodies recognize. The second column shows the approximate molecular weight (MW) of the proteins. The third column shows in which species the antibodies were raised.

8. Time-lapse microscopy

HeLa cells were seeded in 8-wells culture plates (Ibidi). The plates were placed onto a sample stage within an incubator chamber (EMBLEM, Heidelberg, Germany) maintained at a temperature of 37°C, humidity 50%, in an atmosphere of 5% CO2. For part I, imaging was performed using a microscope (Axio Observer Z1; Carl Zeiss, Inc.) equipped with Plan Neofluar 20x and 40x objectives. MetaMorph software was used to collect and process data. For analysis of mitotic timing, a HeLa S3 cell line stably expressing histone H2B-GFP was used. Imaging was performed using a 20x objective and images were captured using 10 ms exposure times for GFP every 3 min, for 16 h. For analysis of spindle rotation, a HeLa Kyoto cell line with a RT-site and stably expressing GFP-α-tubulin/cherry-H2B cell line was used. Imaging was performed using a 40x objective and images were captured using 10 and 80 ms exposure time for cherry and EGFP, respectively, every 3 min.

For part II, following Ska1 and Ska3 siRNAs and plasmids transfection, HeLa S3 cells stably expressing histone H2B-GFP were imaged using a Nikon ECLIPSE Ti microscope equipped with a CoolLED pE-1 excitation system and a 20x/0.75 air Plan Apo objective (Nikon).

Images were acquired at multiple positions every 3 min, for 18 h. GFP signal was acquired at each time point with a 10 ms exposure time. mCherry signal was acquired every 10 time points with a 30 ms exposure time.

9. *In vitro* kinase assay

For CDK1 kinase assay with GST-hSpindly, active cyclin B-CDK1 kinase complex (Millipore) was mixed with the substrate (GST-hSpindly WT or 5A mutant) in BRB buffer (80 mM PIPES pH 6.8, 0.5mM $MgCl_2$, 1 mM EGTA, 5 mM β-glycerophosphate, 1 mM DTT) with 10 μM ATP and 5 μCiγ-^{32}P-ATP. For kinase assay using His_6-Aurora B as kinase and His_6-Ska proteins as substrates, the following buffer was used: 25 mM HEPES pH 7.4, 50 mM NaCl, 1 mM DTT, 2 mM EGTA, 5 mM $MgSO_4$, 10 μM ATP and 5 μCiγ-^{32}P-ATP. *In vitro* kinase assays were performed at 30 ºC. Reactions were stopped after 30 min by addition of sample buffer. Samples were then resolved by SDS-PAGE and visualized by autoradiography. Kodak BioMax MR films were used to detect the signal.

For Aurora B kinase assays on peptide-immobilized cellulose membranes, peptide arrays were constructed using standard Fmoc (*N*-(9-fluorenyl)methoxycarbonyl) chemistry on a MultiPep robotic spotter according to the manufacturer's directions (Intavis). 12-mer peptides containing putative Aurora B sites (S/T) of Ska1 and Ska3 at position 7 were generated and immobilized on cellulose membranes. To determine specificity, control peptides were synthesized with the corresponding phospho-acceptor changed to alanine. Dried membranes were first washed in ethanol and then hydrated in kinase buffer (50 mm Tris-HCl, pH7.5, 10 mm $MgCl_2$, 1 mm DTT, 100 μm NaF, and 10 μm sodium orthovanadate) for 1 h followed by overnight blocking in kinase buffer with 100 mm NaCl and 0.5 mg/ml BSA. The next day, the membranes were blocked again with kinase buffer containing 1 mg/ml BSA, 100 mm NaCl, and 10 μm cold ATP at 30 °C for 45 min. The block was subsequently replaced with kinase reaction buffer containing 0.2 mg/ml BSA, 50 μCi/ml γ-^{32}P-ATP, 10 μg/ml His_6-Aurora B, and 10 μM ATP for 3 h on a shaker at 30 °C. The membranes were then washed extensively (10 × 15 min in 1 m NaCl, 3 × 5 min in H_2O, 3 × 15 min 5% H_3PO_4, and 3 × 5 min in H_2O) and then sonicated overnight in 8 M urea, 1% SDS (w/v), and 0.5% (v/v) β-mercaptoethanol to remove residual

nonspecific radioactivity. The membranes were washed again with 5 times with H_2O followed by ethanol and dried before being visualized by autoradiography.

10. Directed yeast two-hybrid analysis

cDNAs encoding the respective prey or bait proteins were cloned in-frame with the GAL activation domain of pACT2 (in the case of Spc24) or pGAD-C1 (in the case of Ska1, Ska2 and Ska3) vectors or the GAL-binding domain of pFBT9 vector (in the case of Hec1, Nuf2, Spc24 and Spc25). All vectors are from Clontech (Mountain View, CA). Plasmids encoding members of the Mis12 complex, namely Mis12, Mis13, Mis14 and Nnf1 (Kiyomitsu et al., 2010) were a gift from M. Yanagida, Kyoto University, Kyoto. To perform the yeast two-hybrid analysis, 10 µl of competent yeast cells (stain: Py69-4A, resuspended in LiSorb solution (100 mM LiOAc, 10 mM Tris-HCl pH 8.0, 1 mM EDTA pH 8.0, 1 M Sorbitol) with 1 mg/ml carrier DNA (Salmon sperm DNA from Invitrogen)) were transformed with the plasmid DNA encoding the proteins of interest (~100-200 µg each) with 80 µl of LiPEG (100 mM LiOAc, 10 mM Tris-HCl pH 8.0, 1 mM EDTA pH 8.0, 40 % PEG3350) and 10 µl DMSO. The mixture was then incubated 20 min at 42 ºC. The cells were then spun down (2000 rpm for 2 min) and resuspended in ~50 µl of 1X PBS. The yeast cells were seeded into yeast plates without Leu and Trp (-L-W). After 2-3 days, ~10 colonies were picked and dissolved in 1X PBS, OD_{600} was measured and different samples were adjusted to have same concentration of yeast cells. Equal volume of the each solution was then seeded into -L-W plates (as growth control) and yeast plates without Leu, Trp, Ade and His (QDO). The plates were then incubated at 30ºC.

Appendix

1. List of abbreviations

All units are abbreviated according to the International Unit System.

aa:	amino acid
a.u.:	arbitrary units
ATP:	adenosine 5'-triphosphate
BSA:	bovine serum albumin
CCAN:	constitutive centromere-associated network
CDK:	cyclin-dependent kinase
CENP-A NAC:	CENP-A-nucleosome associated complex
CENP-A CAD:	CENP-A-nucleosome distal components
CPC:	chromosomal passenger complex
C-terminus:	carboxy-terminus
DAPI:	4', 6-diamidino-2-phenylindole
DHC:	dynein heavy chain
DIC:	dynein intermediate chain
DTT:	dithiothreitol
ECL:	enhanced chemiluminescence
EDTA:	ethylene-dinitrilo-tetra-acetic acid
EGTA:	ethylene-gycol-tetra-acetic acid
FCS:	Fetal calf serum
HCl:	hydrochloric acid
γTuRC:	Gamma tubulin ring complex
GEF:	Guanosine exchange factor
GFP:	green fluorescent protein
GL2:	*Photinus pyralis* luciferase gene
GTP:	Guanosine 5'-triphosphate
h:	hour
H2B:	Histone 2B

HEPES:	N-2-Hydroxyethylpiperazine-N'-2-ethane sulfonic acid
IgG:	Immunoglobulin G
IPTG:	Isopropyl-beta-D-thiogalactopyranoside
K-fibers:	Kinetochore fibers
kDa:	kilo Daltons
KMN:	KNL-1/Mis12/Ndc80 network
KT:	Kinetochore
KT-MT:	Kinetochore microtubule
LB:	Luria broth
MAP:	Microtubule-associated protein
min:	minute
MCC:	mitotic checkpoint complex
MT:	microtubules
MTOC :	Microtubule organizing center
MW:	Molecular weight
N-terminus:	amino-terminus
NEBD:	Nuclear envelop break down
PBS:	Phosphate-buffered saline
PCR:	polymerase chain reaction
RNAi:	RNA interference
Pfu:	*Pyrococcus furiosus*
PIPES:	1, 4-Piperazinediethansulfonic acid
PMSF:	Phenylmethylsulfonyl fluoride
rpm:	Rounds per minute
RT:	Room temperature
RZZ:	Rod/Zw10/Zwilch
SAC:	Spindle-assembly checkpoint
s.d:	Standard derviation
SDS-PAGE:	Sodium dodecylsulfate polyacrylamid gelelectrophoresis
siRNA:	small interfering RNA
WT:	Wild-type

2. Table of created plasmids

Code	Description	Vector	Tag
GC1	Nek7 cDNA from Open Biosystems	pINCY	
GC2	Nek9 cDNA from Open Biosystems	pCR4-TOPO	
GC3	Myc-Nek6	pcDNA3.1/3x myc-C	Myc
GC4	Myc-Nek7	pcDNA3.1/3x myc-C	Myc
GC5	Myc-Nek9	pcDNA3.1/3x myc-C	Myc
GC6	Myc-hSpindly N term 1-444	pcDNA3.1/3x myc-C	Myc
GC7	Myc-hSpindly C term 443-605	pcDNA3.1/3x myc-C	Myc
GC8	His6-hSpindly N term 1-444-His6	pET-28b-HS2	His6
GC9	His6-hSpindly C term 443-605	pET-28b-HS2	His6
GC10	hZW10 cDNA from Open Biosystems	pINCY	
GC11	hZwilch cDNA from Open Biosystems	pCMV-SPORT6	
GC12	GST-hSpindly	pGEX-5x-1	GST
GC13	FLAG-hSpindly	pcDNA3.1/FLAG-C	FLAG
GC14	FLAG-hSpindly N term 1-444	pcDNA3.1/FLAG-C	FLAG
GC15	FLAG-hSpindly C term 443-605	pcDNA3.1/FLAG-C	FLAG
GC16	Myc-ZW10	pcDNA3.1/3x myc-C	Myc
GC17	His6-ZW10	pET-28b-HS2	His6
GC18	Myc-Zwilch	pcDNA3.1/3x myc-C	Myc
GC19	His6-Zwilch	pET-28b-HS2	His6
GC20	hSpindly-GAL4 AD	pGAD-C1	GAL4 AD
GC21	hSpindly-GAL4 BD	pFBT9'	GAL4 BD
GC22	hRod cDNA from Gene Service	pBluescript II SK+	
GC23	FLAG-ZW10	pcDNA3.1/FLAG-C	FLAG
GC24	Myc-Spindly S515A	pcDNA3.1/3x myc-C	Myc
GC25	Myc-Spindly T597A	pcDNA3.1/3x myc-C	Myc
GC26	Myc-Spindly S515A+S555A	pcDNA3.1/3x myc-C	Myc
GC27	Myc-Spindly T509A+S515A	pcDNA3.1/3x myc-C	Myc
GC28	Myc-Spindly T552A+T597A	pcDNA3.1/3x myc-C	Myc
GC29	Myc-Spindly T552A+S555A+T597A	pcDNA3.1/3x myc-C	Myc
GC30	Myc-Spindly S515A+T552A+S555A+T597A	pcDNA3.1/3x myc-C	Myc
GC31	Myc-Spindly 5A	pcDNA3.1/3x myc-C	Myc
GC32	Myc-Spindly RNAi mutant	pcDNA3.1/3x myc-C	Myc
GC33	Myc-Spindly 5A RNAi mutant	pcDNA3.1/3x myc-C	Myc
GC34	Myc-Spindly S515A+S555A RNAi mutant	pcDNA3.1/3x myc-C	Myc
GC35	Myc-Spindly T597 RNAi mutant	pcDNA3.1/3x myc-C	Myc

GC36	p50-GAL4 AD	pGAD-C1	GAL4 AD
GC37	ZW10-GAL4 AD	pGAD-C1	GAL4 AD
GC38	p50-GAL BD	pFBT9'	GAL4 BD
GC39	cherry-spindly WT RNAi mutant	pcDNA3.1/cherry C	cherry
GC40	cherry-spindly 5A RNAi mutant	pcDNA3.1/cherry C	cherry
GC41	cherry-spindly 2A RNAi mutant	pcDNA3.1/cherry C	cherry
GC42	Myc-Spindly 1-444 RNAi mutant	pcDNA3.1/3x myc-C	Myc
GC43	Myc-Spindly 1-506 RNAi mutant	pcDNA3.1/3x myc-C	Myc
GC44	GST-hSpindly S515A S555A	pGEX-5x-1	GST
GC45	GST-hSpindly 5A	pGEX-5x-1	GST
GC46	GST-ZW10	pGEX-6p-3	GST
GC47	cherry-MAD2	pCDNA3.1/cherry-A	cherry
GC48	pET11d-p50	pET11d	
GC49	Myc-Spindly 5D RNAi mutant	pcDNA3.1/3x myc-C	Myc
GC50	Flag-Rod 1-735	pcDNA3.1/Flag-B	FLAG
GC51	Flag-Rod 715-1485	pcDNA3.1/Flag-B	FLAG
GC52	Flag-Rod 1455-2209	pcDNA3.1/Flag-B	FLAG
GC53	Flag-Zwilch	pcDNA3.1/Flag-C	FLAG
GC54	Flag-Ska3	pcDNA3.1/Flag-A	FLAG
GC55	Cherry-H2B	LW10	cherry
GC56	Myc-p50 91-143aa	pcDNA3.1/3x myc-C	Myc
GC57	Flag-Mis12	pcDNA3.1/Flag-C	FLAG
GC58	Flag-Hec1	pcDNA3.1/Flag-C	FLAG
GC59	Cherry-CenpP	pCDNA3.1/cherry-C	cherry
GC60	CenpA Full length cDNA BC002703		
GC61	Cherry-CenpA	pcDNA 4 TO/cherry	cherry
GC62	CENP-P-EGFP	pcDNA4 TO/c-EGFP	EGFP
GC63	Cherry-hSpindly 5D RNAi resistant	pCDNA3.1/cherry-C	cherry
GC64	Myc-CENP-P 1-156aa	pcDNA3.1/3x myc-C	Myc
GC65	Myc-CENP-P 1-208aa	pcDNA3.1/3x myc-C	Myc
GC66	Myc-CENP-P 208-288aa	pcDNA3.1/3x myc-C	Myc
GC67	Myc-CENP-P 1-72aa	pcDNA3.1/3x myc-C	Myc
GC68	Myc-CENP-P 72-288aa	pcDNA3.1/3x myc-C	Myc
GC69	CENP-P-GAL4 AD	pGAD-C1	GAL4 AD
GC70	CENP-P-GAL4 BD	pFBT9'	GAL4 BD
GC71	Mis13-GAL4 AD	pGAD-C1	GAL4 AD
GC72	Mis13-GAL4 BD	pFBT9'	GAL4 BD

GC73	Hec1 446-642 GAL4 BD	pFBT9'	GAL4 BD
GC74	Spc24 1-69 GAL4 BD	pFBT9'	GAL4 BD
GC75	Hec1 1-445 GAL4 BD	pFBT9'	GAL4 BD
GC76	Spc24 70-198 GAL4 BD	pFBT9'	GAL4 BD
GC77	Mis13 1-130 GAL4 BD	pFBT9'	GAL4 BD
GC78	Mis13 121-356 GAL4 BD	pFBT9'	GAL4 BD
GC79	Hec1 1-230 GAL4 BD	pFBT9'	GAL4 BD
GC80	Hec1 231-642 GAL4 BD	pFBT9'	GAL4 BD
GC81	Ska 1 T205A (RNAi resistant)	pcDNA3.1/3x myc-C	Myc
GC82	Ska 1 S185A T205A (RNAi resistant)	pcDNA3.1/3x myc-C	Myc
GC83	Ska 1 T157A S185A T205A (RNAi resistant)	pcDNA3.1/3x myc-C	Myc
GC84	Ska 1 S185A T205A S242A (RNAi resistant)	pcDNA3.1/3x myc-C	Myc
GC85	Ska 1 4A (157, 185, 205, 242; RNAi resistant)	pcDNA3.1/3x myc-C	Myc
GC86	Ska1 92-255 GAL AD	pGAD-C1	GAL4 AD
GC87	Ska 1 RNAi resistant	pcDNA5/FRT/TO/N-3xmycA	Myc
GC88	Ska 1 4A (157, 185, 205, 242; RNAi resistant)	pcDNA5/FRT/TO/N-3xmycA	Myc
GC89	Ska 1 4D (157, 185, 205, 242; RNAi resistant)	pcDNA5/FRT/TO/N-3xmycA	Myc
GC90	Mis13 RNAi resistant	pcDNA3.1/3x myc-C	Myc
GC91	Ska2 1-97aa GAL4 AD	pGAD-C1	GAL4 AD
GC92	Ska2 D36R S37R S39R E40A GAL4 AD	pGAD-C1	GAL4 AD
GC93	Mis13 S100A S109A RNAi rs	pcDNA3.1/3x myc-C	Myc
GC94	Mis13 S28A S100A S109A RNAi rs	pcDNA3.1/3x myc-C	Myc
GC95	Mis13 S77A S100A S109A RNAi rs	pcDNA3.1/3x myc-C	Myc
GC96	Mis13 S28A S77A S100A S109A RNAi rs	pcDNA3.1/3x myc-C	Myc
GC97	Mis13 S100D S109D RNAi rs	pcDNA3.1/3x myc-C	Myc
GC98	Myc-Ska3 S159A	pcDNA5/FRT/TO/N-3xmycA	Myc
GC99	Myc-Ska3 S159D	pcDNA5/FRT/TO/N-3xmycA	Myc
GC100	Mis13 S28D S77D S100D S109D RNAi rs	pcDNA3.1/3x myc-C	Myc
GC101	Mis13 S28D S100D S109D RNAi rs	pcDNA3.1/3x myc-C	Myc
GC102	Mis13 S77D S100D S109D RNAi rs	pcDNA3.1/3x myc-C	Myc
GC103	Spindly F258A	pcDNA3.1/3x myc-C	Myc
GC104	cherry-Ska3 S159A	pCDNA3.1/cherry-A	cherry
GC105	cherry-Ska3 S159D	pCDNA3.1/cherry-A	cherry
GC106	Flag-Mis13 RNAi re	pcDNA3.1/Flag-C	Flag
GC107	Flag-Mis13 S28A S77A S100A S109A RNAi rs	pcDNA3.1/Flag-C	Flag

GC108	Flag-Mis13 S28D S77D S100D S109D RNAi rs	pcDNA3.1/Flag-C	Flag
GC109	Ska3 S110A S159A	pcDNA5/FRT/TO/N-3xmycA	Myc
GC110	Ska3 S110D S159D	pcDNA5/FRT/TO/N-3xmycA	Myc
GC111	Ska3 S87A S110A S159A	pcDNA5/FRT/TO/N-3xmycA	Myc
GC112	Ska3 S87D S110D S159D	pcDNA5/FRT/TO/N-3xmycA	Myc
GC113	Myc-Ska1 4A	pcDNA3.1/3x myc-A	Myc
GC114	Myc-Ska3 3A	pcDNA3.1/3x myc-A	Myc
GC115	BD-Ska3	pFBT9'	GAL4 BD
GC116	AD-Ska3	pGAD-C1	GAL4 AD
GC117	Flag-Ska1 4A	pcDNA3.1/Flag-A	Flag
GC118	Myc-Ska3 1A	pcDNA3.1/3x myc-A	Myc
GC119	His6-Ska1 4A	pET-28c	His6
GC120	His6-Ska1 4D	pET-28c	His6
GC121	His6-Ska3 3A	pET-28c	His6
GC122	His6-Ska3 3D	pET-28c	His6
GC123	Flag-Ska3 3A	pcDNA3.1/Flag-A	Flag
GC124	Flag-Ska3 3D	pcDNA3.1/Flag-A	Flag
GC125	Ska3 S87A S110A S159A S317A	pcDNA5/FRT/TO/N-3xmycA	Myc
GC126	Ska3 S87D S110D S159D S317D	pcDNA5/FRT/TO/N-3xmycA	Myc
GC127	Ska3 S87A S110A S159A	pcDNA3.1/mCherry A	cherry
GC128	Ska3 S87D S110D S159D	pcDNA3.1/mCherry A	cherry
GC129	AD-Ska1 4A	pGAD-C1	GAL4 AD
GC130	AD-Ska1 4D	pGAD-C1	GAL4 AD
GC131	Ska1 4A-His6	pET-28b-HS-1	His6
GC132	Ska1 4D-His6	pET-28b-HS-1	His6
GC133	BD-Ska3 3A	pFBT9'	GAL4 BD
GC134	BD-Ska3 3D	pFBT9'	GAL4 BD
GC135	cherry-Mis12-Ska3 WT	pcDNA3.1/mCherry A	cherry
GC136	cherry-Mis12-Ska3 3D	pcDNA3.1/mCherry A	cherry

Acknowledgements

I would like to thank Prof. Dr. Erich Nigg for giving me the opportunity to pursue my PhD study in his very well organized and equipped laboratory. I also sincerely thank for his supports and advices on my project, and also for his invaluable advice in my scientific career planning.

I would like to express my gratitude to Dr. Anna Santamaria, who is my supervisor of my PhD studies. I thank Anna for introduced me to the exciting mitosis field, teaching me different techniques and knowledge of mitosis. She is always open for discussion and gave me a lot of good advices for my project. She is very friendly and we have both good working and personal relationships.

Furthermore, I am grateful to Prof. Dr. Thomas Mayer and Prof. Dr. Patrick Meraldi for being the members of my PhD advisory Committee and their professional advices.

For technical help I like to thank Anja Wehner, Elena Nigg, Fabien Cubizolles (for general cellular and molecular biology) and Dr. Timo Glatter (for proteomics). I especially thank Dr. Herman Sillje, Dr. Anja Hanisch and Anja Wehner for initial yeast two-hybrid screens of the Ska proteins. For the important reagents, I thank Dr. A. A. Jeyaprakach and Dr. E. Conti for the Ska2 construct and experiment advice, Dr. Herman Sillje and Anja Wehner for generation of CENP-P antibody, Dr. N. S Gray for the Mps1-In-1 inhibitor, Dr. X. Yao for the His-Aurora B construct and Mis13 antibody, Dr. M Yanagudia for the Mis12 complex constructs, Dr. S. Lens for the Mis12-INCENP plasmids, Dr. I. Cheeseman for the GFP^{LAP}-Ska2 cell line, Dr. D. Gerlich for the GFP-α-tubulin/cherry-H2B cell line, and Dr. A. Uldschmid and Luca Fava for generating and characterizing the MAD2 antibody

Special thanks to the lab members, both in Munich and Basel. They are not only colleagues but also friends: Luca Fava, Tom Gaitanos, Anna Santamaria, Zhen Dou, Bin Wang, Lily Wang, Eunice Chan, Manuel Kaulich, Anna Baron, Gernot Guderian, Katharina Mayer, Christian Arquint, Eduard Anselm, Anna-Maria Gabryjonczyk, Fabien Cubizolles, Manuel Bauer and Conrad Eberhard Von Schubert. I enjoy the stimulating and friendly atmosphere in the lab. We also have a lot of unforgettable time outside the lab.

Lastly, I would like to thank my family for the endless love and continuous support.

References

Abrieu, A., L. Magnaghi-Jaulin, J.A. Kahana, M. Peter, A. Castro, S. Vigneron, T. Lorca, D.W. Cleveland, and J.C. Labbe. 2001. Mps1 is a kinetochore-associated kinase essential for the vertebrate mitotic checkpoint. *Cell*. 106:83-93.

Amaro, A.C., C.P. Samora, R. Holtackers, E. Wang, I.J. Kingston, M. Alonso, M. Lampson, A.D. McAinsh, and P. Meraldi. 2010. Molecular control of kinetochore-microtubule dynamics and chromosome oscillations. *Nat Cell Biol*. 12:319-329.

Andrews, P.D., Y. Ovechkina, N. Morrice, M. Wagenbach, K. Duncan, L. Wordeman, and J.R. Swedlow. 2004a. Aurora B regulates MCAK at the mitotic centromere. *Developmental cell*. 6:253-268.

Andrews, P.D., Y. Ovechkina, N. Morrice, M. Wagenbach, K. Duncan, L. Wordeman, and J.R. Swedlow. 2004b. Aurora B regulates MCAK at the mitotic centromere. *Dev Cell*. 6:253-268.

Barisic, M., B. Sohm, P. Mikolcevic, C. Wandke, V. Rauch, T. Ringer, M. Hess, G. Bonn, and S. Geley. 2010. Spindly/CCDC99 is required for efficient chromosome congression and mitotic checkpoint regulation. *Molecular biology of the cell*. 21:1968-1981.

Basto, R., R. Gomes, and R.E. Karess. 2000. Rough deal and Zw10 are required for the metaphase checkpoint in Drosophila. *Nat Cell Biol*. 2:939-943.

Basto, R., F. Scaerou, S. Mische, E. Wojcik, C. Lefebvre, R. Gomes, T. Hays, and R. Karess. 2004. In vivo dynamics of the rough deal checkpoint protein during Drosophila mitosis. *Curr Biol*. 14:56-61.

Bharadwaj, R., and H. Yu. 2004. The spindle checkpoint, aneuploidy, and cancer. *Oncogene*. 23:2016-2027.

Biggins, S., F.F. Severin, N. Bhalla, I. Sassoon, A.A. Hyman, and A.W. Murray. 1999. The conserved protein kinase Ipl1 regulates microtubule binding to kinetochores in budding yeast. *Genes Dev*. 13:532-544.

Bishop, J.D., and J.M. Schumacher. 2002. Phosphorylation of the carboxyl terminus of inner centromere protein (INCENP) by the Aurora B Kinase stimulates Aurora B kinase activity. *J Biol Chem*. 277:27577-27580.

Buffin, E., C. Lefebvre, J. Huang, M.E. Gagou, and R.E. Karess. 2005. Recruitment of Mad2 to the kinetochore requires the Rod/Zw10 complex. *Curr Biol*. 15:856-861.

Busson, S., D. Dujardin, A. Moreau, J. Dompierre, and J.R. De Mey. 1998. Dynein and dynactin are localized to astral microtubules and at cortical sites in mitotic epithelial cells. *Curr Biol*. 8:541-544.

Carazo-Salas, R.E., O.J. Gruss, I.W. Mattaj, and E. Karsenti. 2001. Ran-GTP coordinates regulation of microtubule nucleation and dynamics during mitotic-spindle assembly. *Nat Cell Biol*. 3:228-234.

Carroll, C.W., K.J. Milks, and A.F. Straight. 2010. Dual recognition of CENP-A nucleosomes is required for centromere assembly. *J Cell Biol*. 189:1143-1155.

Chan, G.K., S.A. Jablonski, D.A. Starr, M.L. Goldberg, and T.J. Yen. 2000. Human Zw10 and ROD are mitotic checkpoint proteins that bind to kinetochores. *Nat Cell Biol*. 2:944-947.

Cheeseman, I.M., S. Anderson, M. Jwa, E.M. Green, J. Kang, J.R. Yates, 3rd, C.S. Chan, D.G. Drubin, and G. Barnes. 2002. Phospho-regulation of kinetochore-microtubule attachments by the Aurora kinase Ipl1p. *Cell*. 111:163-172.

Cheeseman, I.M., J.S. Chappie, E.M. Wilson-Kubalek, and A. Desai. 2006. The conserved KMN network constitutes the core microtubule-binding site of the kinetochore. *Cell*. 127:983-997.

Cheeseman, I.M., and A. Desai. 2008. Molecular architecture of the kinetochore-microtubule interface. *Nat Rev Mol Cell Biol*. 9:33-46.

Cheeseman, I.M., S. Niessen, S. Anderson, F. Hyndman, J.R. Yates, 3rd, K. Oegema, and A. Desai. 2004. A conserved protein network controls assembly of the outer kinetochore and its ability to sustain tension. *Genes Dev*. 18:2255-2268.

Ciferri, C., J. De Luca, S. Monzani, K.J. Ferrari, D. Ristic, C. Wyman, H. Stark, J. Kilmartin, E.D. Salmon, and A. Musacchio. 2005. Architecture of the human ndc80-hec1 complex, a critical constituent of the outer kinetochore. *J Biol Chem*. 280:29088-29095.

Ciferri, C., S. Pasqualato, E. Screpanti, G. Varetti, S. Santaguida, G. Dos Reis, A. Maiolica, J. Polka, J.G. De Luca, P. De Wulf, M. Salek, J. Rappsilber, C.A. Moores, E.D. Salmon, and A. Musacchio. 2008. Implications for kinetochore-microtubule attachment from the structure of an engineered Ndc80 complex. *Cell*. 133:427-439.

Cimini, D., X. Wan, C.B. Hirel, and E.D. Salmon. 2006. Aurora kinase promotes turnover of kinetochore microtubules to reduce chromosome segregation errors. *Curr Biol*. 16:1711-1718.

Cleveland, D.W., Y. Mao, and K.F. Sullivan. 2003. Centromeres and kinetochores: from epigenetics to mitotic checkpoint signaling. *Cell*. 112:407-421.

Conde e Silva, N., B.E. Black, A. Sivolob, J. Filipski, D.W. Cleveland, and A. Prunell. 2007. CENP-A-containing nucleosomes: easier disassembly versus exclusive centromeric localization. *J Mol Biol*. 370:555-573.

Daum, J.R., J.D. Wren, J.J. Daniel, S. Sivakumar, J.N. McAvoy, T.A. Potapova, and G.J. Gorbsky. 2009. Ska3 is required for spindle checkpoint silencing and the maintenance of chromosome cohesion in mitosis. *Curr Biol*. 19:1467-1472.

De Antoni, A., C.G. Pearson, D. Cimini, J.C. Canman, V. Sala, L. Nezi, M. Mapelli, L. Sironi, M. Faretta, E.D. Salmon, and A. Musacchio. 2005. The Mad1/Mad2 complex as a template for Mad2 activation in the spindle assembly checkpoint. *Curr Biol*. 15:214-225.

DeLuca, J.G., Y. Dong, P. Hergert, J. Strauss, J.M. Hickey, E.D. Salmon, and B.F. McEwen. 2005. Hec1 and nuf2 are core components of the kinetochore outer plate essential for organizing microtubule attachment sites. *Mol Biol Cell*. 16:519-531.

DeLuca, J.G., W.E. Gall, C. Ciferri, D. Cimini, A. Musacchio, and E.D. Salmon. 2006. Kinetochore microtubule dynamics and attachment stability are regulated by Hec1. *Cell*. 127:969-982.

DeLuca, K.F., S.M. Lens, and J.G. DeLuca. 2011a. Temporal changes in Hec1 phosphorylation control kinetochore-microtubule attachment stability during mitosis. *Journal of cell science*. 124:622-634.

DeLuca, K.F., S.M. Lens, and J.G. DeLuca. 2011b. Temporal changes in Hec1 phosphorylation control kinetochore-microtubule attachment stability during mitosis. *Journal of cell science*. 124:622-634.

Desai, A., S. Rybina, T. Muller-Reichert, A. Shevchenko, A. Hyman, and K. Oegema. 2003. KNL-1 directs assembly of the microtubule-binding interface of the kinetochore in C. elegans. *Genes Dev*. 17:2421-2435.

Ditchfield, C., V.L. Johnson, A. Tighe, R. Ellston, C. Haworth, T. Johnson, A. Mortlock, N. Keen, and S.S. Taylor. 2003a. Aurora B couples chromosome alignment with anaphase by targeting BubR1, Mad2, and Cenp-E to kinetochores. *The Journal of cell biology*. 161:267-280.

Ditchfield, C., V.L. Johnson, A. Tighe, R. Ellston, C. Haworth, T. Johnson, A. Mortlock, N. Keen, and S.S. Taylor. 2003b. Aurora B couples chromosome alignment with anaphase by targeting BubR1, Mad2, and Cenp-E to kinetochores. *J Cell Biol*. 161:267-280.

Earnshaw, W.C., and B.R. Migeon. 1985. Three related centromere proteins are absent from the inactive centromere of a stable isodicentric chromosome. *Chromosoma*. 92:290-296.

Echeverri, C.J., B.M. Paschal, K.T. Vaughan, and R.B. Vallee. 1996. Molecular characterization of the 50-kD subunit of dynactin reveals function for the complex in chromosome alignment and spindle organization during mitosis. *J Cell Biol*. 132:617-633.

Elbashir, S.M., J. Harborth, W. Lendeckel, A. Yalcin, K. Weber, and T. Tuschl. 2001. Duplexes of 21-nucleotide RNAs mediate RNA interference in cultured mammalian cells. *Nature*. 411:494-498.
Famulski, J.K., and G.K. Chan. 2007. Aurora B kinase-dependent recruitment of hZW10 and hROD to tensionless kinetochores. *Curr Biol*. 17:2143-2149.
Fang, G. 2002. Checkpoint protein BubR1 acts synergistically with Mad2 to inhibit anaphase-promoting complex. *Mol Biol Cell*. 13:755-766.
Fang, G., H. Yu, and M.W. Kirschner. 1998. The checkpoint protein MAD2 and the mitotic regulator CDC20 form a ternary complex with the anaphase-promoting complex to control anaphase initiation. *Genes Dev*. 12:1871-1883.
Faulkner, N.E., D.L. Dujardin, C.Y. Tai, K.T. Vaughan, C.B. O'Connell, Y. Wang, and R.B. Vallee. 2000. A role for the lissencephaly gene LIS1 in mitosis and cytoplasmic dynein function. *Nature cell biology*. 2:784-791.
Fava, L.L., M. Kaulich, E.A. Nigg, and A. Santamaria. 2011. Probing the in vivo function of Mad1:C-Mad2 in the spindle assembly checkpoint. *EMBO J*.
Feng, Y., E.C. Olson, P.T. Stukenberg, L.A. Flanagan, M.W. Kirschner, and C.A. Walsh. 2000. LIS1 regulates CNS lamination by interacting with mNudE, a central component of the centrosome. *Neuron*. 28:665-679.
Feng, Y., and C.A. Walsh. 2004. Mitotic spindle regulation by Nde1 controls cerebral cortical size. *Neuron*. 44:279-293.
Foltz, D.R., L.E. Jansen, B.E. Black, A.O. Bailey, J.R. Yates, 3rd, and D.W. Cleveland. 2006. The human CENP-A centromeric nucleosome-associated complex. *Nat Cell Biol*. 8:458-469.
Fraschini, R., A. Beretta, L. Sironi, A. Musacchio, G. Lucchini, and S. Piatti. 2001. Bub3 interaction with Mad2, Mad3 and Cdc20 is mediated by WD40 repeats and does not require intact kinetochores. *EMBO J*. 20:6648-6659.
Fujita, Y., T. Hayashi, T. Kiyomitsu, Y. Toyoda, A. Kokubu, C. Obuse, and M. Yanagida. 2007. Priming of centromere for CENP-A recruitment by human hMis18alpha, hMis18beta, and M18BP1. *Dev Cell*. 12:17-30.
Fuller, B.G., M.A. Lampson, E.A. Foley, S. Rosasco-Nitcher, K.V. Le, P. Tobelmann, D.L. Brautigan, P.T. Stukenberg, and T.M. Kapoor. 2008. Midzone activation of aurora B in anaphase produces an intracellular phosphorylation gradient. *Nature*. 453:1132-1136.
Gadde, S., and R. Heald. 2004. Mechanisms and molecules of the mitotic spindle. *Curr Biol*. 14:R797-805.
Gaetz, J., and T.M. Kapoor. 2004. Dynein/dynactin regulate metaphase spindle length by targeting depolymerizing activities to spindle poles. *J Cell Biol*. 166:465-471.
Gaglio, T., A. Saredi, J.B. Bingham, M.J. Hasbani, S.R. Gill, T.A. Schroer, and D.A. Compton. 1996. Opposing motor activities are required for the organization of the mammalian mitotic spindle pole. *J Cell Biol*. 135:399-414.
Gaitanos, T.N., A. Santamaria, A.A. Jeyaprakash, B. Wang, E. Conti, and E.A. Nigg. 2009. Stable kinetochore-microtubule interactions depend on the Ska complex and its new component Ska3/C13Orf3. *Embo J*.
Garrett, M.D. 2001. Cell cycle control and cancer. *Current Science*. 81:8.
Gassmann, R., A. Essex, J.S. Hu, P.S. Maddox, F. Motegi, A. Sugimoto, S.M. O'Rourke, B. Bowerman, I. McLeod, J.R. Yates, 3rd, K. Oegema, I.M. Cheeseman, and A. Desai. 2008a. A new mechanism controlling kinetochore-microtubule interactions revealed by comparison of two dynein-targeting components: SPDL-1 and the Rod/Zwilch/Zw10 complex. *Genes Dev*. 22:2385-2399.
Gassmann, R., A. Essex, J.S. Hu, P.S. Maddox, F. Motegi, A. Sugimoto, S.M. O'Rourke, B. Bowerman, I. McLeod, J.R. Yates, 3rd, K. Oegema, I.M. Cheeseman, and A. Desai. 2008b. A new mechanism controlling kinetochore-microtubule interactions revealed by comparison of two dynein-

targeting components: SPDL-1 and the Rod/Zwilch/Zw10 complex. *Genes & development*. 22:2385-2399.
Gassmann, R., A.J. Holland, D. Varma, X. Wan, F. Civril, D.W. Cleveland, K. Oegema, E.D. Salmon, and A. Desai. 2010. Removal of Spindly from microtubule-attached kinetochores controls spindle checkpoint silencing in human cells. *Genes & development*. 24:957-971.
Gatlin, J.C., and K. Bloom. 2010. Microtubule motors in eukaryotic spindle assembly and maintenance. *Semin Cell Dev Biol*. 21:248-254.
Gieni, R.S., G.K. Chan, and M.J. Hendzel. 2008. Epigenetics regulate centromere formation and kinetochore function. *J Cell Biochem*. 104:2027-2039.
Goshima, G., F. Nedelec, and R.D. Vale. 2005. Mechanisms for focusing mitotic spindle poles by minus end-directed motor proteins. *J Cell Biol*. 171:229-240.
Griffis, E.R., N. Stuurman, and R.D. Vale. 2007. Spindly, a novel protein essential for silencing the spindle assembly checkpoint, recruits dynein to the kinetochore. *J Cell Biol*. 177:1005-1015.
Guimaraes, G.J., Y. Dong, B.F. McEwen, and J.G. Deluca. 2008. Kinetochore-microtubule attachment relies on the disordered N-terminal tail domain of Hec1. *Curr Biol*. 18:1778-1784.
Habu, T., S.H. Kim, J. Weinstein, and T. Matsumoto. 2002. Identification of a MAD2-binding protein, CMT2, and its role in mitosis. *EMBO J*. 21:6419-6428.
Hanisch, A., H.H. Sillje, and E.A. Nigg. 2006. Timely anaphase onset requires a novel spindle and kinetochore complex comprising Ska1 and Ska2. *Embo J*. 25:5504-5515.
Hartwell, L.H., and T.A. Weinert. 1989. Checkpoints: controls that ensure the order of cell cycle events. *Science*. 246:629-634.
Hauf, S., R.W. Cole, S. LaTerra, C. Zimmer, G. Schnapp, R. Walter, A. Heckel, J. van Meel, C.L. Rieder, and J.M. Peters. 2003. The small molecule Hesperadin reveals a role for Aurora B in correcting kinetochore-microtubule attachment and in maintaining the spindle assembly checkpoint. *J Cell Biol*. 161:281-294.
Hayden, J.H., S.S. Bowser, and C.L. Rieder. 1990. Kinetochores capture astral microtubules during chromosome attachment to the mitotic spindle: direct visualization in live newt lung cells. *J Cell Biol*. 111:1039-1045.
Heald, R., R. Tournebize, A. Habermann, E. Karsenti, and A. Hyman. 1997. Spindle assembly in Xenopus egg extracts: respective roles of centrosomes and microtubule self-organization. *J Cell Biol*. 138:615-628.
Hemmerich, P., S. Weidtkamp-Peters, C. Hoischen, L. Schmiedeberg, I. Erliandri, and S. Diekmann. 2008. Dynamics of inner kinetochore assembly and maintenance in living cells. *J Cell Biol*. 180:1101-1114.
Hinchcliffe, E.H., F.J. Miller, M. Cham, A. Khodjakov, and G. Sluder. 2001. Requirement of a centrosomal activity for cell cycle progression through G1 into S phase. *Science*. 291:1547-1550.
Hirose, H., K. Arasaki, N. Dohmae, K. Takio, K. Hatsuzawa, M. Nagahama, K. Tani, A. Yamamoto, M. Tohyama, and M. Tagaya. 2004. Implication of ZW10 in membrane trafficking between the endoplasmic reticulum and Golgi. *Embo J*. 23:1267-1278.
Honda, R., R. Korner, and E.A. Nigg. 2003. Exploring the functional interactions between Aurora B, INCENP, and survivin in mitosis. *Mol Biol Cell*. 14:3325-3341.
Hori, T., M. Amano, A. Suzuki, C.B. Backer, J.P. Welburn, Y. Dong, B.F. McEwen, W.H. Shang, E. Suzuki, K. Okawa, I.M. Cheeseman, and T. Fukagawa. 2008a. CCAN makes multiple contacts with centromeric DNA to provide distinct pathways to the outer kinetochore. *Cell*. 135:1039-1052.
Hori, T., M. Okada, K. Maenaka, and T. Fukagawa. 2008b. CENP-O class proteins form a stable complex and are required for proper kinetochore function. *Mol Biol Cell*. 19:843-854.

Howell, B.J., B.F. McEwen, J.C. Canman, D.B. Hoffman, E.M. Farrar, C.L. Rieder, and E.D. Salmon. 2001. Cytoplasmic dynein/dynactin drives kinetochore protein transport to the spindle poles and has a role in mitotic spindle checkpoint inactivation. *J Cell Biol*. 155:1159-1172.

Howell, B.J., B. Moree, E.M. Farrar, S. Stewart, G. Fang, and E.D. Salmon. 2004. Spindle checkpoint protein dynamics at kinetochores in living cells. *Curr Biol*. 14:953-964.

Hoyt, M.A., L. Totis, and B.T. Roberts. 1991. S. cerevisiae genes required for cell cycle arrest in response to loss of microtubule function. *Cell*. 66:507-517.

Hubner, N.C., L.H. Wang, M. Kaulich, P. Descombes, I. Poser, and E.A. Nigg. 2010. Re-examination of siRNA specificity questions role of PICH and Tao1 in the spindle checkpoint and identifies Mad2 as a sensitive target for small RNAs. *Chromosoma*. 119:149-165.

Jansen, L.E., B.E. Black, D.R. Foltz, and D.W. Cleveland. 2007. Propagation of centromeric chromatin requires exit from mitosis. *J Cell Biol*. 176:795-805.

Jelluma, N., A.B. Brenkman, N.J. van den Broek, C.W. Cruijsen, M.H. van Osch, S.M. Lens, R.H. Medema, and G.J. Kops. 2008. Mps1 phosphorylates Borealin to control Aurora B activity and chromosome alignment. *Cell*. 132:233-246.

Joglekar, A.P., K. Bloom, and E.D. Salmon. 2009. In vivo protein architecture of the eukaryotic kinetochore with nanometer scale accuracy. *Curr Biol*. 19:694-699.

Joglekar, A.P., D. Bouck, K. Finley, X. Liu, Y. Wan, J. Berman, X. He, E.D. Salmon, and K.S. Bloom. 2008. Molecular architecture of the kinetochore-microtubule attachment site is conserved between point and regional centromeres. *J Cell Biol*. 181:587-594.

Joglekar, A.P., D.C. Bouck, J.N. Molk, K.S. Bloom, and E.D. Salmon. 2006. Molecular architecture of a kinetochore-microtubule attachment site. *Nat Cell Biol*. 8:581-585.

Joglekar, A.P., and J.G. DeLuca. 2009. Chromosome segregation: Ndc80 can carry the load. *Curr Biol*. 19:R404-407.

Kapoor, T.M., M.A. Lampson, P. Hergert, L. Cameron, D. Cimini, E.D. Salmon, B.F. McEwen, and A. Khodjakov. 2006. Chromosomes can congress to the metaphase plate before biorientation. *Science*. 311:388-391.

Kapoor, T.M., T.U. Mayer, M.L. Coughlin, and T.J. Mitchison. 2000. Probing spindle assembly mechanisms with monastrol, a small molecule inhibitor of the mitotic kinesin, Eg5. *J Cell Biol*. 150:975-988.

Kardon, J.R., and R.D. Vale. 2009. Regulators of the cytoplasmic dynein motor. *Nat Rev Mol Cell Biol*. 10:854-865.

Karess, R. 2005. Rod-Zw10-Zwilch: a key player in the spindle checkpoint. *Trends Cell Biol*. 15:386-392.

Kawashima, S.A., T. Tsukahara, M. Langegger, S. Hauf, T.S. Kitajima, and Y. Watanabe. 2007. Shugoshin enables tension-generating attachment of kinetochores by loading Aurora to centromeres. *Genes & development*. 21:420-435.

Khodjakov, A., R.W. Cole, B.R. Oakley, and C.L. Rieder. 2000. Centrosome-independent mitotic spindle formation in vertebrates. *Curr Biol*. 10:59-67.

Khodjakov, A., L. Copenagle, M.B. Gordon, D.A. Compton, and T.M. Kapoor. 2003. Minus-end capture of preformed kinetochore fibers contributes to spindle morphogenesis. *J Cell Biol*. 160:671-683.

Kim, Y., A.J. Holland, W. Lan, and D.W. Cleveland. 2010. Aurora kinases and protein phosphatase 1 mediate chromosome congression through regulation of CENP-E. *Cell*. 142:444-455.

King, J.M., T.S. Hays, and R.B. Nicklas. 2000. Dynein is a transient kinetochore component whose binding is regulated by microtubule attachment, not tension. *J Cell Biol*. 151:739-748.

King, J.M., and R.B. Nicklas. 2000. Tension on chromosomes increases the number of kinetochore microtubules but only within limits. *Journal of cell science*. 113 Pt 21:3815-3823.

Kirschner, M., and T. Mitchison. 1986. Beyond self-assembly: from microtubules to morphogenesis. *Cell*. 45:329-342.

Kiyomitsu, T., O. Iwasaki, C. Obuse, and M. Yanagida. 2010. Inner centromere formation requires hMis14, a trident kinetochore protein that specifically recruits HP1 to human chromosomes. *J Cell Biol*. 188:791-807.

Kiyomitsu, T., C. Obuse, and M. Yanagida. 2007. Human Blinkin/AF15q14 is required for chromosome alignment and the mitotic checkpoint through direct interaction with Bub1 and BubR1. *Dev Cell*. 13:663-676.

Klein, U.R., E.A. Nigg, and U. Gruneberg. 2006. Centromere targeting of the chromosomal passenger complex requires a ternary subcomplex of Borealin, Survivin, and the N-terminal domain of INCENP. *Mol Biol Cell*. 17:2547-2558.

Kline, S.L., I.M. Cheeseman, T. Hori, T. Fukagawa, and A. Desai. 2006. The human Mis12 complex is required for kinetochore assembly and proper chromosome segregation. *J Cell Biol*. 173:9-17.

Kops, G.J., Y. Kim, B.A. Weaver, Y. Mao, I. McLeod, J.R. Yates, 3rd, M. Tagaya, and D.W. Cleveland. 2005. ZW10 links mitotic checkpoint signaling to the structural kinetochore. *J Cell Biol*. 169:49-60.

Kulukian, A., J.S. Han, and D.W. Cleveland. 2009. Unattached kinetochores catalyze production of an anaphase inhibitor that requires a Mad2 template to prime Cdc20 for BubR1 binding. *Dev Cell*. 16:105-117.

Kwiatkowski, N., N. Jelluma, P. Filippakopoulos, M. Soundararajan, M.S. Manak, M. Kwon, H.G. Choi, T. Sim, Q.L. Deveraux, S. Rottmann, D. Pellman, J.V. Shah, G.J. Kops, S. Knapp, and N.S. Gray. 2010. Small-molecule kinase inhibitors provide insight into Mps1 cell cycle function. *Nat Chem Biol*. 6:359-368.

Lampert, F., P. Hornung, and S. Westermann. 2010. The Dam1 complex confers microtubule plus end-tracking activity to the Ndc80 kinetochore complex. *J Cell Biol*. 189:641-649.

Lampson, M.A., K. Renduchitala, A. Khodjakov, and T.M. Kapoor. 2004. Correcting improper chromosome-spindle attachments during cell division. *Nat Cell Biol*. 6:232-237.

Lan, W., X. Zhang, S.L. Kline-Smith, S.E. Rosasco, G.A. Barrett-Wilt, J. Shabanowitz, D.F. Hunt, C.E. Walczak, and P.T. Stukenberg. 2004a. Aurora B phosphorylates centromeric MCAK and regulates its localization and microtubule depolymerization activity. *Current biology : CB*. 14:273-286.

Lan, W., X. Zhang, S.L. Kline-Smith, S.E. Rosasco, G.A. Barrett-Wilt, J. Shabanowitz, D.F. Hunt, C.E. Walczak, and P.T. Stukenberg. 2004b. Aurora B phosphorylates centromeric MCAK and regulates its localization and microtubule depolymerization activity. *Curr Biol*. 14:273-286.

Lens, S.M., J.A. Rodriguez, G. Vader, S.W. Span, G. Giaccone, and R.H. Medema. 2006. Uncoupling the central spindle-associated function of the chromosomal passenger complex from its role at centromeres. *Mol Biol Cell*. 17:1897-1909.

Levesque, A.A., and D.A. Compton. 2001. The chromokinesin Kid is necessary for chromosome arm orientation and oscillation, but not congression, on mitotic spindles. *J Cell Biol*. 154:1135-1146.

Li, R., and A.W. Murray. 1991. Feedback control of mitosis in budding yeast. *Cell*. 66:519-531.

Li, X., and R.B. Nicklas. 1995. Mitotic forces control a cell-cycle checkpoint. *Nature*. 373:630-632.

Li, Y., W. Yu, Y. Liang, and X. Zhu. 2007. Kinetochore dynein generates a poleward pulling force to facilitate congression and full chromosome alignment. *Cell research*. 17:701-712.

Liang, Y., W. Yu, Y. Li, Z. Yang, X. Yan, Q. Huang, and X. Zhu. 2004. Nudel functions in membrane traffic mainly through association with Lis1 and cytoplasmic dynein. *J Cell Biol*. 164:557-566.

Liang, Y., W. Yu, Y. Li, L. Yu, Q. Zhang, F. Wang, Z. Yang, J. Du, Q. Huang, X. Yao, and X. Zhu. 2007. Nudel modulates kinetochore association and function of cytoplasmic dynein in M phase. *Mol Biol Cell*. 18:2656-2666.

Lin, Y.T., Y. Chen, G. Wu, and W.H. Lee. 2006. Hec1 sequentially recruits Zwint-1 and ZW10 to kinetochores for faithful chromosome segregation and spindle checkpoint control. *Oncogene*. 25:6901-6914.

Liu, D., G. Vader, M.J. Vromans, M.A. Lampson, and S.M. Lens. 2009. Sensing chromosome bi-orientation by spatial separation of aurora B kinase from kinetochore substrates. *Science*. 323:1350-1353.

Liu, D., M. Vleugel, C.B. Backer, T. Hori, T. Fukagawa, I.M. Cheeseman, and M.A. Lampson. 2010. Regulated targeting of protein phosphatase 1 to the outer kinetochore by KNL1 opposes Aurora B kinase. *J Cell Biol*. 188:809-820.

Luo, X., Z. Tang, J. Rizo, and H. Yu. 2002. The Mad2 spindle checkpoint protein undergoes similar major conformational changes upon binding to either Mad1 or Cdc20. *Mol Cell*. 9:59-71.

Maiato, H., C.L. Rieder, and A. Khodjakov. 2004. Kinetochore-driven formation of kinetochore fibers contributes to spindle assembly during animal mitosis. *J Cell Biol*. 167:831-840.

Malureanu, L.A., K.B. Jeganathan, M. Hamada, L. Wasilewski, J. Davenport, and J.M. van Deursen. 2009. BubR1 N terminus acts as a soluble inhibitor of cyclin B degradation by APC/C(Cdc20) in interphase. *Dev Cell*. 16:118-131.

Mapelli, M., F.V. Filipp, G. Rancati, L. Massimiliano, L. Nezi, G. Stier, R.S. Hagan, S. Confalonieri, S. Piatti, M. Sattler, and A. Musacchio. 2006. Determinants of conformational dimerization of Mad2 and its inhibition by p31comet. *EMBO J*. 25:1273-1284.

Mapelli, M., L. Massimiliano, S. Santaguida, and A. Musacchio. 2007. The Mad2 conformational dimer: structure and implications for the spindle assembly checkpoint. *Cell*. 131:730-743.

Martin-Lluesma, S., V.M. Stucke, and E.A. Nigg. 2002. Role of Hec1 in spindle checkpoint signaling and kinetochore recruitment of Mad1/Mad2. *Science*. 297:2267-2270.

Maure, J.F., S. Komoto, Y. Oku, A. Mino, S. Pasqualato, K. Natsume, L. Clayton, A. Musacchio, and T.U. Tanaka. 2011. The Ndc80 loop region facilitates formation of kinetochore attachment to the dynamic microtubule plus end. *Curr Biol*. 21:207-213.

Mayer, T.U., T.M. Kapoor, S.J. Haggarty, R.W. King, S.L. Schreiber, and T.J. Mitchison. 1999. Small molecule inhibitor of mitotic spindle bipolarity identified in a phenotype-based screen. *Science*. 286:971-974.

Mayr, M.I., S. Hummer, J. Bormann, T. Gruner, S. Adio, G. Woehlke, and T.U. Mayer. 2007. The human kinesin Kif18A is a motile microtubule depolymerase essential for chromosome congression. *Curr Biol*. 17:488-498.

McClelland, S.E., S. Borusu, A.C. Amaro, J.R. Winter, M. Belwal, A.D. McAinsh, and P. Meraldi. 2007. The CENP-A NAC/CAD kinetochore complex controls chromosome congression and spindle bipolarity. *EMBO J*. 26:5033-5047.

McIntosh, J.R., E.L. Grishchuk, M.K. Morphew, A.K. Efremov, K. Zhudenkov, V.A. Volkov, I.M. Cheeseman, A. Desai, D.N. Mastronarde, and F.I. Ataullakhanov. 2008. Fibrils connect microtubule tips with kinetochores: a mechanism to couple tubulin dynamics to chromosome motion. *Cell*. 135:322-333.

Mische, S., Y. He, L. Ma, M. Li, M. Serr, and T.S. Hays. 2008. Dynein light intermediate chain: an essential subunit that contributes to spindle checkpoint inactivation. *Mol Biol Cell*. 19:4918-4929.

Moreno-Moreno, O., M. Torras-Llort, and F. Azorin. 2006. Proteolysis restricts localization of CID, the centromere-specific histone H3 variant of Drosophila, to centromeres. *Nucleic Acids Res*. 34:6247-6255.

Morgan, D.O. 2007. The cell cycle : principles of control. New Science Press Ltd 2007, London Sunderland, MA. 297 pp.

Moritz, M., M.B. Braunfeld, V. Guenebaut, J. Heuser, and D.A. Agard. 2000. Structure of the gamma-tubulin ring complex: a template for microtubule nucleation. *Nat Cell Biol*. 2:365-370.

Mountain, V., C. Simerly, L. Howard, A. Ando, G. Schatten, and D.A. Compton. 1999. The kinesin-related protein, HSET, opposes the activity of Eg5 and cross-links microtubules in the mammalian mitotic spindle. *J Cell Biol*. 147:351-366.

Musacchio, A., and E.D. Salmon. 2007. The spindle-assembly checkpoint in space and time. *Nat Rev Mol Cell Biol*. 8:379-393.

Nezi, L., and A. Musacchio. 2009. Sister chromatid tension and the spindle assembly checkpoint. *Curr Opin Cell Biol*. 21:785-795.

Nicklas, R.B., and S.C. Ward. 1994. Elements of error correction in mitosis: microtubule capture, release, and tension. *J Cell Biol*. 126:1241-1253.

Nigg, E.A. 2001. Mitotic kinases as regulators of cell division and its checkpoints. *Nat Rev Mol Cell Biol*. 2:21-32.

Nigg, E.A. 2002. Centrosome aberrations: cause or consequence of cancer progression? *Nat Rev Cancer*. 2:815-825.

Nilsson, J., M. Yekezare, J. Minshull, and J. Pines. 2008. The APC/C maintains the spindle assembly checkpoint by targeting Cdc20 for destruction. *Nat Cell Biol*. 10:1411-1420.

Nousiainen, M., H.H. Sillje, G. Sauer, E.A. Nigg, and R. Korner. 2006. Phosphoproteome analysis of the human mitotic spindle. *Proc Natl Acad Sci U S A*. 103:5391-5396.

Nurse, P. 2000. A long twentieth century of the cell cycle and beyond. *Cell*. 100:71-78.

O'Connell, C.B., and A.L. Khodjakov. 2007. Cooperative mechanisms of mitotic spindle formation. *Journal of cell science*. 120:1717-1722.

O'Connell, C.B., and Y.L. Wang. 2000. Mammalian spindle orientation and position respond to changes in cell shape in a dynein-dependent fashion. *Molecular biology of the cell*. 11:1765-1774.

Obuse, C., O. Iwasaki, T. Kiyomitsu, G. Goshima, Y. Toyoda, and M. Yanagida. 2004. A conserved Mis12 centromere complex is linked to heterochromatic HP1 and outer kinetochore protein Zwint-1. *Nat Cell Biol*. 6:1135-1141.

Ohta, S., J.C. Bukowski-Wills, L. Sanchez-Pulido, L. Alves Fde, L. Wood, Z.A. Chen, M. Platani, L. Fischer, D.F. Hudson, C.P. Ponting, T. Fukagawa, W.C. Earnshaw, and J. Rappsilber. 2010. The protein composition of mitotic chromosomes determined using multiclassifier combinatorial proteomics. *Cell*. 142:810-821.

Okada, M., I.M. Cheeseman, T. Hori, K. Okawa, I.X. McLeod, J.R. Yates, 3rd, A. Desai, and T. Fukagawa. 2006. The CENP-H-I complex is required for the efficient incorporation of newly synthesized CENP-A into centromeres. *Nat Cell Biol*. 8:446-457.

Olsen, J.V., M. Vermeulen, A. Santamaria, C. Kumar, M.L. Miller, L.J. Jensen, F. Gnad, J. Cox, T.S. Jensen, E.A. Nigg, S. Brunak, and M. Mann. 2010. Quantitative phosphoproteomics reveals widespread full phosphorylation site occupancy during mitosis. *Sci Signal*. 3:ra3.

Paweletz, N. 2001. Walther Flemming: pioneer of mitosis research. *Nat Rev Mol Cell Biol*. 2:72-75.

Pearson, C.G., and K. Bloom. 2004. Dynamic microtubules lead the way for spindle positioning. *Nat Rev Mol Cell Biol*. 5:481-492.

Petrovic, A., S. Pasqualato, P. Dube, V. Krenn, S. Santaguida, D. Cittaro, S. Monzani, L. Massimiliano, J. Keller, A. Tarricone, A. Maiolica, H. Stark, and A. Musacchio. 2010. The MIS12 complex is a protein interaction hub for outer kinetochore assembly. *J Cell Biol*. 190:835-852.

Pines, J. 2006. Mitosis: a matter of getting rid of the right protein at the right time. *Trends Cell Biol*. 16:55-63.

Pinsky, B.A., and S. Biggins. 2005. The spindle checkpoint: tension versus attachment. *Trends Cell Biol*. 15:486-493.

Powers, A.F., A.D. Franck, D.R. Gestaut, J. Cooper, B. Gracyzk, R.R. Wei, L. Wordeman, T.N. Davis, and C.L. Asbury. 2009. The Ndc80 kinetochore complex forms load-bearing attachments to dynamic microtubule tips via biased diffusion. *Cell*. 136:865-875.

Przewloka, M.R., Z. Venkei, V.M. Bolanos-Garcia, J. Debski, M. Dadlez, and D.M. Glover. 2011. CENP-C is a structural platform for kinetochore assembly. *Curr Biol*. 21:399-405.

Raaijmakers, J.A., M.E. Tanenbaum, A.F. Maia, and R.H. Medema. 2009. RAMA1 is a novel kinetochore protein involved in kinetochore-microtubule attachment. *Journal of cell science*. 122:2436-2445.

Rieder, C.L. 1981. The structure of the cold-stable kinetochore fiber in metaphase PtK1 cells. *Chromosoma*. 84:145-158.

Rieder, C.L. 2005. Kinetochore fiber formation in animal somatic cells: dueling mechanisms come to a draw. *Chromosoma*. 114:310-318.

Rieder, C.L., and S.P. Alexander. 1990. Kinetochores are transported poleward along a single astral microtubule during chromosome attachment to the spindle in newt lung cells. *J Cell Biol*. 110:81-95.

Rieder, C.L., R.W. Cole, A. Khodjakov, and G. Sluder. 1995. The checkpoint delaying anaphase in response to chromosome monoorientation is mediated by an inhibitory signal produced by unattached kinetochores. *J Cell Biol*. 130:941-948.

Ruchaud, S., M. Carmena, and W.C. Earnshaw. 2007. Chromosomal passengers: conducting cell division. *Nat Rev Mol Cell Biol*. 8:798-812.

Sanchez-Perez, I., S.J. Renwick, K. Crawley, I. Karig, V. Buck, J.C. Meadows, A. Franco-Sanchez, U. Fleig, T. Toda, and J.B. Millar. 2005. The DASH complex and Klp5/Klp6 kinesin coordinate bipolar chromosome attachment in fission yeast. *The EMBO journal*. 24:2931-2943.

Santaguida, S., and A. Musacchio. 2009. The life and miracles of kinetochores. *EMBO J*. 28:2511-2531.

Santaguida, S., A. Tighe, A.M. D'Alise, S.S. Taylor, and A. Musacchio. 2010. Dissecting the role of MPS1 in chromosome biorientation and the spindle checkpoint through the small molecule inhibitor reversine. *J Cell Biol*. 190:73-87.

Santamaria, A., R. Neef, U. Eberspacher, K. Eis, M. Husemann, D. Mumberg, S. Prechtl, V. Schulze, G. Siemeister, L. Wortmann, F.A. Barr, and E.A. Nigg. 2007. Use of the novel Plk1 inhibitor ZK-thiazolidinone to elucidate functions of Plk1 in early and late stages of mitosis. *Mol Biol Cell*. 18:4024-4036.

Santamaria, A., B. Wang, S. Elowe, R. Malik, F. Zhang, M. Bauer, A. Schmidt, H.H. Sillje, R. Korner, and E.A. Nigg. 2011. The Plk1-dependent phosphoproteome of the early mitotic spindle. *Mol Cell Proteomics*. 10:M110 004457.

Sauer, G., R. Korner, A. Hanisch, A. Ries, E.A. Nigg, and H.H. Sillje. 2005. Proteome analysis of the human mitotic spindle. *Molecular & cellular proteomics : MCP*. 4:35-43.

Savoian, M.S., M.L. Goldberg, and C.L. Rieder. 2000. The rate of poleward chromosome motion is attenuated in Drosophila zw10 and rod mutants. *Nat Cell Biol*. 2:948-952.

Schmidt, J.C., T. Kiyomitsu, T. Hori, C.B. Backer, T. Fukagawa, and I.M. Cheeseman. 2010. Aurora B kinase controls the targeting of the Astrin-SKAP complex to bioriented kinetochores. *J Cell Biol*. 191:269-280.

Screpanti, E., A. De Antoni, G.M. Alushin, A. Petrovic, T. Melis, E. Nogales, and A. Musacchio. 2011. Direct binding of Cenp-C to the Mis12 complex joins the inner and outer kinetochore. *Curr Biol*. 21:391-398.

Sessa, F., M. Mapelli, C. Ciferri, C. Tarricone, L.B. Areces, T.R. Schneider, P.T. Stukenberg, and A. Musacchio. 2005. Mechanism of Aurora B activation by INCENP and inhibition by hesperadin. *Mol Cell*. 18:379-391.

Sharp, D.J., H.M. Brown, M. Kwon, G.C. Rogers, G. Holland, and J.M. Scholey. 2000. Functional coordination of three mitotic motors in Drosophila embryos. *Mol Biol Cell*. 11:241-253.

Sillje, H.H., S. Nagel, R. Korner, and E.A. Nigg. 2006. HURP is a Ran-importin beta-regulated protein that stabilizes kinetochore microtubules in the vicinity of chromosomes. *Curr Biol*. 16:731-742.

Sironi, L., M. Mapelli, S. Knapp, A. De Antoni, K.T. Jeang, and A. Musacchio. 2002. Crystal structure of the tetrameric Mad1-Mad2 core complex: implications of a 'safety belt' binding mechanism for the spindle checkpoint. *EMBO J*. 21:2496-2506.

Sivaram, M.V., T.L. Wadzinski, S.D. Redick, T. Manna, and S.J. Doxsey. 2009. Dynein light intermediate chain 1 is required for progress through the spindle assembly checkpoint. *The EMBO journal*.

Skoufias, D.A., P.R. Andreassen, F.B. Lacroix, L. Wilson, and R.L. Margolis. 2001. Mammalian mad2 and bub1/bubR1 recognize distinct spindle-attachment and kinetochore-tension checkpoints. *Proc Natl Acad Sci U S A*. 98:4492-4497.

Starr, D.A., B.C. Williams, T.S. Hays, and M.L. Goldberg. 1998. ZW10 helps recruit dynactin and dynein to the kinetochore. *The Journal of cell biology*. 142:763-774.

Stehman, S.A., Y. Chen, R.J. McKenney, and R.B. Vallee. 2007. NudE and NudEL are required for mitotic progression and are involved in dynein recruitment to kinetochores. *J Cell Biol*. 178:583-594.

Stucke, V.M., H.H. Sillje, L. Arnaud, and E.A. Nigg. 2002. Human Mps1 kinase is required for the spindle assembly checkpoint but not for centrosome duplication. *The EMBO journal*. 21:1723-1732.

Stumpff, J., G. von Dassow, M. Wagenbach, C. Asbury, and L. Wordeman. 2008. The kinesin-8 motor Kif18A suppresses kinetochore movements to control mitotic chromosome alignment. *Dev Cell*. 14:252-262.

Sudakin, V., G.K. Chan, and T.J. Yen. 2001. Checkpoint inhibition of the APC/C in HeLa cells is mediated by a complex of BUBR1, BUB3, CDC20, and MAD2. *J Cell Biol*. 154:925-936.

Sui, S., J. Wang, B. Yang, L. Song, J. Zhang, M. Chen, J. Liu, Z. Lu, Y. Cai, S. Chen, W. Bi, Y. Zhu, F. He, and X. Qian. 2008. Phosphoproteome analysis of the human Chang liver cells using SCX and a complementary mass spectrometric strategy. *Proteomics*. 8:2024-2034.

Tanaka, T.U., and A. Desai. 2008. Kinetochore-microtubule interactions: the means to the end. *Curr Opin Cell Biol*. 20:53-63.

Tanaka, T.U., N. Rachidi, C. Janke, G. Pereira, M. Galova, E. Schiebel, M.J. Stark, and K. Nasmyth. 2002. Evidence that the Ipl1-Sli15 (Aurora kinase-INCENP) complex promotes chromosome bi-orientation by altering kinetochore-spindle pole connections. *Cell*. 108:317-329.

Tang, Z., R. Bharadwaj, B. Li, and H. Yu. 2001. Mad2-Independent inhibition of APCCdc20 by the mitotic checkpoint protein BubR1. *Dev Cell*. 1:227-237.

Tanudji, M., J. Shoemaker, L. L'Italien, L. Russell, G. Chin, and X.M. Schebye. 2004. Gene silencing of CENP-E by small interfering RNA in HeLa cells leads to missegregation of chromosomes after a mitotic delay. *Molecular biology of the cell*. 15:3771-3781.

Thein, K.H., J. Kleylein-Sohn, E.A. Nigg, and U. Gruneberg. 2007. Astrin is required for the maintenance of sister chromatid cohesion and centrosome integrity. *J Cell Biol*. 178:345-354.

Theis, M., M. Slabicki, M. Junqueira, M. Paszkowski-Rogacz, J. Sontheimer, R. Kittler, A.K. Heninger, T. Glatter, K. Kruusmaa, I. Poser, A.A. Hyman, M.T. Pisabarro, M. Gstaiger, R. Aebersold, A. Shevchenko, and F. Buchholz. 2009. Comparative profiling identifies C13orf3 as a component of the Ska complex required for mammalian cell division. *Embo J*. 28:1453-1465.

Tien, J.F., N.T. Umbreit, D.R. Gestaut, A.D. Franck, J. Cooper, L. Wordeman, T. Gonen, C.L. Asbury, and T.N. Davis. 2010. Cooperation of the Dam1 and Ndc80 kinetochore complexes enhances microtubule coupling and is regulated by aurora B. *J Cell Biol*. 189:713-723.

Torras-Llort, M., O. Moreno-Moreno, and F. Azorin. 2009. Focus on the centre: the role of chromatin on the regulation of centromere identity and function. *EMBO J*. 28:2337-2348.

Toso, A., J.R. Winter, A.J. Garrod, A.C. Amaro, P. Meraldi, and A.D. McAinsh. 2009. Kinetochore-generated pushing forces separate centrosomes during bipolar spindle assembly. *J Cell Biol*. 184:365-372.

Toyoshima, F., S. Matsumura, H. Morimoto, M. Mitsushima, and E. Nishida. 2007. PtdIns(3,4,5)P3 regulates spindle orientation in adherent cells. *Dev Cell*. 13:796-811.

Toyoshima, F., and E. Nishida. 2007. Integrin-mediated adhesion orients the spindle parallel to the substratum in an EB1- and myosin X-dependent manner. *Embo J*. 26:1487-1498.

Vaisberg, E.A., M.P. Koonce, and J.R. McIntosh. 1993. Cytoplasmic dynein plays a role in mammalian mitotic spindle formation. *J Cell Biol*. 123:849-858.
Varma, D., P. Monzo, S.A. Stehman, and R.B. Vallee. 2008. Direct role of dynein motor in stable kinetochore-microtubule attachment, orientation, and alignment. *J Cell Biol*. 182:1045-1054.
Verdaasdonk, J.S., and K. Bloom. 2011. Centromeres: unique chromatin structures that drive chromosome segregation. *Nat Rev Mol Cell Biol*. 12:320-332.
Vergnolle, M.A., and S.S. Taylor. 2007. Cenp-F links kinetochores to Ndel1/Nde1/Lis1/dynein microtubule motor complexes. *Curr Biol*. 17:1173-1179.
Vorozhko, V.V., M.J. Emanuele, M.J. Kallio, P.T. Stukenberg, and G.J. Gorbsky. 2008. Multiple mechanisms of chromosome movement in vertebrate cells mediated through the Ndc80 complex and dynein/dynactin. *Chromosoma*. 117:169-179.
Wadsworth, P., and A. Khodjakov. 2004. E pluribus unum: towards a universal mechanism for spindle assembly. *Trends Cell Biol*. 14:413-419.
Wan, X., R.P. O'Quinn, H.L. Pierce, A.P. Joglekar, W.E. Gall, J.G. DeLuca, C.W. Carroll, S.T. Liu, T.J. Yen, B.F. McEwen, P.T. Stukenberg, A. Desai, and E.D. Salmon. 2009. Protein architecture of the human kinetochore microtubule attachment site. *Cell*. 137:672-684.
Wang, E., E.R. Ballister, and M.A. Lampson. 2011. Aurora B dynamics at centromeres create a diffusion-based phosphorylation gradient. *The Journal of cell biology*. 194:539-549.
Waters, J.C., R.H. Chen, A.W. Murray, and E.D. Salmon. 1998. Localization of Mad2 to kinetochores depends on microtubule attachment, not tension. *J Cell Biol*. 141:1181-1191.
Wei, R.R., P.K. Sorger, and S.C. Harrison. 2005. Molecular organization of the Ndc80 complex, an essential kinetochore component. *Proc Natl Acad Sci U S A*. 102:5363-5367.
Weiss, E., and M. Winey. 1996. The Saccharomyces cerevisiae spindle pole body duplication gene MPS1 is part of a mitotic checkpoint. *J Cell Biol*. 132:111-123.
Welburn, J.P., E.L. Grishchuk, C.B. Backer, E.M. Wilson-Kubalek, J.R. Yates, 3rd, and I.M. Cheeseman. 2009. The human kinetochore Ska1 complex facilitates microtubule depolymerization-coupled motility. *Dev Cell*. 16:374-385.
Welburn, J.P., M. Vleugel, D. Liu, J.R. Yates, 3rd, M.A. Lampson, T. Fukagawa, and I.M. Cheeseman. 2010. Aurora B phosphorylates spatially distinct targets to differentially regulate the kinetochore-microtubule interface. *Mol Cell*. 38:383-392.
Whyte, J., J.R. Bader, S.B. Tauhata, M. Raycroft, J. Hornick, K.K. Pfister, W.S. Lane, G.K. Chan, E.H. Hinchcliffe, P.S. Vaughan, and K.T. Vaughan. 2008. Phosphorylation regulates targeting of cytoplasmic dynein to kinetochores during mitosis. *The Journal of cell biology*.
Williams, B.C., and M.L. Goldberg. 1994. Determinants of Drosophila zw10 protein localization and function. *Journal of cell science*. 107 (Pt 4):785-798.
Wittmann, T., A. Hyman, and A. Desai. 2001. The spindle: a dynamic assembly of microtubules and motors. *Nat Cell Biol*. 3:E28-34.
Wojcik, E., R. Basto, M. Serr, F. Scaerou, R. Karess, and T. Hays. 2001. Kinetochore dynein: its dynamics and role in the transport of the Rough deal checkpoint protein. *Nat Cell Biol*. 3:1001-1007.
Wollman, R., E.N. Cytrynbaum, J.T. Jones, T. Meyer, J.M. Scholey, and A. Mogilner. 2005. Efficient chromosome capture requires a bias in the 'search-and-capture' process during mitotic-spindle assembly. *Curr Biol*. 15:828-832.
Xia, G., X. Luo, T. Habu, J. Rizo, T. Matsumoto, and H. Yu. 2004. Conformation-specific binding of p31(comet) antagonizes the function of Mad2 in the spindle checkpoint. *EMBO J*. 23:3133-3143.
Yamamoto, T.G., S. Watanabe, A. Essex, and R. Kitagawa. 2008. SPDL-1 functions as a kinetochore receptor for MDF-1 in Caenorhabditis elegans. *J Cell Biol*. 183:187-194.
Yang, M., B. Li, D.R. Tomchick, M. Machius, J. Rizo, H. Yu, and X. Luo. 2007a. p31comet blocks Mad2 activation through structural mimicry. *Cell*. 131:744-755.

Yang, Y., F. Wu, T. Ward, F. Yan, Q. Wu, Z. Wang, T. McGlothen, W. Peng, T. You, M. Sun, T. Cui, R. Hu, Z. Dou, J. Zhu, W. Xie, Z. Rao, X. Ding, and X. Yao. 2008. Phosphorylation of HsMis13 by Aurora B kinase is essential for assembly of functional kinetochore. *J Biol Chem*. 283:26726-26736.

Yang, Z., U.S. Tulu, P. Wadsworth, and C.L. Rieder. 2007b. Kinetochore dynein is required for chromosome motion and congression independent of the spindle checkpoint. *Curr Biol*. 17:973-980.

Yasui, Y., T. Urano, A. Kawajiri, K. Nagata, M. Tatsuka, H. Saya, K. Furukawa, T. Takahashi, I. Izawa, and M. Inagaki. 2004. Autophosphorylation of a newly identified site of Aurora-B is indispensable for cytokinesis. *J Biol Chem*. 279:12997-13003.

Yingling, J., Y.H. Youn, D. Darling, K. Toyo-Oka, T. Pramparo, S. Hirotsune, and A. Wynshaw-Boris. 2008. Neuroepithelial stem cell proliferation requires LIS1 for precise spindle orientation and symmetric division. *Cell*. 132:474-486.

Zhou, J., J. Yao, and H.C. Joshi. 2002. Attachment and tension in the spindle assembly checkpoint. *Journal of cell science*. 115:3547-3555.

Curriculum Vitae

Personal Information

First name: Ying Wai

Family name: Chan

Date of birth: 2nd July 1984

Place of birth: Hong Kong

Family status: Single

Nationality: Chinese

Working address: Growth & Development, Biozentrum, University of Basel, Klingelbergstr. 50/70, 4056 Basel, Switzerland

Email: gary.chan@unibas.ch

Office phone no: +41 61 267 20 36

Mobile: +41 76 764 00 89

Education

September 2009 onwards	PhD student at the Biozentrum, University of Basel, Switzerland Supervisors: Prof. Dr. Erich A. Nigg and Dr. Anna Santamaria
September 2007- August 2009	PhD student at the Max Planck Institute of Biochemistry, Department of Cell Biology, Am Klopferspitz 18, D-8215 Martinsried Supervisors: Prof. Dr. Erich A. Nigg and Dr. Anna Santamaria
September 2005- August 2007	Master student at the Hong Kong University of Science and Technology, Hong Kong, China Supervisors: Prof. Dr. Randy Poon Master of Philosophy (MPhil) in Biochemistry obtained on 19th November 2007

September 2002- August 2005	Bachelor student at the Hong Kong University of Science and Technology, Hong Kong, China Bachelor of Science (BSc) in Biochemistry obtained on 19th November 2005 (First Class Honors)

Publications

Chan, Y.W., Fava, L.L, Uldschmid, A., Schmitz, M.H.A., Gerlich, D.W., Nigg, E.A. and Santamaria, A.
Mitotic control of kinetochore-associated dynein and spindle orientation by human Spindly. *Journal of Cell Biology* 185: 859-874 (2009)

Chan, Y.W., Chen, Y., and Poon, R.Y.C.
Generation of an indestructible cyclin B1 by caspase-6-dependent cleavage during mitotic catastrophe. *Oncogene* 28: 170-83 (2009).

Chan, Y.W., Ma, H.T., Wong, W., Ho, C.C., On, K.F., and Poon, R.Y.C.
CDK1 inhibitors antagonize the immediate apoptosis triggered by spindle disruption but promote apoptosis following the subsequent rereplication and abnormal mitosis. *Cell Cycle* 7: 1149-61 (2008).

Chan, Y.W., On, K.F., Chan, W.M., Wong, W., Siu, H.O., Hau, P.M., and Poon, R.Y.C.
The kinetics of p53 activation versus cyclin E accumulation underlies the relationship between the spindle-assembly checkpoint and the postmitotic checkpoint. *Journal of Biological Chemistry* 283: 15716-23 (2008).

Meetings

25th June -1st July 2011
Gordon Research Conference: Cell growth and proliferation in Biddeford, USA
Poster presentation
Title: Regulation of the Ska complex by Aurora B-mediated phosphorylation

23rd -25th Septemper 2008

10th Young Scientist Meeting "Biology of Cell Division" in Heidelberg, Germany

Poster presentation and oral presentation

Title: Human Spindly is required for kinetochore localization of dynein but not for the stripping of checkpoint proteins.

Extra curriculum activity

2005-2007	Hall Tutor at the Hong Kong University of Science and Technology
2003-2004	Academic Secretary of the Science Student Association, the Hong Kong University of Science and Technology

Awards

2008	Postgraduate Student Research Award
2005	Academic Achievement Medal: Average of A in all courses taken throughout the Bachelor study

Teaching experience

I have been teaching undergraduate practical courses during both my Master study and PhD study.